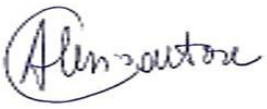
UNIVERSITA' VITA-SALUTE SAN RAFFAELE

CORSO DI DOTTORATO DI RICERCA INTERNAZIONALE IN MEDICINA MOLECOLARE

Curriculum in Terapia Genica e Cellulare

EVALUATION OF THE EFFICACY AND SAFETY OF GENE THERAPY STRATEGIES FOR LIVER METABOLIC DISEASES

DoS: Prof. Alessio Cantore 

Second Supervisor: Prof. Mario Amendola

Tesi di DOTTORATO DI RICERCA di Chiara Simoni

Matr. 019196

Ciclo di Dottorato XXXVII

SSD BIO/11 BIO/17

Anno Accademico 2023/2024

CONSULTAZIONE TESI DI DOTTORATO DI RICERCA

Il/la sottoscritto/*I*	Chiara Simoni
Matricola / *registration number*	019196
nato a/ *born at*	Verona
il/*on*	04/04/1995

autore della tesi di Dottorato di ricerca dal titolo / *author of the PhD Thesis titled*

Evaluation of the efficacy and safety of gene therapy strategies for liver metabolic diseases

☐ AUTORIZZA la Consultazione della tesi / AUTHORIZES *the public release of the thesis*

☒ NON AUTORIZZA la Consultazione della tesi per 12 mesi /DOES NOT AUTHORIZE *the public release of the thesis for* 12 *months*

a partire dalla data di conseguimento del titolo e precisamente */ from the PhD thesis date, specifically*

Dal / *from* 15/11/2024 Al / *to* 15/11/2025

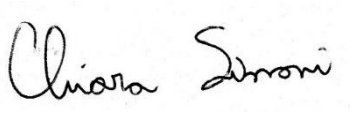
Poiché /*because*:

□ l'intera ricerca o parti di essa sono potenzialmente soggette a brevettabilità/ *The whole project or part of it might be subject to patentability;*

☒ ci sono parti di tesi che sono già state sottoposte a un editore o sono in attesa di pubblicazione/ *Parts of the thesis have been or are being submitted to a publisher or are in press;*

□ la tesi è finanziata da enti esterni che vantano dei diritti su di esse e sulla loro pubblicazione/ *the thesis project is financed by external bodies that have rights over it and on its publication.*

È fatto divieto di riprodurre, in tutto o in parte, quanto in essa contenuto / *Copyright the contents of the thesis in whole or in part is forbidden*

Data /Date 18/10/2024 Firma /Signature 

DECLARATION

This thesis has been:

- composed by myself and has not been used in any previous application for a degree. Throughout the text I use both 'I' and 'We' interchangeably.

- has been written according to the editing guidelines approved by the University.

All the results presented here were obtained by myself, except for:

1) *Large-scale IDLV and LV preparations* were performed with the help of Mauro Biffi and Maria Lucia Longo, SR-TIGET, Milan, Italy.
2) *AAV preparations carrying donor DNAs* (Results, chapter 3.3, 3.4, 3.5, 3.6; figure 3, 4, 5, 6, 7) were produced by Innovavector, while *AAVs carrying mCherry or hFIX* (Results, chapter 3.7, 3.8, 3.10, 3.12, 3.13; figure 8, 9, 12, 14, 15) were produced by Giuseppe Ronzitti laboratory, Genethon, Evry-Courcouronnes, France.
3) *Mice intravenous injections* were performed with the help of Elena Barbon, Francesco Starinieri, or Camilla Negri, SR-TIGET, Milan, Italy.
4) *Immune fluorescence image analysis* was performed with the help of Francesco Starinieri, SR-TIGET, Milan, Italy who created the programs on Matlab.
5) *ALT, AST, ALP serum concentrations* were evaluated by Micol Rava in the "mouse clinic" facility, IRCCS San Raffaele Scientific Institute, Milan, Italy
6) *Liver for histopathology analysis* were embedded in formalin, cut, and stained by Rossana Norata and Martina Rocchi, GLP test facility, IRCCS San Raffaele Scientific Institute, Milan, Italy; *histopathology images were analyzed* by Francesca Sanvito, who completed the corresponding tables (table 2, 3, 4).
7) *Mice perfusions* (Results, chapter 3.9; figure 10, 11) were performed with the help of Elena Barbon, SR-TIGET, Milan, Italy.
8) *Liver subpopulations* were separated (Results, chapter 3.9; figure 10, 11) with the help of Elisabetta Manta, SR-TIGET, Milan, Italy.
9) *Selection of antibodies for liver subpopulation sorting and design of sorting panels* were performed with the help of Andrea Annoni, SR-TIGET, Milan, Italy.
10) *Sorting of liver subpopulations* (Results, chapter 3.9; figure 10, 11) was performed by FRACTAL facility, IRCCS San Raffaele Scientific Institute, Milan, Italy

11) *p24 measurement in serum* (Results, chapter 3.9; figure 10) was performed with the help of Valeria Mollica, SR-TIGET, Milan, Italy.
12) *Injections and sacrifice of Agl$^{-/-}$ and WT age-matched controls* (Results, chapter 3.13; figure 15) were performed by Giuseppe Ronzitti laboratory, Genethon, Evry-Courcouronnes, France.

Some parts of the thesis have already been published in a review (doi: 10.3389/fgeed.2024.145803) where I am the first author, in particular, Introduction:

- Chapter 1.1.2, 1.2, 1.2.1, 1.2.2, 1.2.3, 1.2.4, 1.2.5, 1.2.6, 1.3, 1.3.1, 1.3.2, 1.3.3, 1.3.4, 1.3.5, 1.4, 1.5, 1.6.
- Figure II, III, IV.
- Table I, II.

Some parts of the thesis are currently under review in Nature Communication and have been published as a preprint (doi: 10.21203/rs.3.rs-4011604/v1), in particular:

- Results Chapter 3.7, 3.8, 3.10, 3.12, 3.13; Figure 8, 9, 12, 14, 15; Table 2, 3, 4
- Discussion Chapter 4.4, 4.7, 4.8
- Materials and methods Chapter 5.2, 5.3, 5.7, 5.9, 5.11, 5.12, 5.13, 5.14, 5.15, 5.18

All sources of information are acknowledged by means of reference.

Acknowledgments

Il primo ringraziamento va ad Alessio per avermi accolta nel suo gruppo nel 2019, quando ero solamente una studentessa di magistrale, e per aver creduto in me dandomi la possibilità di fare questo dottorato. Grazie a te e al Tiget ho avuto la possibilità di imparare più di quanto avrei immaginato.

L'altro ringraziamento di uguale importanza va ad Elena che ha lavorato con me a questo progetto. Grazie per tutti i tuoi preziosi consigli che vanno dagli esperimenti, alla scrittura di paper, fino alla scelta dei colori per grafici e poster. Grazie anche per essere un'amica, sempre pronta ad ascoltare i miei scleri e a gioire insieme per le cose positive.

Grazie agli amici che credono in me più di quando faccia io stessa, a Francesco e Thomas perché come all'incirca disse un saggio "non si sopravvive a un tirocinio magistrale + fellow + dottorato senza dei buoni amici, fuori e dentro il lab", e a Cesare per le discussioni su qualsiasi argomento e per spingermi a fare sempre meglio.

Grazie poi a tutti i membri presenti e passati del lab Cantore, a Elisabetta, Matteo e Camilla, per il vostro aiuto negli esperimenti e per le risate che portate tutti i giorni, ma anche a Mauro, Marilù, Michela, Anna, Sofia, Francesca e Maurizio, per il vostro contributo e per aver reso migliori le lunghe giornate di lavoro.

Grazie anche a Martina, Chiara e Margherita che con i loro sorrisi e le lamentele condivise hanno reso questi anni più leggeri.

C'è bisogno di ringraziare anche le persone fuori dal laboratorio. In primis i miei genitori che mi hanno permesso di avere tutto nella vita, dalla casa delle Barbie fino ad una casa vera a Milano, niente di quello che fate è scontato. Mi avete regalato anche Erica che è una sorella perfetta con cui passare la vita.

Grazie poi a tutte le amiche di una vita sparpagliate per il mondo, Emily, Elena, Letizia, Elisa, Marta, Debora, Lucia, Sara, Anna, Michela, Chiara, Serena, sempre pronte a fare il tifo le une per le altre nonostante la distanza. E grazie agli amici nuovi scoperti a Milano Marika, Assunta, Federica, Donato, Giorgio per avermi fatto sentire un po' a casa.

Ultimo ma decisamente non ultimo, grazie ad Adriano, che è stato al mio fianco in questi tre anni, che ha condiviso con me la vita di una dottoranda a Milano e l'ha resa molto più bella. Sono pronta a vedere cosa ci riserverà il futuro insieme. Intanto prometto che d'ora in poi tornerò a casa prima la sera.

Abstract

The liver is a major metabolic organ involved in many genetic diseases. Over the years *in vivo* liver-directed gene therapy strategies have been developed as therapeutic approaches. Gene addition based on adeno-associated viral vectors (AAVs) has become an approved drug for the inherited coagulation disease hemophilia. However, other strategies, such as gene editing, are being developed to modify the hepatocyte genome. With CRISPR/Cas9-based gene editing it is possible to obtain targeted transgene insertions maintained upon hepatocyte proliferation. Transgene maintenance is fundamental for the treatment of metabolic disorders that have rapid manifestation and decline. Two of these metabolic disorders are Maple syrup urine disease (MSUD) and Progressive familial intrahepatic cholestasis type 2 (PFIC2). MSUD is caused by mutations in one of four different genes, we are concentrating on *DBT*, while PFIC2 is due to mutations of *ABCB11*. Gene editing may become a therapeutic strategy for MSUD and PFIC2, by integrating transgene cDNA in the first intron of *DBT* and *ABCB11* genes, respectively, to maintain as much as possible physiological gene regulation. In this work, we tested different integration strategies and demonstrated that donor DNAs with short homology arms are the most efficient in integrating and expressing the transgene. Then, we showed that the coadministration of lipid nanoparticles (LNPs) and AAVs resulted in the highest integration rate. However, to develop gene editing for PFIC2 it is important to consider liver fibrosis, which causes alteration of liver architecture and metabolism. Here, we exploited two chemically induced and two genetic mouse models with different types and grades of liver fibrosis. We report that both pericentral and periportal fibrosis partially inhibited lentiviral vector (LV) and LNP-mediated hepatocyte gene transfer, while the efficiency of AAV-mediated transduction was reduced only in the presence of periportal fibrosis. Gene transfer was less impacted when liver fibrosis was milder. We also investigated the biodistribution of LV transduction among different organs and liver cell types, and the zonation in the liver lobule of LV-, AAV-, and LNP-mediated gene transfer. Overall, this work informs about the optimal strategy and timeframe of *in vivo* liver-directed genome editing for the treatment of MSUD and PFIC-2 and sheds light on the impact of liver fibrosis on hepatic gene transfer.

Table of contents

Acronyms and abbreviations 5

List of figures and tables 12

1. Introduction 14

1.1 Liver-directed gene therapy 14

1.1.1 The liver 14

1.1.2 The liver as a target organ for gene therapy 16

1.2 Gene editing strategies 19

1.2.1 NHEJ-based gene editing approaches 21

1.2.2 MMEJ-based gene editing approaches 23

1.2.3 HDR-based targeted integration approaches 24

1.2.4 Liver-targeted base editing approaches 26

1.2.5 Liver-targeted prime editing approaches 28

1.2.6 Liver gene silencing/activation 30

1.3 *In vivo* delivery methods to the liver 32

1.3.1 Adeno-Associated viral vectors 33

1.3.2 Adenoviral vectors 35

1.3.3 Lentiviral vectors 35

1.3.4 Lipid nanoparticles 36

1.3.5 Virus-like particles 38

1.4 Liver-directed genome editing clinical trials 39

1.5 Genome editing-related potential adverse events 43

1.6 Liver-directed genome editing future perspectives 45

1.7 Inherited metabolic diseases 47

1.7.1 Maple syrup urine disease 47

1.7.2 Progressive familial intrahepatic cholestasis type 2 51
1.8 Liver fibrosis 54
1.8.1 Pathophysiology of liver fibrosis 54
1.8.2 Etiology of liver fibrosis 57
1.8.3 Liver fibrosis mouse models 59
1.8.4 Liver fibrosis regression and treatments 60
2. Aim of the work 63
3. Results 64
3.1 Selection of the best-performing sgRNAs 64
3.2 Comparison of HDR- and non-HDR-based donor DNAs in murine and human cell lines 66
3.3 Comparison of HDR- and non-HDR-based donor DNAs administration to juvenile Cas9 mice 69
3.4 Comparison of HDR- and non-HDR-based donor DNAs administration to newborn Cas9 mice 73
3.5 Delivery test of donor DNA with viral vectors in combination with LNP carrying Cas9 and sgRNA 75
3.6 Assessment of the best time of LNP administration in combination with viral vectors to deliver the gene editing machinery 78
3.7 CCl_4-induced liver fibrosis negatively affects LV but not AAV transduction 80
3.8 DDC-induced biliary fibrosis negatively affects both LV and AAV transduction 84
3.9 Liver fibrosis reduces LV transduction of hepatocytes and spleen 87
3.10 Milder fibrosis, induced by CCl_4 or DDC, reduces LV and AAV transduction efficiency 91
3.11 Hepatocyte transfection mediated by LNP is impaired by CCl_4 and DDC-induced fibrosis 93

3.12 Liver fibrosis due to *Abcb11* deficiency slightly reduces LV and AAV transduction 94

3.13 LV and AAV transduction is not significantly impaired in *Agl*$^{-/-}$ mice 97

3.14 Liver fibrosis modifies the distribution of gene transfer within the liver lobule 98

4. Discussion 101

4.1 Selection of the best-performing sgRNA and donor DNA for *in vivo* liver-directed gene editing 101

4.2 Selection of the best delivery vehicles and time of administration for the editing machinery 102

4.3 Future development of a gene-editing strategy for the treatment of MSUD and PFIC2 104

4.4 Impact of liver fibrosis on gene transfer to hepatocytes 105

4.5 LV biodistribution in liver subpopulation and different organs in the presence of fibrosis 107

4.6 Transduction and transfection zonation with liver fibrosis 108

4.7 Speculation on the mechanism causing impairment of gene transfer 109

4.8 Limitations of the study and its relevance for human pathologies 110

4.9 Conclusions 111

5. Materials and methods 113

5.1 Bioinformatic analysis 113

5.2 Generation of plasmids 115

5.3 LV and IDLV production and titration 116

5.4 Cell line experiments 117

5.5 T7 and TIDE assays 118

5.6 Determination of integrations by ddPCR 119

5.7 AAV production and titration 121

5.8 LNP production and quality assessment 121
5.9 Mice experiments 121
5.10 Gene expression assays 123
5.11 Liver immunofluorescence imaging 123
5.12 Determination of hepatic clinical chemistry 124
5.13 Liver histopathology analysis 124
5.14 Enzyme-linked immunosorbent assay (ELISA) 125
5.15 VCN determination 125
5.16 p24 measurement in serum 126
5.17 Sorting of liver subpopulations 126
5.18 Statistical analysis 127
References 128

Acronyms and abbreviations

AAV	Adeno-associated viral vector
AAV8	AAV serotype 8
Abcb11$^{-/-}$	Abcb11 knock-out
ABE	Adenine base editor
AdV	Adenoviruses vector
Agl$^{-/-}$	Agl knock-out
AIH	Autoimmune hepatitis
ALD	Alcoholic liver disease
ALP	Alkaline phosphatase
ALT	Alanine aminotransferase
ApoE	Apolipoprotein E
ASBT	Apical sodium-dependent bile salt transporter
ASGPR	Asialoglycoprotein receptor
AST	Aspartate transaminase
BCAA	Branched-chain amino acids
BCKDH	Branched-chain α-ketoacid dehydrogenase
BDL	Bile duct ligation
BE	Base editor
bGH	Bovine growth hormone
bp	Base pairs
BSA	Bovine serum albumin
BSEP	Bile salt export pump

CAST	CRISPR-associated transposase
CAST-seq	Chromosomal aberrations analysis by single targeted linker-mediated PCR sequencing
CBE	Cytidine base editor
CCL2	C-C motif ligand 2
CCl_3	Trichloromethyl
CCl_4	Carbon tetrachloride
CCL5	C-C motif ligand 5
CDAA	Choline-deficient, L-amino acid-defined
cDNA	Complementary DNA
CK7	Cytokeratin 7
CRISPR/Cas9	Clustered Regularly Interspaced Short Palindromic Repeats and associated protein 9
CRISPRa	CRISPR activator
CRISPRi	CRISPR interference
CYP2E1	Cytochrome P450 2E1
DAMP	Damage-associated molecular pattern
dCas9	Dead Cas9
DDC	3,5-diethoxycarbonyl-1,4-dihydrocollidine
ddPCR	Digital droplet PCR
DSB	Double-strand break
ECM	Extracellular matrix
eVLPs	Engineered VLP
FiCAT	Find and cut-and-transfer

Fw	Forward
FXR	Farnesoid X receptor
GalNAc	N-acetylgalactosamine
gDNA	Genomic DNA
GS	Glutamine synthetase
GSD III	Glycogen storage disease type III
hAAT	Human alpha1-antitrypsin
HA-L	Homology arm left
HA-R	Homology arm right
HBSS	Hank's balanced salt solution
HBV	Hepatitis B virus
HCC	Hepatocellular carcinoma
HCV	Hepatitis C virus
HDR	Homology-directed repair
HEK	Human embryonic kidney
Hepa	Hepatocytes
HEPES	(4-(2-hydroxyethyl)-1-piperazineethanesulfonic acid
HFHFC	High-fat, high-fructose, and high-cholesterol
hFIX	Human FIX
HITI	Homology-independent targeted integration strategy
HIV	Human immunodeficiency virus
HSC	Hepatic stellate cell
IDLV	Integrase-deficient lentiviral vector

IL-1	Interleukin-1
IL-10	Interleukin-10
IL-13	Interleukin-13
IL-6	Interleukin-6
IMDM	Iscove’s modified Dulbecco’s medium
iMSUD	Intermediate MSUD
Indels	Insertions or deletions
ITR	Inverted terminal repeat
IU	International units
KC	Kupffer cells
KIC	α-ketoisocaproic acid
KIV	α-ketoisovaleric acid
KMV	α-keto-β-methylvaleric acid
LDL	Low-density lipoprotein
LDLR	Low-density lipoprotein receptor
LNP	Lipid nanoparticle
LSEC	Liver sinusoidal endothelial cell
LTR	Long terminal repeat
LV	Lentiviral vector
MASH	Metabolic dysfunction-associated steatohepatitis
MASLD	Metabolic dysfunction–associated steatotic liver disease
MLV	Murine leukemia virus
MMEJ	Micro homology-mediated end joining

MMLV	Moloney murine leukemia virus
MMP	Matrix metalloproteinase
MOI	Multiplicity of infection
mRNA	Messenger RNA
MSUD	Maple syrup urine disease
nCas9	Nickase Cas9
NEB	New England Biolabs
NHEJ	Non-homologous end joining
NHP	Non-human primate
nPC	Non-parenchymal cells
PAM	Protospacer adjacent motif
PASSIGE	Prime-editing-assisted site-specific integrase gene editing
PASTE	Programmable addition via site-specific targeting elements
PBC	Primary biliary cholangitis
PBS	Phosphate saline buffer
PC	Pericentral zone
pDC	Plasmacytoid dendritic cells
PDGF	Platelet-derived growth factor
PE	Prime editor
PEDAR	PE-Cas9-based deletion and repair
PEG	Polyethylene glycol
pegRNA	Prime editing gRNA
PFIC2	Progressive familial intrahepatic cholestasis type 2

PITCh	Precise integration into target chromosome
PP	Periportal zone
Prb	Probes
PSC	Primary sclerosing cholangitis
RNP	Ribonucleoprotein
RT	Reverse transcriptase
Rv	Reverse
SA	Splice acceptor
SaCas9	*Staphylococcus aureus* Cas9
SAE	Severe adverse event
SEM	Standard error of the mean
sgRNA	Single-guide RNA
sgRNA CS	sgRNA cut site
SIN	Self-inactivating
siRNA	Short-interfering RNA
SpCas9	*Streptococcus pyogenes* Cas9
ssDNA	Single-stranded DNA
TAA	Thioacetamide
TALEN	Transcription activator-like effector nucleases
TGF-β	Transforming growth factor-beta
TIMP	Tissue inhibitors of metalloproteinase
TJ	Template jumping
TNF-α	Tumor necrosis factor-alpha

TU	Transducing units
TwinPE	Twin prime editing
UGI	Uracil glycosylase inhibitor
VCN	Vector genome copy number
vg	Vector genomes
VLP	Virus-like particles
VPR	VP64-p65-Rta
VSV.G	Vesicular stomatitis virus glycoprotein G
WT	Wild type
ZFN	Zinc finger nuclease

List of figures and tables

Figure I……15

Figure II……...…19

Table I……..20

Figure III……..……31

Figure IV……...…39

Table II……..…42

Figure V……..….48

Figure VI……...…52

Table 1……..64

Figure 1...……65

Figure 2...……67

Figure 3...……70

Figure 4...……72

Figure 5...……74

Figure 6...……77

Figure 7...……79

Figure 8...……81

Table 2……..83

Figure 9...……85

Table 3……..86

Figure 10...……..88

Figure 11...……..90

Figure 12...……..……..92

Figure 13...……..……..94

Figure 14...……..……..95

Table 4……..96

Figure 15...……..……..97

Figure 16...……..……..99

1. Introduction

1.1 Liver-directed gene therapy

The idea behind gene therapy is to modify the genomic material inside the cells to treat acquired or genetic diseases. This could be obtained by exploiting several strategies, for example by adding a gene that is the corrected version of the one mutated (gene replacement), or that confers new functions to the cell (gene addition). Moreover, in recent years, the evolution of gene editing allowed site-specific modification of a gene that can be disrupted, corrected, silenced, or activated. Gene therapy can be performed *ex vivo* by harvesting target cells from the body, modifying and reinfusing them back to the individual. This strategy has been very effective, e.g. in the context of diseases where the modification of cells of the hematopoietic compartment, which are relatively easy to harvest, could be therapeutic. Indeed, it led to the approval of several drugs (Ginn *et al*, 2024). However, this strategy is not feasible for the majority of target organs, so *in vivo* gene therapy has been developed. In this case, target cells are directly modified inside the body by systemic or *in situ* delivery of gene therapy agents. Systemic administration is the most exploited approach used to target the liver.

1.1.1 The liver

The liver is a major metabolic organ that performs many essential biological functions. It is mainly composed of parenchymal cells, the hepatocytes (70%). The remaining 30% is made of non-parenchymal cells (nPCs). The most abundant nPCs are liver sinusoidal endothelial cells (LSECs) (15%) that shape the sinusoids, the liver microvasculature. Sinusoids carry blood between hepatocytes and are characterized by the presence of fenestrations that allow contact between liver cells and the blood. In the perisinusoidal space, there are Kupffer cells (KC) (5%), which are resident macrophages, and hepatic stellate cells (HSC) (5%), which store vitamin A and are involved in the fibrosis process. The remaining 5% are cholangiocytes, which form the bile ducts, and other cells like fibroblasts and immune cells, including plasmacytoid dendritic cells (pDC) (Racanelli & Rehermann, 2006). The blood arrives at the liver from the aorta through the hepatic artery (25%), and from the spleen and the gastrointestinal tract through the portal vein (75%).

The blood flow merges in the sinusoids and empties into the central vein. The bile is produced by hepatocytes and is secreted in the bile canaliculi, initially made by the plasma membranes of neighboring hepatocytes. Bile canaliculi converge into progressively larger bile ducts that bring the bile into the gallbladder. The branches of the hepatic artery and portal vein delimitate the lobules which are the functional units of the liver (Fig. I). The lobule has a hexagonal shape with the central vein in the center and six portal triads in the corners that create the hexagon. The portal triad comprises a hepatic artery, a portal vein, and a bile duct which are close in space. Therefore, the blood flow goes from the portal triads to the central vein, while bile goes in the opposite direction. Thus, hepatocytes along the lobule are exposed to diverse stimuli, so they are conventionally divided into three zones. Zone 1 is near the portal triad and is called periportal. Hepatocytes in this zone are in an environment rich in oxygen and nutrients, and they perform, among other functions, gluconeogenesis, lipid metabolism, urea, and protein synthesis. Zone 2 is in the middle and hepatocytes located there are considered the most active in homeostasis repopulation and regeneration (He *et al*, 2021). Finally, Zone 3 hepatocytes are near the central vein, in the so-called pericentral zone with a low-oxygen environment, thus performing mainly glycolysis, xenobiotic metabolism, and glutamine synthesis. Recently, technological advancements in single-cell analyses allowed for a better partition of the hepatic lobule, which can be divided into 9 layers with differential gene expressions (Halpern *et al*, 2017).

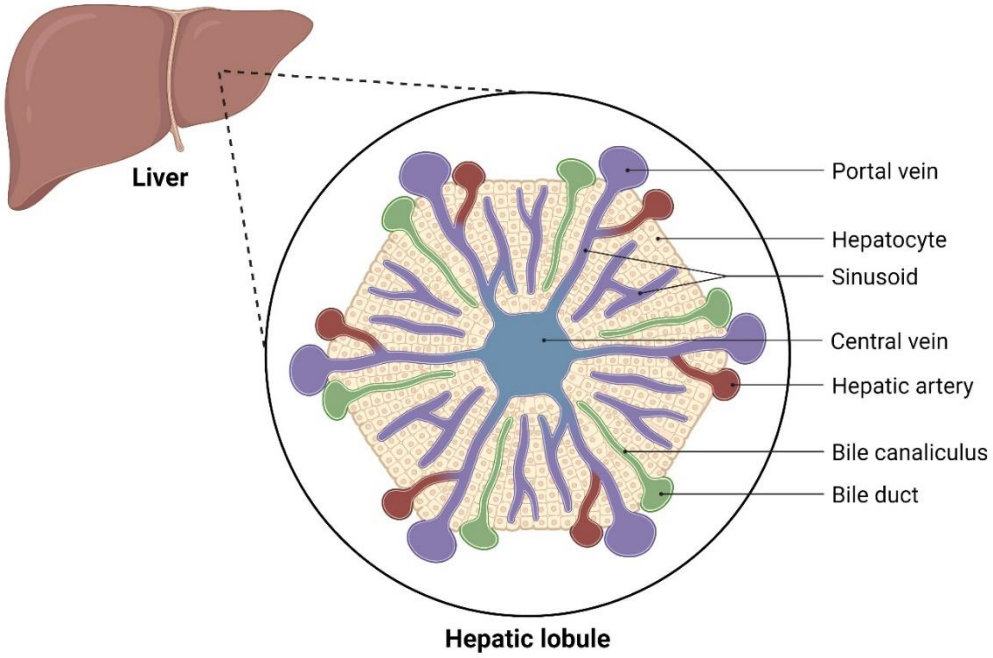


Figure I. Liver structure. Schematic representation of the hepatic lobule, the repeated functional unit that composes the liver. Created with BioRender.com.

The liver performs around 500 essential biological functions, among them carbohydrate, fat, protein metabolism, and the production and secretion of bile and coagulation factors. For this reason, impairment of liver functionality is the cause of many genetic diseases (Elijah Trefts *et al*, 2017). For some of these disorders, available treatment that allows the restoration of the missing function relies on enzyme replacement therapy or orthotopic liver transplantation. Enzyme replacement therapy requires life-long repeated administrations of the therapeutic protein. It can be performed only when the infused enzyme works in the blood, such as in plasma protein deficiencies, or can be uptaken by the target cells allowing cross-correction, such as in the case of lysosomal storage disorders (Bonam *et al*, 2019). On the other hand, liver transplantation is an invasive treatment that presents risks of organ rejection and graft failure and requires a life-long immunosuppressive regimen (Khalil *et al*, 2023). For these reasons, in the past few decades, liver-directed gene therapy has been investigated as a promising alternative therapeutic strategy.

1.1.2 The liver as a target organ for gene therapy

To date, the most advanced approach is based on gene replacement or addition exploiting adeno-associated viral vectors (AAVs) injected systemically (Baruteau *et al*, 2024). AAVs targeting the liver to replace coagulation factors have been shown to provide multi-year benefits in hemophilic patients, leading to the approval of three gene therapy products, Etranacogene Dezaparvovec and Fidanacogene Elaparvovec for the treatment of hemophilia B (Heo, 2023; U.S. FDA Approves Pfizer's BEQVEZTM (fidanacogene elaparvovec-dzkt), a One-Time Gene Therapy for Adults with Hemophilia B, 2024), and Valoctocogene Roxaparvovec for the treatment of hemophilia A (Blair, 2022; Ozelo *et al*, 2022). Moreover, AAV-based therapeutic approaches are currently being tested in pre-clinical and clinical studies for the treatment of other diseases linked to the liver. Examples of disorders treated in active clinical trials are ornithine transcarbamylase deficiency, Wilson disease, glycogen storage disease type Ia, phenylketonuria, Crigler–Najjar syndrome, and mucopolysaccharidosis type VI (Baruteau *et al*, 2024; Zabaleta *et al*, 2023). Results of mucopolysaccharidosis type VI

phase I/II clinical trial have been published (Brunetti-Pierri *et al*, 2022). Nine patients have been treated with three escalating doses of AAV8 expressing *ARSB*, the mutated gene causing the disorder. No adverse events were detected, however, only patients treated with the highest dose showed maintenance of phenotype correction up to 2 years post-gene therapy, with no reintroduction of enzyme replacement therapy needed. Also, results of the Crigler–Najjar syndrome phase I/II clinical trial have been published (D'Antiga *et al*, 2023). Five patients received two escalating doses of AAV8 encoding *UGT1A1*, the mutated gene causing the disorder. Even in this trial, no adverse events were reported, and only patients treated at the highest dose showed effective reduction of the toxic substrate up to 1.5 years after gene therapy. Despite these achievements, some limitations remain to the usage of AAVs (Wang *et al*, 2019a). One major limitation is represented by their non-integrative nature, AAV genome remains mainly episomal, thus leading to a progressive loss of transgene expression following cell replication (Cunningham *et al*, 2008; Wang *et al*, 2012). This would represent a challenge for the treatment of pediatric patients in which the liver is actively growing, especially in the context of severe inherited metabolic disorders, where an early intervention would be essential to prevent disease progression and related complications (Yilmaz *et al*, 2020). To overcome this limitation, a possibility is to exploit integrative vectors such as lentiviral vectors (LVs), which have been shown to provide long-lasting transgene expression from the liver in hemophilia mouse models, dogs, and non-human primates (NHPs) (Milani *et al*, 2022, 2019b; Cantore *et al*, 2015). Other strategies aiming at guaranteeing a stable transgene expression throughout post-natal liver growth and homeostatic turnover rely on the usage of transposon-based integration of a therapeutic cassette (Kebriaei *et al*, 2017). For both LV and transposon-based platforms, however, the semi-random integration profile and the usage of heterologous promoters cause concerns about genotoxicity. Moreover, employing constitutive promoters may not be ideal for applications in which a regulated transgene expression is preferred, such as when the overexpression of a protein could be detrimental to the cell, or when the gene expression is tightly regulated in response to specific stimuli. In this context, genome editing approaches are being increasingly explored to provide precise genomic interventions such as gene disruption, insertion of a therapeutic gene in a desired locus, correction of a specific disease-causing mutation, gene silencing, or gene activation (Adlat *et al*, 2023). The first reported genome

editing tools were meganucleases, microbial-derived homing endonucleases adapted for targeted DNA modification (Stoddard, 2011). Next, synthetic fusion proteins called zinc finger nucleases (ZFNs) have been established by combining multiple zinc finger DNA binding domains with the catalytic domain of FokI, a restriction enzyme that cleaves the double-strand DNA (Urnov *et al*, 2010). Finally, the same FokI domain has also been exploited in combination with transcription activator-like effector proteins to generate transcription activator-like effector nucleases (TALENs) (Christian *et al*, 2010). However, redirecting the DNA targeting specificity of these genome editing tools based on protein-DNA interactions requires laborious steps of protein engineering, thus these reagents never gained widespread usage in the field. By contrast, most genome editing approaches nowadays rely on the usage of Clustered Regularly Interspaced Short Palindromic Repeats and associated protein 9 (CRISPR/Cas9), which has become over the years the system of choice, thanks to the fact that targeting specificity is based on RNA-DNA complementarity (Wang & Doudna, 2023). A ribonucleoprotein (RNP) composed of a simple and short single-guide RNA (sgRNA) and the Cas9 nuclease can indeed target a wide range of DNA sequences (Wang & Doudna, 2023). CRISPR/Cas9 is a family of proteins divided into two classes, each further divided into three types and several subtypes (Makarova *et al*, 2020). The most exploited is class 2 since the proteins involved are smaller than those in class 1. CRISPR/Cas class 2 system can be divided into type II/Cas9, type V/Cas12, and type VI/Cas13. The target of Cas9 and Cas12 is double-strand DNA while Cas13 targets RNA. Cas9 and Cas12 differ in their mechanism of action and dimensions since Cas12 is smaller and requires a shorter sgRNA compared to Cas9 (van der Oost & Patinios, 2023). The description of this mechanism by the work of Doudna and Charpentier was revolutionary for modern biotechnology and was indeed recognized with the Nobel Prize for chemistry in 2020 (Jinek *et al*, 2012). All meganucleases, TALENs, ZFNs, and Cas nucleases can thus be programmed to perform site-specific DNA double-strand breaks (DSBs). The DSBs can be repaired by exploiting different endogenous repair pathways such as the non-homologous end joining (NHEJ), the micro homology-mediated end joining (MMEJ), or the homology-directed repair (HDR) (Chen *et al*, 2024a). It is possible to take advantage of all these cellular DNA repair mechanisms depending on the intended genomic modification. Since the presence of DBS can potentially give rise to genotoxicity concerns (Tao *et al*, 2023), the nucleases

have also been engineered to perform a single strand cut (*i.e.* nickase Cas9, nCas9), or to be catalytically inactive (*i.e.* dead Cas9, dCas9). These modified Cas9 have been fused to deaminases, retro-transcriptases, transcriptional activators, or silencing proteins to obtain, theoretically, safer genomic or epigenomic modifications (Tao *et al*, 2023). All the rapid advances in this field have led to the approval of the first CRISPR/Cas9-based gene editing product, Casgevy, in December 2023 (FDA NEWS RELEASE FDA Approves First Gene Therapies to Treat Patients with Sickle Cell Disease, 2023; Sheridan, 2024). The drug is based on the *ex vivo* modification of patients' hematopoietic stem cells to disrupt the expression of *BCL11A*, a repressor of the fetal γ-globin gene, for the treatment of sickle cell disease and transfusion-dependent β-thalassemia. As a result of the *BCL11A* inactivation, the reactivation of fetal hemoglobin allows for restoring erythropoietic homeostasis (Frangoul *et al*, 2021). Treatments for various other diseases are currently under investigation exploiting the *ex vivo* modification of hematopoietic stem cells. However, genome editing is more difficult to apply in the context of diseases linked to solid organs like the liver (Baruteau *et al*, 2024), which require an *in-situ* delivery of the editing machinery. Nevertheless, in recent years great improvements have been performed, opening the possibility for liver-directed genome editing to become a treatment for inherited and acquired diseases (Fig. II).

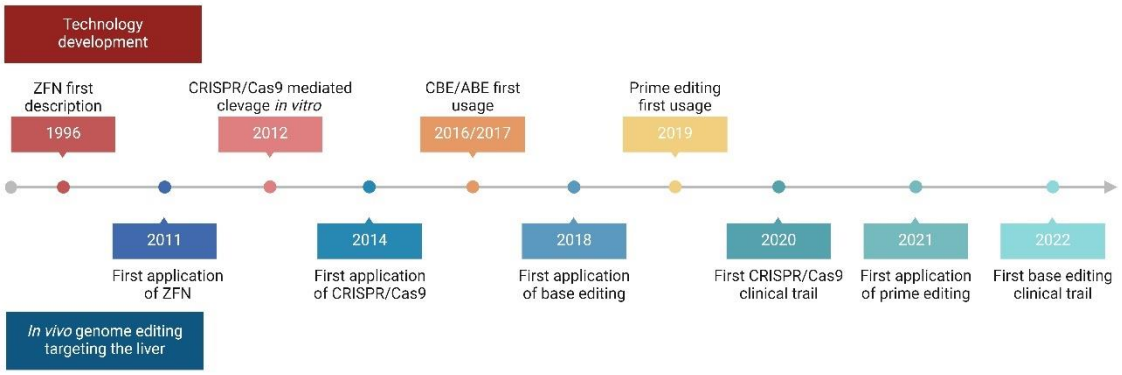


Figure II. Timeline of in vivo liver-directed genome editing. Timeline chart highlighting crucial events regarding technological advancement and applications of *in vivo* liver-directed genome editing. Created with BioRender.com.

1.2 Gene editing strategies

The technological advances in genome editing opened the way to many different approaches that can be exploited to treat liver genetic diseases. Simple gene disruption

has been achieved by exploiting the NHEJ pathway, giving rise to insertions or deletions (indels) able to abrogate gene expression (Stinson & Loparo, 2021). On the other end, the different pathways of DSB repair (NHEJ, MMEJ, and HDR) have been exploited to obtain the insertion of the transgene of interest, carried by a donor DNA, in the desired locus (Chen *et al*, 2024a). More recently, base editing and prime editing have been developed to target specific disease-causing mutations with the advantage of greatly reducing the generation of DSB events (Anzalone *et al*, 2020). Lastly, some strategies have been developed that completely avoid breaks of DNA, based on the modification of the epigenome to transcriptionally silence or activate a specific gene (Villiger *et al*, 2024). In the following subsections, we reviewed representative works on the above-mentioned approaches, which are also listed in Table I.

Table I – Non-exhaustive representative list of studies employing genome editing therapeutic approaches targeting the liver

Strategy	Target	Disease indication	Delivery method	References
NHEJ-mediated gene disruption	*TTR*	Transthyretin Amyloidosis	CRISPR/Cas9 delivered by LNPs	(Finn *et al*, 2018; Gillmore *et al*, 2021)
	KLKB1	Hereditary Angioedema		(Longhurst *et al*, 2024)
HITI-mediated gene insertion	*ALB*	Mucopolysaccharidosis type VI	CRISPR/Cas9 and donor DNA delivered by AAVs	(Tornabene *et al*, 2022; Esposito *et al*, 2024)
		Hemophilia A, B		(Chen *et al*, 2019; He *et al*, 2022; Esposito *et al*, 2024)
	SERPINC1	Hemophilia A, B	CRISPR/Cas9 and donor DNA delivered by LNPs + AAVs	(Lee *et al*, 2023; Han *et al*, 2023)
MMEJ-mediated gene disruption	*HAO1*	Primary Hyperoxaluria type 1	CRISPR-Cas9 nickase delivered by AAVs	(Torella *et al*, 2024)
MMEJ-mediated gene insertion	*FAH*	Hereditary tyrosinemia type 1	CRISPR-Cas9 plasmids by hydrodynamic injection	(Yao *et al*, 2017)
HDR-mediated gene insertion (without nucleases)	*ALB*	Hemophilia B, Crigler-Najjar, methylmalonic acidemia, Wilson disease	Promoterless donor DNA delivered by AAVs	(Barzel *et al*, 2015; Porro *et al*, 2017; Chandler *et al*, 2021; Venturoni *et al*, 2022; Padula *et al*, 2023)
HDR-mediated gene insertion (with nucleases)	*F9*	Hemophilia B, Crigler Najjar	CRISPR/Cas9 and donor DNA delivered by AAVs + LNPs, or dual AAVs	(Wang *et al*, 2019b; Lisjak *et al*, 2022)
	ALB			(De Caneva *et al*, 2019)
	PAH	Phenylketonuria		(Richards *et al*, 2020)

	SPF	Ornithine transcarbamylase deficiency		(Wang *et al*, 2020)
	ASS1	Citrullinemia type I		(Lisjak *et al*, 2023)
	F9	Hemophilia B	ZFN and donor DNA delivered by AAVs	(Sharma *et al*, 2015; Li *et al*, 2011)
	IDUA	Mucopolysaccharidosis type I		(Ou *et al*, 2019)
	GLA	Fabry disease		(Pagant *et al*, 2021)
Base editing-mediated gene correction	*PAH*	Phenylketonuria	ABE reagents delivered by LNPs	(Brooks *et al*, 2023, 2024)
	IDUA	Mucopolysaccharidosis type I	ABE delivered by dual AAVs	(Su *et al*, 2023)
	HFE	Hemochromatosis		(Rovai *et al*, 2022)
	AGXT	Primary Hyperoxaluria type 1		(Chen *et al*, 2024b)
	PAH	Phenylketonuria		(Villiger *et al*, 2018)
	SERPINA1	Alpha-1 antitrypsin deficiency	ABE or CBE reagents delivered by LNPs	(Packer *et al*, 2022)
Base editing-mediated gene disruption	*PCSK9*	Familiar hypercholesterolemia	ABE reagents delivered by LNP	(Rothgangl *et al*, 2021; Musunuru *et al*, 2021)
Prime editing-mediated gene correction	*SERPINA1*	Alpha-1 antitrypsin deficiency	PE delivered by dual AAVs	(Liu *et al*, 2021)
	PAH	Phenylketonuria	PE delivered by AdV	(Böck *et al*, 2022)
	FAH	Hereditary tyrosinemia type 1	PE-plasmids delivered by hydrodynamic injection	(Jang *et al*, 2021)
	PCSK9	Coronary diseases	PE delivered by dual AAVs	(Zheng *et al*, 2022; Davis *et al*, 2024)
Prime editing-based deletion and replacement of long DNA sequences	*FAH*	Hereditary tyrosinemia type 1	PE-plasmids delivered by hydrodynamic injection	(Jiang *et al*, 2022; Zheng *et al*, 2023a)
	ACTB	/	PE delivered by AdV	(Yarnall *et al*, 2023)
Epigenome editing-mediated gene activation	*EPO*	Chronic renal anemia	Epigenome editors delivered by LNPs	(Beyersdorf *et al*, 2022)
Epigenome editing-mediated gene repression	*PCSK9*	Coronary diseases	Epigenome editors delivered by dual AAVs	(Thakore *et al*, 2018; Gemberling *et al*, 2021)
			Epigenome editors delivered by LNPs	(Cappelluti *et al*, 2024)

1.2.1 NHEJ-based gene editing approaches

NHEJ is the DSB repair pathway most exploited by the cells and is active in all phases of the cell cycle (Pannunzio *et al*, 2018). During the repair process, DNA-free ends are processed to obtain blunt ends that are directly ligated. This system is therefore prone to

the introduction of indel mutations since there are no mechanisms of DNA proofreading (Stinson & Loparo, 2021) (Fig. IIIA). For this reason, NHEJ is typically exploited to target monogenic disorders caused by a gain-of-function or dominant negative mutations, by inactivating the target gene (Schambach *et al*, 2024). One of the most advanced approaches is the one developed for the treatment of Transthyretin Amyloidosis, an autosomal dominant condition resulting from mutations in the *TTR* gene, leading to transthyretin accumulation in tissues. The strategy developed exploits CRISPR/Cas9 and the NHEJ pathway to disrupt the *TTR* gene in hepatocytes (Finn *et al*, 2018; Gillmore *et al*, 2021). A similar strategy has been developed for the treatment of Hereditary Angioedema, a dominant genetic disorder due to C1-inhibitor overexpression. In this case, a CRISPR/Cas9-based strategy aims at disrupting the *KLKB1* gene, which is involved in the overproduction of the C1-inhibitor (Longhurst *et al*, 2024). Both strategies were shown to be effective and are now being tested in clinical trials (see "Liver-directed genome editing clinical trials" section below). The NHEJ pathway has also been exploited to achieve targeted integration of a therapeutic transgene. In 2016 Suzuki et al. first described the homology-independent targeted integration strategy (HITI) (Suzuki *et al*, 2016), based on the usage of a donor DNA flanked by the sgRNA target sequences in reverse orientation. In this way, Cas9 can cut both the genomic target locus and the donor DNA to improve the genomic integration rate. Moreover, if the genomic insertion occurs in the wrong orientation, an intact sgRNA target sequence may be recreated and re-cut, thus favoring donor integration in the proper orientation (Suzuki *et al*, 2016) (Fig. IIIA). This strategy has been investigated in a preclinical study for the treatment of the lysosomal storage disease Mucopolysaccharidosis type VI. It resulted in therapeutic efficiency and stable integration in the liver of mice treated as newborns (Tornabene *et al*, 2022). The HITI strategy has been applied also in the context of hemophilia A and B, caused by mutations in coagulation factor 8 or 9 (*F8* or *F9*) genes respectively. In recent studies, the corrective donor DNA was inserted in the albumin locus, to exploit the strength of the albumin promoter and achieve high expression of the coagulation factor transgene and its secretion into the bloodstream (He *et al*, 2022). The power of HITI-mediated gene insertion for disease treatment has been confirmed recently in another preclinical study for Mucopolysaccharidosis type VI and hemophilia A (Esposito *et al*, 2024). The targeted integration of a transgene in the albumin locus is particularly

beneficial in the context of non-autonomous cell disorders or disorders in which the organism can be detoxified by cross-correction mechanisms. In this way, even a relatively low targeting efficiency paralleled by a low percentage of corrected hepatocytes may guarantee therapeutic levels of transgene expression thanks to the strong activity of the albumin promoter. Another strategy tested in the context of hemophilia consisted of the integration of the corrective complementary DNA (cDNA) into the *Serpinc1* locus. The integration was based on a bidirectional construct containing the *F8* or *F9* cDNA. In this way, the transgene can always be expressed, despite the orientation of the insertion (Lee *et al*, 2023; Han *et al*, 2023) (Fig. IIIA). An additional potential application of NHEJ-mediated gene disruption is the treatment of hepatitis B virus (HBV) infection, which can lead to liver cirrhosis and cancer (Yuen *et al*, 2018). Recently, some strategies have been developed to disrupt essential genes of the virus (Kasianchuk *et al*, 2023), showing a reduction of viral proteins in both serum and liver of HBV-infected mice (Yan *et al*, 2021). However, this approach still requires optimization to further reduce viral load and HBV DNA in CRISPR-treated mice (Stone *et al*, 2021).

1.2.2 MMEJ-based gene editing approaches

MMEJ is an alternative pathway for the repair of DSB, which exploits 5-25 base pairs (bp)-long micro homologous sequences present in the two broken DNA strands. This pathway results in deletions or insertions that are longer compared to those usually introduced by NHEJ. Moreover, MMEJ is more active during the S/G2 phase of the cell cycle and seems to compete with NHEJ in the G1 phase (Sallmyr & Tomkinson, 2018). Given the fact that the MMEJ pathway has mutagenic properties, it has been exploited for therapeutic gene disruption purposes (Fig. IIIB). A recent application has been described for the treatment of primary hyperoxaluria type 1, an autosomal recessive metabolic disease caused by mutations in the *AGXT* gene and leading to oxalate accumulation in the liver and kidney, leading to renal dysfunction and ultimately kidney failure. Two paired nCas9 were employed to introduce nicks on the two opposite strands of the *HAO1* gene, at a distance of 28 nucleotides. The nicks were repaired mainly by MMEJ and led to the introduction of indels that abolished the gene function, resulting in therapeutic efficacy in a disease mouse model (Torella *et al*, 2024). MMEJ can be also exploited for targeted genomic integration. In a strategy called PITCh (precise integration

into target chromosome), micro-homology arms flank the donor DNA allowing for the genomic integration mediated by the MMEJ pathway. As for the HITI strategy, sgRNA target sequences can be added at the side of the donor DNA to increase the rate of insertion (Nakade *et al*, 2014) (Fig. IIIB). PITCh strategy has been tested by injection of the MMEJ components into the liver of mice with the inherited metabolic disease hereditary tyrosinemia type I, to insert a *Fah* therapeutic cDNA into the endogenous genomic locus. The strategy resulted in reduced liver damage and a better survival rate of the treated animals, indicating the rescue of *Fah* expression from those hepatocytes in which a functional integration occurred (Yao *et al*, 2017).

1.2.3 HDR-based targeted integration approaches

HDR is the most precise mechanism that cells exploit to repair DSB in the genome. It relies on the presence of the sister chromatid, so it is active during the S/G2 phase of the cell cycle. It involves the recognition, protection, and processing of the DNA ends, that are paired with the homologous regions. Subsequentially, DNA polymerase can synthesize the complementary sequence that is missing. The two complementary regions are then annealed, processed, and ligated to restore the intact genome (Douglass Wright *et al*, 2018). This precise repair pathway is the most commonly exploited in the genome editing field to allow for insertion of the sequences of interest in a site-specific manner. It has been demonstrated that the HDR pathway can be exploited even without nucleases to perform gene targeting. Several studies highlighted the potential of inserting a promoterless therapeutic cDNA into the albumin locus as a safe harbor to exploit the high activity of the albumin promoter for transgene expression (Barzel *et al*, 2015; Porro *et al*, 2017). In particular, in the approach named GeneRide, the cDNA of interest is inserted in-frame into the 3' end of the albumin gene along with an upstream 2A-peptide coding sequence, to allow for the translation of both the albumin-2A peptide and the therapeutic protein (Fig. IIIC). This approach has been tested in pre-clinical proof of concept studies for the treatment of hemophilia B and Crigler-Najjar syndrome, resulting in therapeutic efficacy even at low targeting efficiencies, since in these disorders even a relatively low enzyme activity results in clinical benefit (Barzel *et al*, 2015; Porro *et al*, 2017). The nuclease-free strategy has been investigated also in the context of Wilson disease, an autosomal disorder of copper accumulation caused by mutations in the *ATP7B* gene,

encoding a transporter involved in copper excretion into the bile. A promoterless mini-*ATP7B* transgene inserted in the albumin locus resulted in extensive liver repopulation by edited hepatocytes and amelioration of liver injury and copper metabolism (Padula *et al*, 2023). The same strategy has been also tested in the context of methylmalonic acidemia, a severe organic acidemia caused by a mitochondrial enzymatic defect. In this case, the initial low targeting efficiency was compensated over time by a progressive expansion of the corrected cells harboring a selective advantage over non-corrected ones, with a concomitant amelioration of the disease-related biomarkers (Chandler *et al*, 2021; Venturoni *et al*, 2022). These results supported the initiation of a phase I/II clinical trial in pediatric patients with severe methylmalonic acidemia sponsored by LogicBio Therapeutics, which however is now terminated due to lack of efficacy and the occurrence of severe adverse events (SAEs) in some patients (Gene Therapy With hLB-001 in Pediatric Patients With Severe Methylmalonic Acidemia (SUNRISE), 2024; Marie Payton *et al*, 2024). Efforts have been made to increase the targeting efficiency. It has been demonstrated that fludarabine, a ribonucleotide reductase inhibitor, could increase *in vivo* nuclease-free HDR efficiency by around 3 to 4-fold in the murine liver (Tsuji *et al*, 2022). Nevertheless, the nuclease-free strategy is difficult to apply to most diseases where there is no proliferative advantage of the corrected hepatocytes or in which an initial high targeting efficiency is required to prevent disease-related complications. For this reason, HDR-based donor DNA is usually coupled with a nuclease such as Cas9, to generate a DSB in the locus of interest favoring the HDR-mediated integration rate (Fig. IIIC) (Rouet *et al*, 1994). This strategy has been applied in the context of hemophilia B, to insert a corrective *F9* cDNA into the second exon of the *F9* gene using ZFN or CRISPR/Cas9 (Wang *et al*, 2019b; Sharma *et al*, 2015; Li *et al*, 2011) or at the 3' end of the albumin safe harbor (Lisjak *et al*, 2022). In the first approach, ZFNs were used to target adult mice hepatocytes with an *F9* cDNA bearing a splice site acceptor upstream of the coding region. On the other hand, Wang et al. delivered the CRISPR/Cas9 machinery in both newborn and adult hemophilia B mice, showing around 10% and 4% of hepatocytes targeted by HDR respectively, thus resulting in stable FIX expression even after partial hepatectomy (Wang *et al*, 2019b). In the second approach, Lisjak et al. also exploited the CRISPR/Cas9 components and the donor DNA, confirming a higher HDR efficiency in the liver of newborn mice (around 4%) compared to adults (less than 1%).

This resulted in therapeutic efficacy only in mice treated as newborns (Lisjak *et al*, 2022), highlighting the challenge of performing efficient HDR-targeting in the post-mitotic adult liver in which NHEJ is preferentially exploited as repair mechanism. The potential of HDR-based targeting coupled with a nuclease was demonstrated also in other preclinical studies aiming at integrating the donor DNA into the endogenous genomic locus or in a safe harbor, in the context of inherited metabolic diseases, such as phenylketonuria (Richards *et al*, 2020), ornithine transcarbamylase deficiency (Wang *et al*, 2020), citrullinemia type I (Lisjak *et al*, 2023), and Crigler-Najjar syndrome (De Caneva *et al*, 2019). These studies confirmed a generally higher efficiency of integration when using the nuclease compared to the GeneRide approach. Not only Cas9 but also ZFNs were employed coupled with the donor DNA for site-specific insertion of a corrective transgene into the hepatocyte albumin locus, resulting in some therapeutic efficacy in mouse models of the lysosomal storage diseases mucopolysaccharidosis type I, Gaucher, Hurler, and Fabry disease (Ou *et al*, 2019; Pagant *et al*, 2021; Sharma *et al*, 2015).

1.2.4 Liver-targeted base editing approaches

Base editing is an innovative technology that has been developed by the group of David Liu to perform precise nucleotide modification without the need for potentially harmful DSB (Komor *et al*, 2016; Gaudelli *et al*, 2017). Base editors (BEs) are composed of nCas9 fused to a deaminase enzyme, which catalyzes the deamination of a nucleobase. The strategy relies on the positioning of the deaminase on the target locus by the sgRNA and Cas9. Once Cas9 binds the genome the double-stranded DNA is open so that the deaminase can act precisely on a short stretch of single-stranded DNA (ssDNA), named the editing window. Modified nucleobases create a mismatch in the genome that is then solved by cellular DNA repair mechanisms. Concomitantly, the nCas9 cuts the non-modified strand favoring the usage of the other strand as a template for DNA repair, thus maintaining the edited nucleotide (Porto *et al*, 2020). The two most exploited and advanced editors are the cytidine base editor (CBE) and adenine base editor (ABE). CBE is designed to convert cytidine into uridine. This modification is read by the replication and transcription machinery as a thymidine, obtaining a C-G to T-A conversion. CBE has been derived from a natural cytidine deaminase coupled with Cas9 and with the uracil glycosylase inhibitor (UGI). UGI has been added to avoid the removal of the uracil, which

occurs frequently since the base excision repair pathway is very active in cells (Komor *et al*, 2016). On the other hand, ABE was laboratory-evolved to act on DNA starting from RNA-targeting adenosine deaminases, then fused to nCas9. They can deaminate adenosine resulting in inosine, which is read by replication and transcription machinery as a guanine, resulting in an A-T to G-C base pair conversion (Gaudelli *et al*, 2017). BEs can be exploited to obtain different outputs. They can directly correct a disease-causing point mutation, or they can disrupt the expression of a gene. The disruption can be achieved by generating a premature stop codon or by creating an alternative splice site that will disrupt the original reading frame (Fig. IIID). The correction of a pathogenic mutation has been performed in the context of phenylketonuria, an autosomal recessive disorder caused by mutations in the *PAH* gene, leading to the accumulation of phenylalanine in the blood. A mouse model harboring one of the most common *PAH* pathogenic variants has been treated with an ABE, resulting in the normalization of circulating phenylalanine (Brooks *et al*, 2023, 2024). ABE-mediated correction of pathogenic mutations was also assessed in preclinical studies for the treatment of mucopolysaccharidosis type I (Su *et al*, 2023), hemochromatosis (Rovai *et al*, 2022), and primary hyperoxaluria type 1 (Chen *et al*, 2024b). Furthermore, CBE was exploited for the treatment of phenylketonuria, restoring the physiological blood phenylalanine and ameliorating the disease phenotype (Villiger *et al*, 2018). Another work investigated two strategies for the treatment of alpha-1 antitrypsin deficiency. The first was based on the use of CBE to introduce a mutation with a compensatory functional effect, the second was based on the use of ABE to correct a disease-causing point mutation. Both strategies resulted in a therapeutically relevant increase in serum alpha-1 antitrypsin and improved liver histopathology (Packer *et al*, 2022). Besides genetic disorders, liver base editing has been investigated also for the treatment of hepatocellular carcinoma (HCC). In particular, Zhao et al. employed ABEs to correct a *TERT* promoter mutation, which frequently occurs in HCC and other human cancers. The correction of the mutation with an ABE resulted in significant inhibition of the growth of liver tumors in a mouse model (Zhao *et al*, 2024). BEs for gene disruption purposes have been extensively investigated also for the treatment of familial hypercholesterolemia, an autosomal dominant disease characterized by high circulating low-density lipoprotein (LDL) cholesterol (Canepari & Cantore, 2023). In 2021 two reports were published describing the usage of ABE for the

disruption of a splice site, resulting in the knock-out of *PCSK9* in macaques. Since *PCSK9* is a negative modulator of the LDL receptor (LDLR), its inhibition resulted in LDLR upregulation in the liver, in turn leading to a therapeutic reduction of blood LDL cholesterol (Rothgangl *et al*, 2021; Musunuru *et al*, 2021). In 2023, these findings rapidly led to the initiation of a clinical trial in patients affected by familial hypercholesterolemia (see "Liver-directed genome editing clinical trials" section below).

1.2.5 Liver-targeted prime editing approaches

Prime editors (PEs) represent one of the latest advances in the genome editing field. They were developed to broaden the possibilities for precise genomic modification that cannot be fully covered by BEs. PEs are composed of a nCas9 coupled with a reverse transcriptase (RT). The sgRNA has been modified to generate a prime editing gRNA (pegRNA). The pegRNA is similar to a standard sgRNA, with the addition of the primer binding site and the RT template. The mechanism of action consists of the binding and nicking of the DNA template by Cas9. The cut DNA strand is then recognized by the pegRNA which anneals *via* the primer binding site. This annealing is exploited by the RT which retrotranscribes the template to install the desired DNA sequence. In the latest version of PEs, an additional sgRNA was added to introduce a nick in the non-edited strand, to favor the insertion of the modified DNA strand (Anzalone *et al*, 2019). PEs can be exploited to achieve short integrations, deletions, and all the possible base-to-base conversions (Fig. IIIE). In comparison to standard editing with nucleases or with BEs, PEs display some advantages. For instance, they allow the minimization of DBS and modification of sequences far from the protospacer adjacent motif (PAM) (Anzalone *et al*, 2019). One of the first applications of PEs was related to the treatment of alpha-1 antitrypsin deficiency. The most frequent pathogenic mutation is a G to A mutation in the *SERPINA1* gene. In this genomic region, however, there is no optimal PAM to be used for editing. Therefore, Liu et al. investigated a prime editing strategy that resulted in the correction of around 7% of pathogenic alleles in the liver (Liu *et al*, 2021). Another study applied prime editing for the treatment of phenylketonuria, reaching a correction efficiency of around 11% in the liver of newborn mice, sufficient to provide therapeutic benefit (Böck *et al*, 2022). PEs were also delivered *in vivo* to the liver of mice with hereditary tyrosinemia, resulting in a significant amelioration of the disease phenotype

without detectable off-target edits (Jang *et al*, 2021). Another relevant target for liver prime editing is *PCSK9*, as previously described for base editing strategies for the treatment of hypercholesterolemia. Thus, some works described the selection and optimization of efficient PEs to be delivered *in vivo* to target *PCSK9* (Zheng *et al*, 2022; Davis *et al*, 2024). Several studies have in common the continuous development of PEs to allow easier delivery to the liver and to increment the editing efficiency (Liu *et al*, 2021; Böck *et al*, 2022; Zheng *et al*, 2022; Davis *et al*, 2024). In this context, it would be beneficial to achieve integrations or deletions of large DNA fragments to correct defects arising from multiple mutations or large insertions/deletions. However, PEs can effectively insert only up to around 50 base pairs or delete up to around 80 base pairs (Anzalone *et al*, 2019). To address this issue different strategies have been developed, but few of them have already been tested *in vivo*. The strategy called PEDAR (PE-Cas9-based deletion and repair) exploits a fully active Cas9 combined with a retro transcriptase and two different pegRNAs (Fig. IIIE). In this way, the region between the two pegRNAs can be deleted, since Cas9 will perform a DBS. Subsequently, the two pegRNAs will be retrotranscribed to form two complementary strands that will be ligated, resulting in the deletion of the undesired sequence and the insertion of a specific edit. PEDAR has been applied in a mouse model of tyrosinemia I leading to the deletion of 1.38 kilobases (kb) and the insertion of 19bp (Jiang *et al*, 2022). A strategy tested *in vivo* for large DNA insertions is the so-called template jumping (TJ) prime editing, based on the presence of two primer-biding sites on the pegRNA. In this case, PEs act as previously described, creating a ssDNA harboring another primer binding site at the end. The PE can then generate another nick on the opposite strand, *via* the other sgRNA. The primer binding site present on the ssDNA can bind the DNA at the nick site and the retro transcriptase can generate the second strand of DNA. Thus, the synthesized DNA is inserted in the target locus, allowing the deletion of the sequence that was present between the two nicks (Fig. IIIE). This strategy has been exploited in a mouse model of tyrosinemia I to replace an exon of the *Fah* gene. This resulted in 0.1% of corrected hepatocytes that acquired a proliferative advantage (Zheng *et al*, 2023a). Other systems combine the activity of PEs with the ability of serine integrase to insert long sequences of DNA. Examples are TwinPE (twin prime editing) (Anzalone *et al*, 2022), PASTE (programmable addition via site-specific targeting elements) (Yarnall *et al*, 2023), and PASSIGE (prime-editing-

assisted site-specific integrase gene editing) (Pandey *et al*, 2024). They exploit PEs to insert in a specific locus the landing sequence recognized by the serine integrase, which then can insert a double-strand donor DNA. All the systems reached more than 10kb of cargo insertion cell lines and primary cells (Fig. IIIE). PASSIGE is the latest evolution and allows the highest rate of integration *in vitro* (up to 60%) (Pandey *et al*, 2024). Among these approaches, PASTE was the only one tested *in vivo,* achieving around 1-2% of integration in hepatocytes (Yarnall *et al*, 2023). Despite the great potential for precise genomic modification, prime editing requires optimization to increase efficiency and be applied in different liver-related indications.

1.2.6 Liver gene silencing/activation

Among the possible liver-directed therapeutic approaches, epigenome editing represents a strategy in active evolution for those indications that can benefit from gene silencing or gene activation. Indeed, epigenome editing aims at rewriting the epigenetic code to control gene expression without directly modifying the primary DNA sequence. Since epigenome editing does not intervene in disease-causing mutations, its application is limited to specific indications, for instance, to suppress the expression of a gene involved in a dominant genetic disease. The epigenome editors are based on proteins that can recognize and bind a specific region of the genome, like multiple zinc finger domains, transcription activator-like effector proteins, or dCas9, coupled to epigenome modifier enzymes (Ueda *et al*, 2023). The most commonly exploited epigenome activators are VP64 or the combination VP64-p65-Rta (VPR), while the most used repressors are KRAB, DNMT3A with DNMT3L, or the combination KRAB-MeCP2 (Bendixen *et al*, 2023; Amabile *et al*, 2016) (Fig. IIIF). For their easy-to-assemble and easy-to-use properties, the most employed strategies are based on dCas9 fused to an activator (CRISPRa) or a repressor for interference (CRISPRi) (Bendixen *et al*, 2023). The potency of CRISPRa *in vivo* in hepatocytes has been demonstrated for the upregulation of erythropoietin, a target therapeutically relevant for several conditions. CRISPRa was

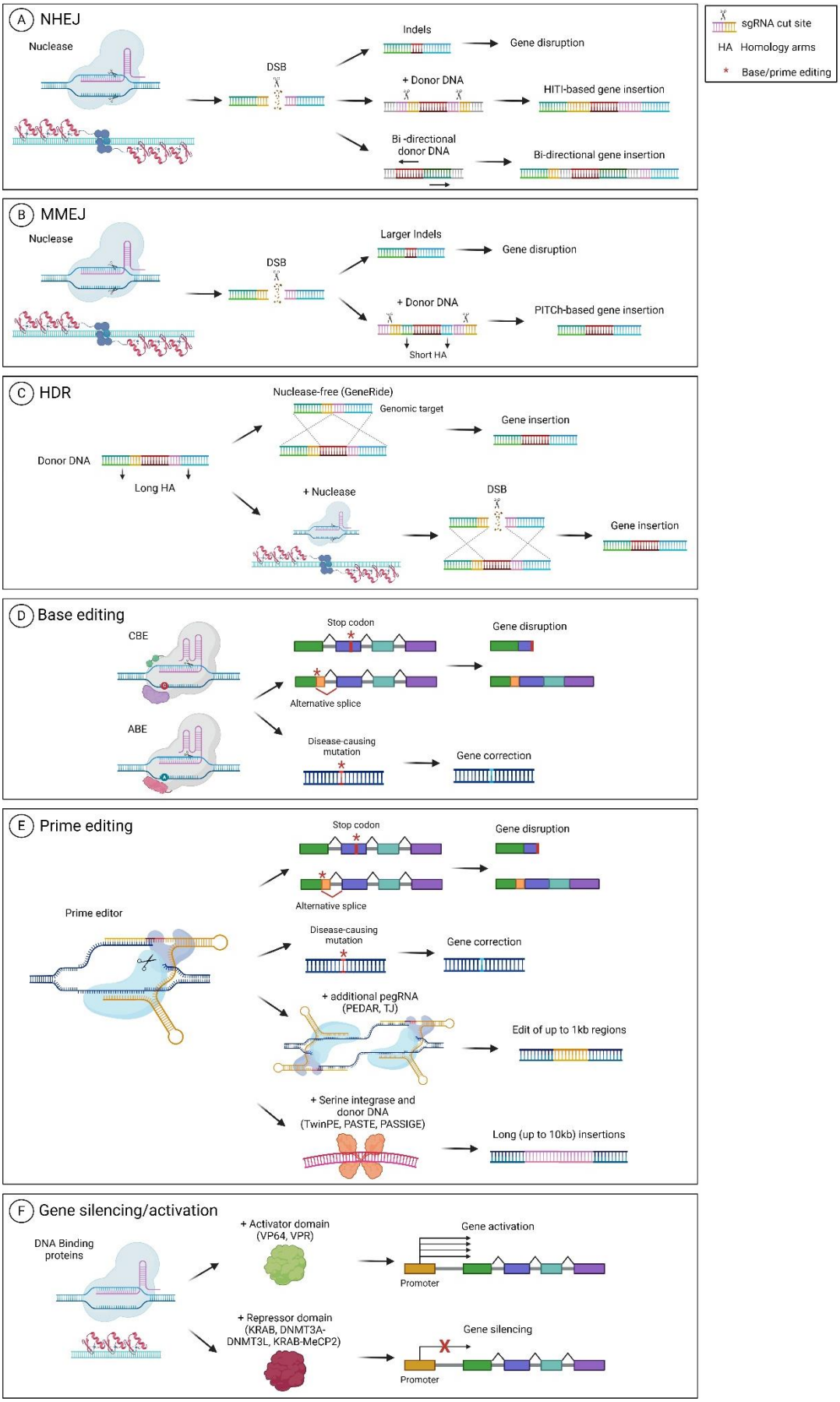

A NHEJ
Nuclease
DSB
Indels
Gene disruption
+ Donor DNA
HITI-based gene insertion
Bi -directional donor DNA
Bi-directional gene insertion
B MMEJ
Nuclease
DSB
Larger Indels
Gene disruption
+ Donor DNA
PITCh-based gene insertion
Short HA
C HDR
Nuclease-free (GeneRide)
Genomic target
Gene insertion
Donor DNA
Long HA
+ Nuclease
DSB
Gene insertion
D Base editing
CBE
Stop codon
Gene disruption
Alternative splice
ABE
Disease-causing mutation
Gene correction
E Prime editing
Stop codon
Gene disruption
Alternative splice
Prime editor
Disease-causing mutation
Gene correction
+ additional pegRNA (PEDAR, TJ)
Edit of up to 1kb regions
+ Serine integrase and donor DNA (TwinPE, PASTE, PASSIGE)
Long (up to 10kb) insertions
F Gene silencing/activation
DNA Binding proteins
+ Activator domain (VP64, VPR)
Gene activation
Promoter
+ Repressor domain (KRAB, DNMT3A-DNMT3L, KRAB-MeCP2)
Gene silencing
Promoter
sgRNA cut site
HA Homology arms
* Base/prime editing

Figure III. Gene editing strategies. A) Scheme of non-homologous end joining (NHEJ)-based gene editing approaches and their possible outcomes, *i.e.* gene disruption *via* indels formation or gene insertion in the presence of a donor DNA (HITI-based or bi-directional). B) Scheme of microhomology-mediated end joining (MMEJ)-based gene editing approaches and their possible outcomes, *i.e.* gene disruption *via* larger indels formation or gene insertion in the presence of a donor DNA (PITCh). C) Scheme of homology-directed repair (HDR)-mediated gene insertion mechanisms, achieved *via* recombination with or without nucleases. D) Scheme of base editing approaches and their possible outcomes, *i.e.* gene disruption *via* stop codon or alternative splice formation, or gene correction of a point mutation. E) Scheme of prime editing approaches and their possible outcomes, *i.e.* gene disruption *via* stop codon or alternative splice formation, gene correction, editing of up to 1kb with two pegRNAs (PEDAR, TJ), or serine integrase-mediated long insertions (TwinPE, PASTE, PASSIGE). F) Scheme of gene silencing or activation mechanisms, *via* the combination of DNA-binding proteins with repressor or activator domains, respectively. Created with BioRender.com.

delivered *in vivo*, obtaining sustained overexpression of erythropoietin for up to 7 days (Beyersdorf *et al*, 2022). On the other hand, liver-targeted CRISPRi has been exploited in different works aimed at silencing *PCSK9* (Thakore *et al*, 2018; Gemberling *et al*, 2021). These studies showed a stable up-to-6-month reduction of the protein in the serum of treated mice. Of note, another recent work demonstrated that zinc-finger-based epigenome editors outperform CRISPR or TALE-based editors for the durable silencing of *PCSK9*, allowing for up to a one-year reduction in circulating PCSK9, also after partial hepatectomy (Cappelluti *et al*, 2024). These works highlight the potential of epigenome editors for further development towards clinical applications.

1.3 *In vivo* delivery methods to the liver

A crucial aspect to be considered when developing liver-directed genome editing approaches is the delivery of editing components *in vivo*. The editing machinery can be encoded by DNA or RNA templates, or it can be delivered directly as a protein or RNP complex. All these macromolecules are fragile and can be easily degraded in circulation. Moreover, they need to reach the target tissue, interact with components of the plasma membrane or extracellular matrix, enter the cell, escape the endosome, and get to the appropriate intracellular compartment (Khirallah *et al*, 2023). For these reasons, optimal delivery vehicles should allow to efficiently encapsulate the editing components and then bring them to target cells, without toxicities for the recipient. This is a challenging endeavor, thus a significant effort has been put into developing different *in vivo* delivery

strategies over the years. Delivery systems can be divided into viral and non-viral ones. Among the viral vectors, AAVs are currently the most utilized vehicles for genome editing applications *in vivo*, even if LVs and adenoviruses-derived vectors (AdVs) may also be considered as alternatives. Among non-viral methods, lipid nanoparticles (LNPs) are the most exploited and reached clinical application. Finally, virus-like particles (VLP) have recently been adopted in preclinical studies (Raguram *et al*, 2022).

1.3.1 Adeno-Associated viral vectors

AAVs are derived from naturally occurring non-pathogenic viruses. They have an icosahedral capsid composed of 60 copies of structural proteins VP1, VP2, and VP3 with a diameter of ~26 nm. Their genome is an ssDNA of ~4.7kb, flanked by two inverted terminal repeats (ITRs) that are essential for genome packaging during vector production (Wang *et al*, 2019a). Once in the nucleus of the host cells, their genome remains mostly episomal, with a low rate of genomic integration (<1%), and it is therefore progressively diluted during cell replication (Wang *et al*, 2019a; Cunningham *et al*, 2008) (Fig. IVA). To develop vectors suitable for gene therapy applications, only ITRs were maintained, while all viral genes were eliminated and substituted with the therapeutic cassette of interest (Wang *et al*, 2019a). AAV-mediated liver gene transfer has shown promising efficacy and safety profile in several preclinical and clinical studies (Baruteau *et al*, 2024). Several native or engineered AAV-capsid variants have been exploited for specific applications, to reach different target cells (Pupo *et al*, 2022). For all these reasons they have become one of the most common methods to deliver gene editing machinery. However, one limitation is their cargo capacity, limited to ~4.7kb. This is a relevant drawback for genome editing since the most exploited nuclease is the *Streptococcus pyogenes* Cas9 (SpCas9) which is ~4kb in length. Thus, the residual space available for regulatory elements and sgRNA expression cassettes is limited. Therefore, SpCas9-expressing AAVs typically contain very short promoters (up to 300 bp), whether constitutive (Suzuki *et al*, 2016; He *et al*, 2022) or liver-specific (Tornabene *et al*, 2022; Richards *et al*, 2020). Usually, a second AAV is needed for the delivery of the donor DNA and the sgRNA-expression cassette. In this case, an efficient genome editing output can be achieved only when the target cell is co-transduced by the two AAVs. The capacity of AAV to co-transduce the target cell was leveraged to develop the dual AAV vector

strategy, in which a single gene product is split in half and then reconstituted upon co-transduction. The most successful dual AAV approach is based on protein trans-splicing using split inteins. The method was originally optimized for gene addition and gene replacement applications to deliver large transgenes (Barbon *et al*, 2023; Padula *et al*, 2022; Jauze *et al*, 2024; Trapani *et al*, 2014) and then applied also to BEs, PEs, silencers, and activators for genome editing purposes (Levy *et al*, 2020; Davis *et al*, 2024). Upon co-transduction and transgene expression, the split inteins dimerize and undergo trans-splicing, generating the complete form of the transgene protein (Aranko *et al*, 2014). Dual AAV allowed successful base editing in the liver in the context of mucopolysaccharidosis type I (Su *et al*, 2023), hemochromatosis (Rovai *et al*, 2022), and phenylketonuria (Villiger *et al*, 2018). The dual AAV system was explored also for delivering PEs or epigenetic silencers in the context of alpha-1 antitrypsin deficiency (Liu *et al*, 2021), or to inactivate *PCSK9* expression (Zheng *et al*, 2022; Thakore *et al*, 2018). Since dual AAV approaches present efficiency, safety, and manufacturing-related limitations, different groups have tried to develop alternatives, such as smaller editing components. Smaller Cas9 orthologs or engineered Cas9 have been tested. The most exploited small Cas9 is derived from *Staphylococcus aureus* (SaCas9), which has a size of ~3.2kb. SaCas9 has been successfully applied in preclinical works in the context of several inherited metabolic diseases and hemophilia (Wang *et al*, 2020; Lisjak *et al*, 2023; De Caneva *et al*, 2019; Chen *et al*, 2019; Wang *et al*, 2019b; Torella *et al*, 2024). Recently, different laboratories developed smaller BEs and PEs that could potentially fit in a single vector (Davis *et al*, 2022; Zheng *et al*, 2022). Ideally, delivering the genome editing machinery by a single AAV would not only allow to achieve higher efficiency but also to potentially reduce the administered vector dose. Besides the cargo limitations, AAVs present additional challenges such as the persistent expression of the transgene in the transduced cells, if quiescent, which could increase the risk of unwanted off-target editing (Anzalone *et al*, 2020). Another risk is related to the potential immunogenicity of Cas9 and all the other components of the gene editing machinery which represent non-self-antigens (Wagner *et al*, 2021). These problems could be overcome by non-viral delivery methods, which we will discuss below.

1.3.2 Adenoviral vectors

AdVs are derived from adenoviruses, non-enveloped viruses with an icosahedral capsid of ~100nm in size. They have a linear double-stranded DNA genome of ~36kb, which is maintained as an episome in the nucleus of transduced cells (Lee *et al*, 2017) (Fig. IVB). They were among the first vectors to be exploited for *in vivo* gene delivery, taking advantage of the knowledge of the biology of the parental virus and its capability of efficiently transducing the target cells (Lee *et al*, 2017). One of the most important advantages of AdV is the large cargo capacity, which has been exploited also for the delivery of genome editing machinery to the liver. They have been tested as an all-in-one platform for the delivery of Cas9 and sgRNA to knock out *PCSK9* (Ding *et al*, 2014), or together with another AdV carrying the donor DNA to allow insertion of the therapeutic transgene in the context of alpha-1-antitrypsin deficiency (Stephens *et al*, 2018) or hereditary tyrosinemia (Shao *et al*, 2018). AdV has been also explored to incorporate the coding sequences of BEs and PEs for *in vivo* delivery (Chadwick *et al*, 2017; Böck *et al*, 2022), as well as for the PASTE approach (Yarnall *et al*, 2023). However, the major concern related to the use of AdV is their immunogenic profile, which resulted in major adverse events in past gene therapy clinical trials employing these vectors (Raper *et al*, 2003). Moreover, AdV-derived Cas9 expression induced an anti-Cas9 immune response leading to the killing of corrected cells (Wang *et al*, 2015). For these reasons, the usage of AdV for *in vivo* genome editing will require further investigation before clinical testing.

1.3.3 Lentiviral vectors

An additional delivery vehicle is represented by LVs, which are enveloped vectors derived from human immunodeficiency virus (HIV), with a single-stranded RNA genome of ~10kb that is reverse-transcribed and integrated in a semi-random way into the genome of the transduced cells (Naldini *et al*, 1996) (Fig. IVC). LVs are replication-defective and are composed of HIV-1 capsid and enzymatic proteins, encoded by *gag* and *pol* genes, and the envelope protein that is derived from a different virus and can redirect the tropism of vectors. The most commonly used envelope protein is the vesicular stomatitis virus glycoprotein G (VSV.G), which makes LVs pantropic and allows the transduction of hepatocytes (Dull *et al*, 1998; Zufferey *et al*, 1997). To obtain replication-defective and self-inactivating vectors the different components necessary for the production have been

split into four different constructs, and the 3' long terminal repeat (LTR), which flank the genome, has been partially deleted (Zufferey *et al*, 1997). Moreover, to generate a non-integrative vector, the integrase protein has been inactivated to generate integrase-deficient lentiviral vectors (IDLVs), so the viral genome after retro-transcription is maintained as an episome in the nucleus of the transduced cells (Wanisch & Yáñez-Muñoz, 2009) (Fig. IVC). LVs have been exploited mainly for *ex vivo* applications and have already reached the clinic and the market for different indications (Tucci *et al*, 2022; Labbé *et al*, 2021). Their possible application for *in vivo* delivery to the liver has been investigated in different preclinical studies in dogs and NHP for hemophilia A and B (Milani *et al*, 2019b, 2022; Cantore *et al*, 2015), and in mice for inherited metabolic disorders (Elena Barbon *et al*, 2024; Cesare Canepari *et al*, 2024). However, despite their cargo capacity could allow for relatively easy packaging of all the gene editing machinery in a single vector, they have not been used yet as an *in vivo* delivery of genome editing components to hepatocytes. In this regard, IDLVs have been demonstrated to be effective as HDR templates *ex vivo* (Lombardo *et al*, 2007) without raising concerns about integration-related genotoxicity. However, the risks related to the persistent expression of the editing agents and the off-target effects are shared with the AAV platform.

1.3.4 Lipid nanoparticles

LNPs have been developed in the past years for the *in vivo* delivery of short-interfering RNAs (siRNA) and messenger RNAs (mRNAs). Recently, they have been tested also for gene editing applications becoming one of the most exploited vehicles for liver targeting, for instance in clinical trials delivering genome editing reagents (Gillmore *et al*, 2021; Longhurst *et al*, 2024) (Fig. IVD). LNPs are typically composed of four primary elements: phospholipids, cholesterol, polyethylene glycol (PEG) lipids, and ionizable cationic lipids (Kazemian *et al*, 2022). Phospholipids and cholesterol secure the structural stability of the LNP. PEG lipids have been introduced to coat LNP with PEG molecules to prevent particle aggregation, decrease immunogenicity, and increase the LNP half-life *in vivo* (Kazemian *et al*, 2022). Lastly, the use of ionizable cationic lipids has significantly improved the delivery mediated by LNP. Briefly, these lipids are positively charged during LNP production, allowing the interaction and encapsulation of negatively charged nucleic acids. On the other hand, LNPs are in an uncharged state at a neutral pH, such as

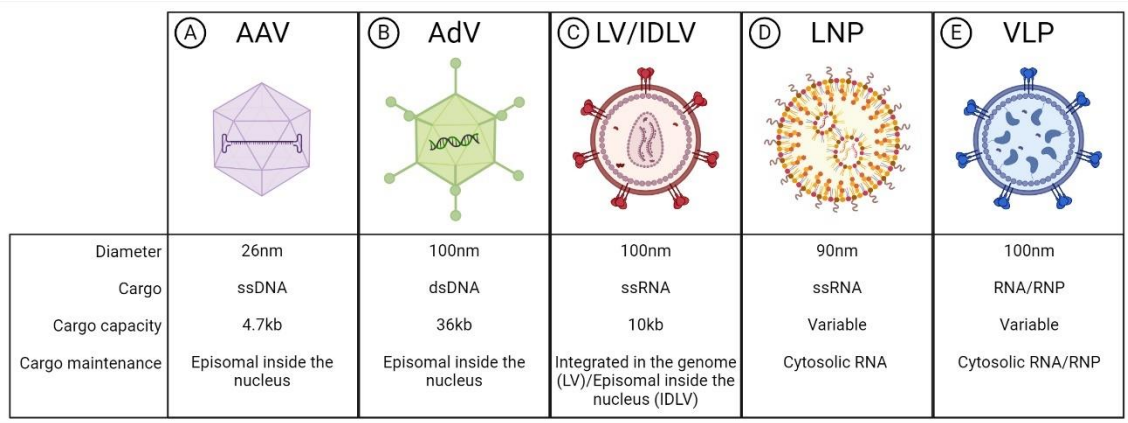
when they are delivered *in vivo*, thus preventing immune system reaction. Once LNPs are internalized into target cells by endocytosis, they become positively charged again due to the lowering of the endosomal pH. This provokes the rupture of the endosome membrane enabling the release of the nucleic acids into the cytosol (Paunovska *et al*, 2022). Up to now, the efficient encapsulation into LNPs is limited to nucleic acids, which remain in the cytosol and cannot access the nucleus, after delivery to target cells. Since the persistence of nucleic acids in the cytosols is limited in time, LNPs allow for transient delivery of their cargo, overcoming the limitation related to the stable expression of the editing agents by viral vectors. Once injected into the bloodstream, LNPs are coated with ApoE lipoproteins that interact with the LDLR. Since LDLR is highly expressed by hepatocytes, LNPs efficiently accumulate in the liver (Paunovska *et al*, 2022). Not only the LNPs' chemical composition but also the cargo ones have to be fine-tuned for efficient delivery. For example, RNA molecules have been optimized to increase their stability and decrease their immunogenic profile. Cas9 mRNAs have been modified by exploiting pseudouridine, 5-methylcytidine, and capping (Karikó *et al*, 2008; Mauer *et al*, 2017), while 2'OMe, 2'F, and phosphorothioate have been included in sgRNA in a specific order (Yin *et al*, 2017). All these improvements led to preclinical studies aimed at evaluating the potency of LNPs to deliver gene-editing agents to hepatocytes for the treatment of different disorders. The delivery of Cas9 mRNA together with sgRNA has been tested for the disruption of genes in the context of hereditary transthyretin amyloidosis or hereditary angioedema and led to the initiation of two clinical trials (Finn *et al*, 2018; Longhurst *et al*, 2024; Gillmore *et al*, 2021). LNPs have also been extensively tested for the delivery of BEs in mouse models of phenylketonuria (Brooks *et al*, 2024, 2023) and alpha-1 antitrypsin deficiency (Packer *et al*, 2022) and in NHPs for the disruption of *PCSK9* (Rothgangl *et al*, 2021; Musunuru *et al*, 2021). Moreover, gene activators and gene silencers have been efficiently delivered to hepatocytes via LNPs to activate erythropoietin (Beyersdorf *et al*, 2022) and silence *PCSK9* (Cappelluti *et al*, 2024). Noticeably, combinations of different delivery methods have been exploited for genome editing applications involving the use of donor DNA. In this case, LNPs were used for the transient delivery of Cas9 and sgRNA, and AAVs for the nuclear delivery of donor DNA. This strategy has been tested in the context of hemophilia A and B, leading to the insertion in approximately 2-3% of the target loci (Lee *et al*, 2023; Han *et al*, 2023).

Notwithstanding the need for further optimizations to achieve higher efficiency, this combined delivery method is promising since it condensates the advantages of both LNPs and AAVs. Recently, LNPs have been further modified to allow their uptake in hepatocytes of patients lacking sufficient levels of LDLR, such as those with homozygous familial hypercholesterolemia. This outcome has been obtained by adding the N-acetylgalactosamine (GalNAc)-targeting ligand to the LNP, to generate GalNAc-LNP. This ligand is recognized by the asialoglycoprotein receptor (ASGPR), which is highly expressed in the liver and allows rapid endocytosis. In the work describing the strategy, Kasiewicz et al. demonstrated the ability of these GalNAc-LNP to deliver gene editing agents to hepatocytes of both wild-type or LDLR knock-out mice and NHPs (Kasiewicz *et al*, 2023).

1.3.5 Virus-like particles

VLPs are derived mainly from retroviruses from which they maintain the envelope and the capsid, while the viral genome is substituted by the gene editing agents incorporated as RNA or protein (Lyu *et al*, 2020). In this way, VLPs can exploit the virus's capacity to enter the cell while allowing transient delivery of the editors, reducing the risk of off-target events and immunogenicity. Retroviruses were selected since their immature particles are 100nm-long in diameter, spherical, and relatively flexible, allowing the packaging of large cargo such as Cas9 or BEs (Raguram *et al*, 2022). The first tested VLPs were packaged with mRNA templates. However, without the addition of proper chemical mRNA modifications, this template is rapidly degraded once inside the cells, thus resulting in low editing efficiency. On the other hand, the most efficient strategy developed for *in vivo* applications is based on the packaging of proteins or RNPs (Fig. IVE). To allow for their encapsulation, proteins or RNP have been fused to structural viral proteins, usually *gag*. Subsequently, the release of the cargo occurs during virion maturation by exploiting a cleavable peptide. Upon cell transduction, the VLP cargo is released inside the cytosol (Kaczmarczyk *et al*, 2011). The formation of the RNPs takes place during VLP production thanks to the expression of the sgRNA from an additional plasmid. Different configurations have been tested in cell lines or for *ex vivo* applications but just two of them achieved efficient editing in the liver. The first one is called “nanoblade” and contains SpCas9-RNP fused to murine leukemia virus (MLV) *gag*.

Nanoblades were shown to achieve 10% of editing in the liver of a hereditary tyrosinemia type 1 mouse model (Mangeot *et al*, 2019). Other tools are engineered VLPs (eVLPs), based on Moloney MLV (MMLV), in which Cas9 or base editor-RNP are fused to the MMLV *gag* with an engineered linker peptide. eVLPs delivered *in vivo* to the liver achieved up to 63% editing efficiency to disrupt the *PCSK9* gene (Banskota *et al*, 2022). eVLPs were also optimized to package PEs as RNP, but up to date they were only tested for *in vivo* editing of the retina (An *et al*, 2024). Despite the promise of eVLPs for efficient hepatic delivery, their immunogenic profile should be the object of careful evaluation since they are of viral origins.



	A AAV	B AdV	C LV/IDLV	D LNP	E VLP
Diameter	26nm	100nm	100nm	90nm	100nm
Cargo	ssDNA	dsDNA	ssRNA	ssRNA	RNA/RNP
Cargo capacity	4.7kb	36kb	10kb	Variable	Variable
Cargo maintenance	Episomal inside the nucleus	Episomal inside the nucleus	Integrated in the genome (LV)/Episomal inside the nucleus (IDLV)	Cytosolic RNA	Cytosolic RNA/RNP

Figure IV. Delivery vehicles to the liver. Schematic representation of adeno-associated viral vectors (AAV) (A), adenoviruses vectors (AdV) (B), lentiviral vectors (LV) or integrase-deficient lentiviral vectors (IDLV) (C), lipid nanoparticles (LNP) (D), virus-like particles (VLP) (E), and their respective features. Created with BioRender.com.

1.4 Liver-directed genome editing clinical trials

There are currently seven clinical trials which employ *in vivo* liver-directed gene editing approaches (Table II). The first one started in 2020, sponsored by Intellia Therapeutics, for the treatment of Transthyretin Amyloidosis with polyneuropathy or cardiomyopathy (Study to Evaluate Safety, Tolerability, Pharmacokinetics, and Pharmacodynamics of NTLA-2001 in Patients With Hereditary Transthyretin Amyloidosis With Polyneuropathy (ATTRv-PN) and Patients With Transthyretin Amyloidosis-Related Cardiomyopathy (ATTR-CM), 2023). This disease is caused by acquired or hereditary dominant mutations in the *TTR* gene and is characterized by the accumulation of misfolded transthyretin in tissues. The genome editing treatment is based on the intravenous administration of LNPs carrying SpCas9 mRNA and sgRNA targeting

the *TTR* gene in hepatocytes, to disrupt its expression and avoid the toxic transthyretin accumulation. Results published from the patients treated in this phase I clinical trial showed a significant and durable reduction in serum transthyretin, with no SAEs (Gillmore *et al*, 2021; Intellia Presents New Interim Data from the Ongoing Phase 1 Study of NTLA-2001 at the 4th International ATTR Amyloidosis Meeting, 2023). Those promising results lead to the initiation of the first Phase III clinical trial for *in vivo* liver-directed gene editing, with more than 30 patients dosed so far (MAGNITUDE: A Phase 3 Study of NTLA-2001 in Participants With Transthyretin Amyloidosis With Cardiomyopathy (ATTR-CM), 2024; Intellia Therapeutics Announces First Quarter 2024 Financial Results and Highlights Recent Company Progress, 2024). The second clinical trial started in 2021, sponsored again by Intellia Therapeutics, for the treatment of Hereditary Angioedema (NTLA-2002 in Adults With Hereditary Angioedema (HAE) (NTLA-2002), 2024). The disease is characterized by unpredictable swelling caused by mutations of the gene encoding for C1-inhibitor. This causes dysregulation of the complement contact activation pathway which can be restored by disrupting the kallikrein expression from the *KLKB1* gene. The treatment is again based on intravenous administration of LNPs carrying SpCas9 mRNA and sgRNA targeting the *KLKB1* gene in hepatocytes. The results of the first 10 treated patients were published in 2024, showing no major SAEs, a dose-dependent reduction in kallikrein plasma levels up to 95%, and an overall 80-91% reduction in angioedema episodes (Longhurst *et al*, 2024). The study is now completed with 37 patients enrolled and Intellia is planning to start a Phase III study in the second half of 2024 (Intellia Therapeutics Announces First Quarter 2024 Financial Results and Highlights Recent Company Progress, 2024). The third study, sponsored by Verve Therapeutics, was the first to evaluate a base editing platform using an ABE to disrupt the expression of the *PCSK9* gene, to treat heterozygous familial hypercholesterolemia (A Study of VERVE-101 in Patients With Familial Hypercholesterolemia and Cardiovascular Disease, 2024). The treatment is based on the intravenous administration of LNPs carrying ABE-mRNA and sgRNA targeting the *PCSK9* gene in hepatocytes. Thirteen patients were dosed with 4 different doses of LNPs, achieving an average of 46% LDL cholesterol reduction at a dose of 0.45mg/kg. However, one of the patients treated with this LNP dose experienced an SAE, presenting with Grade 3 elevation of serum alanine aminotransferase (ALT) and drug-induced thrombocytopenia

within the first four days after dosing. For this reason, the trial is currently on hold (Verve Therapeutics Announces Updates on its PCSK9 Program, 2024). The sponsor hypothesized the SAE to be related to the LNP formulation exploited for the delivery. For this reason, a new clinical trial started in May 2024, by employing a new delivery method based on GalNAc-LNPs (A Study of VERVE-102 in Patients With Familial Hypercholesterolemia or Premature Coronary Artery Disease, 2024). Data on this trial will be released in 2025 (Verve Therapeutics Announces Pipeline Progress and Reports First Quarter 2024 Financial Results, 2024). At the end of 2023, CRISPR Therapeutics announced the start of two Phase I clinical trials to treat cardiovascular diseases. The trials are based on LNPs delivering Cas9 mRNA and sgRNA targeting either ANGPTL3 or lipoprotein(a) in LDLR knock-out human livers (CRISPR Therapeutics Provides Business Update and Reports Fourth Quarter and Full Year 2023 Financial Results, 2023). Up to date, no data about these trials have been released. Finally, in June 2024, Beam Therapeutics announced the dosing of the first patient in a clinical trial for Alpha-1 antitrypsin deficiency (A Study to Evaluate the Safety and Efficacy of BEAM-302 in Adult Patients With Alpha-1 Antitrypsin Deficiency (AATD), 2024; Beam Therapeutics Announces First Patient Dosed in the Phase 1/2 Study of BEAM-302 in Alpha-1 Antitrypsin Deficiency (AATD), 2024). A severe form of the disease is characterized by a point mutation in the *SERPINA1* gene, which causes an inefficient secretion of the alpha-1 antitrypsin protein that accumulates in hepatocytes. The treatment is based on the systemic administration of liver-targeting LNP carrying ABE-mRNA and sgRNA to correct the abovementioned point mutation. Other trials are supposed to start between the end of 2024 and the beginning of 2025. For instance, Intellia Therapeutics is developing an *in vivo* liver-directed CRISPR/Cas9-based therapy for treating Alpha-1 antitrypsin deficiency. The treatment exploits LNPs to deliver Cas9 mRNA and sgRNA, and an AAV to deliver the donor DNA encoding the alpha-1 antitrypsin protein. The strategy is designed to insert the *AAT*-donor DNA into the albumin safe harbor locus (Intellia Therapeutics Announces First Quarter 2024 Financial Results and Highlights Recent Company Progress, 2024). Moreover, Verve Therapeutics is proposing another base editing program to inactivate the *ANGPTL3* gene in the liver for the treatment of homozygous familial hypercholesterolemia (Verve Therapeutics Announces Pipeline Progress and Reports First Quarter 2024 Financial Results, 2024). The rapid development

of genome editing technologies from basic science tools to clinical-stage therapeutic products highlights their potential for the treatment of liver genetic diseases and opens the possibility for their application even to acquired diseases. As an example, Verve Therapeutics included acquired cardiovascular diseases in the company research pipeline (https://www.vervetx.com/our-programs/our-pipeline). However, several challenges remain to be addressed to increase editing efficiency, safety, and clinical translatability.

Table II – Current status of Liver genome editing active clinical trials

Disease indication	Strategy	Delivery	Sponsor	Study type	References
Hereditary transthyretin amyloidosis with polyneuropathy, hereditary transthyretin amyloidosis with cardiomyopathy, or wild-type cardiomyopathy	TTR gene disruption TTR gene disruption	LNPs encoding SpCas9 + sgRNA mRNA	Intellia Therapeutics	Phase I	-ClinicalTrials.gov Identifier: NCT04601051 (Gillmore *et al*, 2021)
				Phase III	-ClinicalTrials.gov Identifier: NCT06128629
Hereditary Angioedema	KLKB1 gene disruption	LNPs encoding SpCas9 + sgRNA mRNA	Intellia Therapeutics	Phase I/II	-ClinicalTrials.gov Identifier: NCT05120830 (Longhurst *et al*, 2024)
Heterozygous familial hypercholesterolemia, atherosclerotic cardiovascular disease	PCSK9 gene disruption	LNPs encoding ABE + sgRNA mRNA	Verve Therapeutics	Phase I	-ClinicalTrials.gov Identifier: NCT05398029
				Phase I	-ClinicalTrials.gov Identifier: NCT06164730
Cardiovascular diseases	ANGPL3 gene disruption	LNPs encoding SpCas9 + sgRNA mRNA	CRISPR Therapeutics	Phase I	(CRISPR Therapeutics Provides Business Update and Reports Fourth Quarter and Full Year 2023 Financial Results, 2023)
	Lipoprotein(a)			Phase I	
Alpha-1 Antitrypsin Deficiency	SERPINA1 gene correction	LNPs encapsulating ABE mRNA + sgRNA	Beam Therapeutics	Phase I/II	-ClinicalTrials.gov Identifier: NCT06389877

1.5 Genome editing-related potential adverse events

When exploiting the CRISPR/Cas9 system with nucleases one major concern is related to the potential off-target effects that could lead to genomic alterations following DSB (Tao *et al*, 2023). Examples of genomic alterations are undesired indels, large deletions, or even chromosomal rearrangements with chromothripsis in both on- and off-target sites (Tao *et al*, 2023; Leibowitz *et al*, 2021). Over the years different methods have been developed to predict and detect off-target events. One of the most used in-silico tools that allows the prediction of sequences with high similarity to the one recognized by the sgRNA is Cas-OFFinder (Bae *et al*, 2014). Other strategies exploit *in vitro* digestion of genomic DNA by the nuclease. One of the latest *in vitro* assays is CIRCLE-seq, based on the linearization and amplification of the DNA fragment containing a Cas9 cleavage site followed by its sequencing (Tsai *et al*, 2017). However, in both in-silico and cell-free methods, the possibility of retrieving false positives is high, thus their results need validation. In this context, methods based on Cas activity directly inside the cells are more reliable. The most used method is GUIDE-seq, based on the insertion of short double-stranded oligodeoxynucleotides into the DSBs created by the nuclease. The regions with the insertion are then sequenced to identify the off targets (Tsai *et al*, 2015). A limitation of this method is the requirement for cells that can be easily transfected. Other strategies have been developed to find larger deletions or translocations. For instance, chromosomal aberrations analysis by single targeted linker-mediated PCR sequencing (CAST-seq) is now extensively used because it can quantitatively calculate the frequency of those aberrations (Turchiano *et al*, 2021; Klermund *et al*, 2024). The major limitation of CAST-seq is the high amount of input genomes required to detect translocation events since those chromosomal aberrations are relatively rare events. However, the results obtained with all approaches need to be always experimentally validated by targeted sequencing of the putative off-target region or long-read sequencing of the chromosomal aberrations, to verify the off-target cleavage or to detect eventual technical bias (Tao *et al*, 2023; Torella *et al*, 2024). To reduce the off targets, many high-fidelity Cas9 have been developed, among others HIFI Cas9 (Vakulskas *et al*, 2018) and EvoCas9 (Casini *et al*, 2018). In parallel, a careful selection of the optimal sgRNA has to be always performed to balance the cutting efficiency and the probability of off-target effects. When employing BEs, a major concern is to provoke unintended edits, in either the on-target or the off-

target sites. The so-called “bystander edits” can occur on the on-target locus if in the spatial activity window of the deaminase are present nucleotides that can be modified other than the target one (Porto & Komor, 2023). BEs can present the same sgRNA-dependent off-target events as Cas9, but they can also present sgRNA-independent off-targets (Porto & Komor, 2023). The sgRNA-dependent off-targets are due to the pairing of the gRNA on homologous loci and can be detected and solved using the same methods developed for Cas9, as above described. The sgRNA-independent off-targets can occur both at DNA and RNA levels, and they are very difficult to detect and analyze. The methods exploited are genome-wide (Zuo *et al*, 2019) or transcriptome-wide sequencing (Grünewald *et al*, 2019). However, they are very expensive, and data retrieved from this kind of analysis require specific bioinformatics expertise to be analyzed. To reduce the sgRNA-independent off-targets, deaminases with a higher fidelity have been developed. However, the increase in specificity is often at the expense of reduced efficiency (Doman *et al*, 2020; Neugebauer *et al*, 2023). As Cas9 and BEs, also PEs can generate off-target editing caused by the recognition of homologous sequences by the sgRNA, which can be prevented by using high-fidelity Cas9 (Kim *et al*, 2020a). The possibility of sgRNA-independent off-target of PEs has been investigated but without significant findings, at least so far (Gao *et al*, 2022). Nevertheless, it has been shown that PEs could eventually retro-transcribe part of the sgRNA scaffold, resulting in its potentially detrimental insertion at the edited site (Tao *et al*, 2022). Moreover, studies performed in hematopoietic stem cells have shown the introduction of chromosomal aberration when using BEs and PEs, even if to a lower extent compared to Cas9. This is due to the usage of nCas9, which can, in some cases, induce the formation of a DSB (Fiumara *et al*, 2024). In the context of hematopoietic stem cells, it has been also demonstrated that all the different gene editing agents can cause an inflammatory response together with the activation of detrimental pathways for cell fitness (Fiumara *et al*, 2024; Schiroli *et al*, 2019). Many of these aspects have not yet been investigated for *in vivo* genome editing approaches directed to the liver. A way to limit potential toxicities is to transiently deliver the editing components, as obtained by the use of LNP-mRNA as previously described. However, even the potential toxicity related to the vehicle itself has to be evaluated. Regarding LNPs, important concerns have been raised during the first trial from Verve Therapeutics, which has been paused due to toxicity possibly related to the LNP formulation (Verve

Therapeutics Announces Updates on its PCSK9 Program, 2024). Concerning viral delivery vehicles, multi-year pre-clinical and clinical experience has demonstrated their therapeutic potential but also highlighted some related toxicities. Among these, the vector-induced immune responses can lead to the elimination of transduced cells or even to SAEs, especially when administering high vector doses (Shirley *et al*, 2020). Furthermore, many viral vectors present a non-null risk of genotoxicity due to vector integration (Baruteau *et al*, 2024). Recently, it has been demonstrated that AAVs generate insertions of concatemers in almost half of the edited cells when used as delivery vehicles for donor DNA (Suchy *et al*, 2024). The phenotypic variability that can derive from those insertions must be carefully evaluated. Another aspect to be considered before the treatment of patients is the pre-existing immunity either against the vehicle or the genome editing components. AAV vector immunity has a very high prevalence (30-60%) in the population since wild-type AAV infection is very common (Weber, 2021). This is currently an exclusion criterion in most of the gene therapy clinical trials using those vectors for liver targeting. Moreover, it has been demonstrated that the presence of anti-Cas9 immunity is high in the population, however, it remains debated whether immune tolerance also occurs toward Cas9-derived antigens (Simhadri *et al*, 2018; Charlesworth *et al*, 2019). Since Cas9 is of bacterial origin, this aspect has to be taken into account when administering a gene editing product *in vivo* because it can cause an immune response against cells that are transduced/transfected (Li *et al*, 2020). In the latest trials, the presence of anti-Cas9 antibodies has been investigated before the administration of the genome editing product, but it has not been included among the exclusion criteria (Longhurst *et al*, 2024).

1.6 Liver-directed genome editing future perspectives

The future of gene editing looks bright. Clinical trials are generating very promising results, and we are probably not far away from the approval of the first *in vivo* gene editing product. Those results are impressive considering that only around a decade has passed between the discovery of CRISPR/Cas9 and its approval in the clinic. For now, strategies that reached the clinic for liver-directed gene editing are based on Cas9 or BEs to disrupt a specific gene. Gene disruption is the simplest and most efficient modification that can

be achieved so far. Efficient small genomic insertions have been obtained only for *ex vivo* applications, such as in the PEs-based program for the treatment of Chronic Granulomatous Disease by Prime Medicine (Prime medicine reports first quarter 2024 financial results and provides business updates, 2024). Likely, PE efficiencies still need to be improved to enable *in vivo* clinical applications. The introduction of large genomic insertions remains a major challenge. The development of a unique strategy based on the insertion of a corrective cDNA would be ideal for correcting at once multiple gene mutations. In this context, positive results have been obtained by Intellia, exploiting the insertion of a corrective donor DNA for the treatment of Alpha-1 antitrypsin deficiency, leading to the initiation of a clinical trial (Intellia Therapeutics Announces First Quarter 2024 Financial Results and Highlights Recent Company Progress, 2024). Intellia is applying a similar genome editing strategy in hemophilia A and B pre-clinical studies. Other strategies aiming at introducing large insertions are under investigation. These are based on serine integrases, such as PASTE and PASSIGE methods described above, or on transposases, such as the FiCAT (find and cut-and-transfer) system. FiCAT exploits an engineered piggyBac transposase combined with Cas9 (Pallarès-Masmitjà *et al*, 2021), to achieve a transposase-mediated insertion of a donor DNA upon Cas9-induced DBS, bypassing the requirement of the TTAA motif at the insertion site. The system was tested *in vivo* but with low efficacy of the integration rate (Pallarès-Masmitjà *et al*, 2021). An interesting discovery to be mentioned was the CRISPR-associated transposase (CAST) bacterial system. Two different CAST types have been described, type V-K CAST (Strecker *et al*, 2019) and type I-F CAST (Klompe *et al*, 2019). Both are based on a nuclease-inactive Cas that, upon DNA binding *via* the sgRNA, can recruit the transposon that allows the site-specific insertion of large sequences. To date, those systems demonstrated very high integration capacity in the bacterial genome but a low integration rate in mammalian cells, suggesting the requirement of additional efforts to advance these tools (Lampe *et al*, 2024; Tou *et al*, 2023). Lastly, RNA editing technologies are emerging to avoid potential genotoxicity due to DNA editing. The most exploited system is based on Cas13a, which was tested to reduce gene expression by the site-specific cleavage of a target RNA (Abudayyeh *et al*, 2017). In addition, RNA-base editing technologies have been developed exploiting enzymes of the ADAR family which catalyze A-to-I editing. Those enzymes have been tested in mouse models of ornithine transcarbamylase

(Katrekar *et al*, 2019) and mucopolysaccharidosis type I syndrome (Yi *et al*, 2022; Katrekar *et al*, 2022). However, the low *in vivo* efficiencies mandate the need for further improvement to achieve therapeutic efficacy. All the scientific advancements obtained in the last years hold great promises for the beginning of an era in which liver-targeted genome editing could become a standard of care for both genetic and acquired diseases. Importantly, the rapid development of these genomic technologies has to be paralleled by a concomitant careful investigation of safety and ethical aspects related to their usage.

1.7 Inherited metabolic diseases

Inherited metabolic diseases or inborn errors of metabolism are a large group of genetic diseases due to defects in the synthesis, degradation, storage, or transport of macronutrients. For example, they can be due to disorders of carbohydrate metabolism, amino acids metabolism, urea cycle, or lysosomal storage. Several inherited metabolic diseases are linked to the liver, given the high number of biological functions that it carries out (Baruteau *et al*, 2024). If the mutated protein that causes the disease is expressed in different tissues the pathology is systemic. Otherwise, if the deficient protein is normally active just in the liver the pathology will affect just this organ. The inborn errors of metabolism that can be treated by liver transplantation are considered good targets also for liver-directed gene therapy. Two representative inherited metabolic disorders with more systemic involvement or more liver-specific dysfunctions are Maple syrup urine disease (MSUD) and Progressive familial intrahepatic cholestasis type 2 (PFIC2), respectively, which are taken as paradigmatic targets of the *in vivo* genome editing strategy presented in this dissertation.

1.7.1 Maple syrup urine disease

MSUD is an autosomal recessive metabolic disease caused by deficiency of the branched-chain α-ketoacid dehydrogenase complex (BCKDH) (Strauss *et al*, 2020b). This enzymatic complex is involved in the catabolism of branched-chain amino acids (BCAAs), leucine, isoleucine, and valine. BCKDH comprises 4 different subunits E1α, E1β, E2, and E3 encoded by *BCKDHA*, *BCKDHB*, *DBT*, and *DLD* genes (Blackburn *et al*, 2017). Mutation in one of those genes can result in MSUD, in particular for the DBT

gene, more than 200 mutations have been described as pathological (The Human Gene Mutation Database). The disease has an incidence of one in 185,000 live births, which is much higher in closed populations such as the Old Order Mennonites of Pennsylvania, where it arrives at one in every 200 live births (Morton *et al*, 2002). In normal conditions, BCAA catabolism starts in the mitochondria with the branched-chain aminotransferases that convert them into α-ketoacids: α-ketoisocaproic acid (KIC), α-ketoisovaleric acid (KIV), or α-keto-β-methylvaleric acid (KMV). The second step involved the BCKDH complex which performs oxidative decarboxylation and converts the α-ketoacids into isovaleryl-CoA, α-methylbutyryl-CoA, Isolutyryl-CoA, acetoacetate, acetyl-CoA, and succinyl-CoA (Fig. V) (Burrage *et al*, 2014).

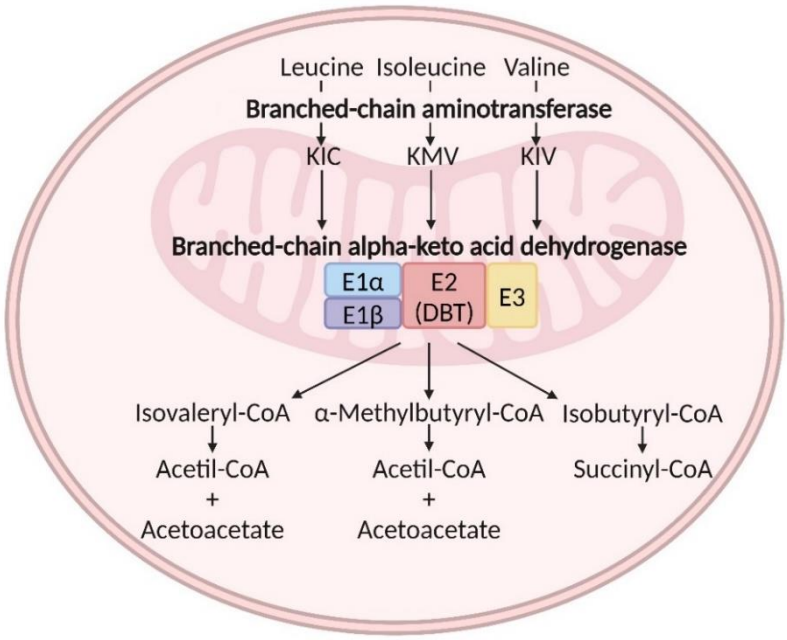


Figure V. Scheme of BCAAs catabolic pathway. Representation of the enzymes and the intermediate product involved in the catabolism of BCAAs. Created with BioRender.com.

BCAAs are among the nine essential amino acids for humans and are involved in protein synthesis, glucose metabolism, and cellular signaling. BCKDH subunits are expressed in all tissues, but mainly in the liver, kidney, and muscles. When the activity of BCKDH is defective, BCAAs and their α-ketoacids accumulate in blood, tissues, and urine. This causes dysfunctions of the muscles, the central nervous system, and the immune system leading to intellectual disability and physical retardation, feeding problems, and a characteristic maple syrup odor in urine that gives the name to the

disorder (Strauss *et al*, 2020b). The most severe symptoms affect the nervous system even if the mechanism is not completely understood. Leucine and KIC accumulation are highly neurotoxic, causing metabolic encephalopathy, cerebral edema, intellectual disability, and psychiatric illness (Burrage *et al*, 2014). Those symptoms can be due to the alteration of water homeostasis, which causes brain swelling, to the impairment in nitrogen homeostasis, which causes glutamate depletion and neurotransmitter imbalance, and to the competition with other amino acids such as tyrosine, which causes protein signaling abnormalities (Muelly *et al*, 2013). Depending on the severity of the symptoms, the age at onset, and the possible treatment, MSUD patients can be classified into five types (Ogier de Baulny & Saudubray, 2002). MSUD patients are usually treated with a dietary restriction of BCAAs and the clinical outcomes are good if the treatment starts very early. However, all the MSUD forms are at constant risk of metabolic decompensation, especially during infections, trauma, or surgery which can lead to neurological decline. The classic MSUD has a neonatal onset with less than 2% of BCKDH residual activity. If left untreated the affected neonatal can develop hypertonia, spasticity, opisthotonus, and poor feeding, which can be rapidly followed by coma and death. The older patient can develop anorexia, muscle fatigue, psychiatric symptoms, and ataxia (Treacy *et al*, 1992). The intermediate form appears healthy at birth, but they start to experience feeding problems, intellectual disability, and physical retardation during the first year of life. The residual enzymatic activity of BCKDH is up to 30%. The intermitted MSUD patients have a normal development and are asymptomatic in the normal state. However, when they experience stress, infections, or trauma they undergo metabolic crises with the same symptoms as the classic MSUD. Some pathogenic mutations of *DBT* can cause thiamine-responsive MSUD. The symptoms are similar to the intermediate form, however, they also need supplementation of thiamine, a co-factor of BCKDH. Finally, since the E3 subunit is common between three enzymatic complexes, mutations of the *DLD* gene affect BCKDH, but also α-ketoglutarate dehydrogenase, and pyruvate dehydrogenase. Depending on the residual activity of E3, MSUD patients with E3 deficiencies can have a wide spectrum of phenotypes from the most common neonatal onset, with symptoms similar to the classic form, to the adult onset, with only liver manifestations. Newborn screening for MSUD, based on the quantification of plasma amino acids, has been implemented in a lot of countries since the dietary restriction is very effective in

preventing the onset of symptoms (Chace *et al*, 2003). However, this screening does not identify the milder forms that usually can be detected just later in life or during acute illness. Orthotopic liver transplantation was demonstrated to be an effective treatment in pediatric patients. In different studies where MSUD patients were transplanted, all of them displayed long-term metabolic stability and became free from the restricted diet (Ewing *et al*, 2021; Strauss *et al*, 2020a). Transplanted patients demonstrated to arrest the neurological decline, but not to revert it, highlighting the need for an early intervention to avoid metabolic crisis and neurological damage (Strauss *et al*, 2020a). However, liver transplantation is not the primary option for MSUD patients since they are usually controlled with the diet and the transplant is a risky procedure with many possible side effects and few liver donors are available. Furthermore, since the protein is normally expressed in all tissues, the normal activity levels are not reached just with a liver transplant, so transplanted patients are still at risk of metabolic decompensation (Muelly *et al*, 2013). Nevertheless, since liver transplantation is therapeutic, bringing approximately 10% of BCKDH activity (Suryawan *et al*, 1998), MSUD is a good candidate for *in vivo* liver-directed gene therapy. In the first published work about MSUD gene therapy, authors developed a *Bckdha* knock-out (KO) mice that recapitulate the human phenotype and tested an AAV serotype 8 (AAV8)-based therapy. They generated two AAV cassettes with *Bckdha* under the control of either a ubiquitous or a liver-specific promoter. They observed a rescue of the disease with the ubiquitous promoter. The rescue was only partial when treating mice with the liver-specific cassette, suggesting that the contribution of extrahepatic organs is important in the gene therapy context (Pontoizeau *et al*, 2022). The same strategy exploiting AAV8 and the ubiquitous promoter was also tested in *Bckdhb* KO mice. Also in this mouse model, the treatment provided long-term rescue of the disease phenotype (Pontoizeau *et al*, 2024). Another work compared the efficiency of liver- or muscle-directed gene therapy in a mouse model called intermediate MSUD (iMSUD). This mouse model is KO for the murine *Dbt* gene while it has the human *DBT* gene knocked in. The low activity of the human gene, around 5%, allows the survival of the mice until weaning, since *Dbt* KO mice usually die 2 days post-birth (Skvorak, 2009). iMSUD mice were used to test two strategies based on the systemic administration of AAVs carrying *DBT* cDNA under the control either of a liver-specific or a ubiquitous promoter. Liver expression allowed only partial control of the disorder,

while the disease phenotype was better controlled in the presence of constitutive expression (Greig *et al*, 2021). Lastly, a strategy based on the repetitive administration of LNP carrying *BCKDHA*, *BCKDHB*, and *DBT* mRNA was tested in the three mouse models described before. The strategy increased survival and ameliorated the disease in all the models (Greig *et al*, 2024). However, all these strategies are based either on AAV or LNP administration. As we said before, AAVs are maintained as episomes in the nucleus of cells so they are diluted with cell replications and LNPs carry mRNA that is quickly degraded. The stability of the transgene is a major problem for diseases like MSUD where the majority of patients display symptoms very early in life.

1.7.2 Progressive familial intrahepatic cholestasis type 2

PFIC2 is an autosomal recessive disease caused by more than 200 described mutations in the *ABCB11* gene (The Human Gene Mutation Database), which encodes for the bile salt export pump (BSEP) protein. BSEP is the main active transporter of bile salts from hepatocyte cytosol to the bile canaliculi. It is a transmembrane protein almost exclusively expressed by hepatocytes and localized in their apical membrane (Kubitz *et al*, 2012). Mutations in *ABCB11* impair BSEP function, leading to reduced bile salt secretion with subsequent accumulation in hepatocytes and circulation that causes hepatic damage and cholestatic disease (Davit-Spraul *et al*, 2009). The liver damage induces liver fibrosis that rapidly progresses to cirrhosis, and end-stage liver disease in the first few years of life (Srivastava, 2014). The first symptoms of PFIC2 are jaundice and pruritus, with prevalently a neonatal onset. The disease is usually severe, with portal hypertension, and a high risk of developing HCC. The incidence is between one in 50,000 to one in 100,000 (Jacquemin, 2012). Patients undergo medical treatment to alleviate pruritus since it is the most debilitating symptom affecting sleep, behavior, and concentration, worsening the quality of life (Lazaridis *et al*, 2001). Moreover, they need to implement a diet with fat-soluble vitamins like A, D, E, and K. Indeed, bile acids, in normal conditions, are synthesized by hepatocytes starting from cholesterol and they are secreted with BSEP in the bile canaliculi, forming micelles. Bile acids reach the intestine following release from the gall bladder. Once in the intestine, the micelles incorporate fat and fat-soluble components such as vitamins. Then, bile acids are reabsorbed by enterocytes using the apical sodium-dependent bile salt transporter (ASBT). Successively, they are secreted

with the OSTα/β transporter in blood where they circle back to the liver and are captured by hepatocytes exploiting NTCP protein. This process is called enterohepatic circulation and involves the majority of bile salts since only 5% are lost in feces (Fig. VI) (Saeed *et al*, 2017).

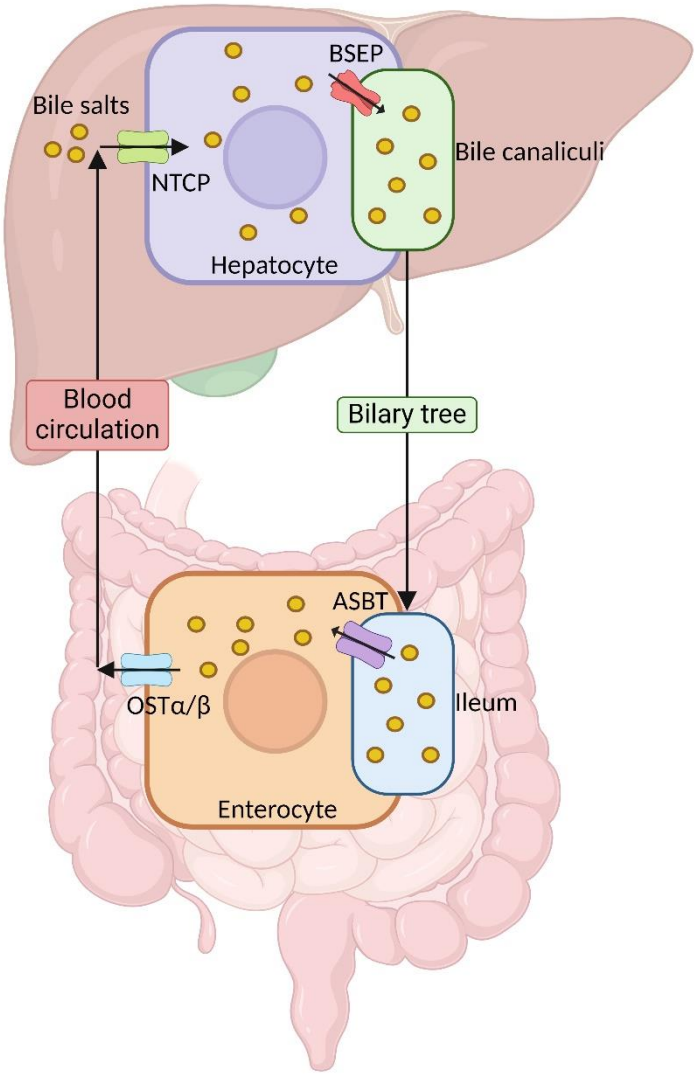


Figure VI. Scheme of enterohepatic circulation of bile salts. Representation of the transporter, the tissues, and the cells involved in the enterohepatic circulation of bile salts from the liver to the intestine and back. Created with BioRender.com.

Since the enterohepatic circulation is altered in PFIC2, patients develop vitamin A, D, E, and K deficiency. Moreover, in healthy conditions, bile salt synthesis, secretion, and circulation are tightly regulated by the farnesoid X receptor (FXR) (Modica *et al*, 2010). FXR is a nuclear receptor highly expressed in hepatocytes and enterocytes. In hepatocytes, after binding bile acids in the cytosol, FXR translocates in the nucleus and

downregulates genes involved in bile salt synthesis and the uptake transporter NTCP, while upregulating BSEP expression. In enterocytes, when FXR binds bile acids, it inhibits the expression of the ileal transporter ASBT and induces the release of FGF19 which acts on hepatocytes by inducing the decrease of bile salt production (Kullak-ublick *et al*, 2004). Enterohepatic circulation is also the main focus of PFIC2 therapies that aim at increasing bile salt secretion from the body. A common surgical intervention is the partial biliary diversion which can be external or internal (Schukfeh *et al*, 2012). The aim is to avoid the passage of bile salt into the ileum where they are reabsorbed. The external biliary diversion connects the gall bladder with a stoma created in the abdominal wall, while the internal connects the gall bladder with the colon. Those techniques were shown to reduce bile salt in circulation, improve liver functions, and reduce liver fibrosis progression (Davis *et al*, 2009). More recently, pharmacological inhibitors of ileal ASBT emerged as efficient medical interventions for PFIC2 patients. Odevixibat (Bylvay) was the first ASBT inhibitor approved by the FDA and EMA in 2021 for the treatment of PFIC2 patients (Deeks, 2021), in 2024 Maralixibat (Livmarli) has also been approved (Mirum's LIVMARLI Now Approved for PFIC in Patients 12 Months and Older, 2024). They reduce the reabsorption of bile salts in the ileum, allowing an increased execration in the feces. They demonstrated to reduce bile salts in circulation and to alleviate PFIC2 symptoms (Deeks, 2021). Finally, liver transplantation is the treatment offered to patients who do not respond to any other medical or surgical intervention. Since *ABCB11* expression is confined to the liver and PFIC2 has only liver manifestations, transplantation is curative, improving cholestasis, pruritus, and all the other symptoms associated with the disease (Srivastava, 2014). However, few cases of recurrence of the disorder after transplantation have been observed. Those were caused by the development of anti-BSEP antibodies in patients with mutations that completely prevent the expression of BSEP (Stindt *et al*, 2016; Kubitz *et al*, 2015). Moreover, liver transplant presents different side effects and risks, as described before. For the above-mentioned reasons, it is possible to consider liver-directed gene therapy for the treatment of PFIC2. However, no reports about gene therapy for PFIC2 have been published yet. This could be due to the length of the *ABCB11* gene which is difficult to fit inside a single AAV. Liver-directed gene therapy strategies have been tested in the context of PFIC type 3 (PFIC3). PFIC3 is another autosomal recessive cholestatic disease caused by mutations in the *ABCB4* gene

(Martínez-García *et al*, 2022). *Abcb4* KO mice, the mouse model of PFIC3, were treated in two independent studies with AAV8 carrying a hepatocyte-specific cassette for the expression of *ABCB4*. The treatment allowed long-term correction of the disease phenotypes, indicating the feasibility of liver-directed gene therapy for genetic cholestasis (Weber *et al*, 2019; Aronson *et al*, 2019). Another tested strategy for PFIC3 is based on the piggyBac transposase to insert the *ABCB4* gene in the genome of target cells in a semi-random way, exploiting AAV8 for delivery. Also, in this case, the strategy allowed the prevention of the disease phenotype (Siew *et al*, 2019b). Lastly, a work demonstrated that repetitive administration of LNP carrying ABCB4 mRNA improved serum biomarkers and liver fibrosis (Wei *et al*, 2021). Those strategies could be possibly applied also to PFIC2 disease. Nevertheless, when developing a gene therapy strategy for a pathology like PFIC2, it is important to consider the alteration of liver architecture present in patients even before one year of age.

1.8 Liver fibrosis

Liver fibrosis is characterized by excessive accumulation of extracellular matrix (ECM) leading to an alteration of liver architecture and functions (Roehlen *et al*, 2020). Fibrosis is a result of chronic liver diseases that are not solved, causing an imbalance between pro-fibrogenic and anti-fibrogenic mechanisms. Chronic liver diseases are among the most common causes of mortality worldwide, accounting for approximately 2 million deaths per year (Asrani *et al*, 2019). They can be caused by viral infection (HBV or hepatitis C virus, HCV), alcoholic steatohepatitis, metabolic dysfunction-associated steatohepatitis (MASH), autoimmune or genetic diseases. Fibrosis characterizes the progression of chronic liver disease, which if not treated can eventually lead to cirrhosis, liver failure, and HCC. Moreover, liver fibrosis causes portal hypertension that can provoke hydropic decompensation, bleeding events, and hepatic encephalopathy (D'Amico *et al*, 2018).

1.8.1 Pathophysiology of liver fibrosis

Chronic liver diseases are characterized by an initial stage of hepatocyte damage. Hepatocytes after necrosis release damage-associated molecular patterns (DAMPs), such

as nucleic acids, and mitochondrial or nucleic proteins, which can be sensed by the surrounding cells, mainly HSCs and KCs (Mihm, 2018). KCs initiate an inflammatory response, releasing pro-inflammatory cytokines like tumor necrosis factor-alpha (TNF-α), interleukin-1 (IL-1), interleukin-6 (IL-6), chemokine (C-C motif) ligand 2 (CCL2), and CCL5 (Tacke & Zimmermann, 2014). The initial inflammation allows the recruitment of other immune cells to the site of injury and induces the activation of HSCs. HSC activation is central to the development of fibrosis. In a healthy liver, HSCs reside in a quiescent state, storing vitamin A. After liver damage and inflammation, HSCs acquire an activated myofibroblast phenotype, characterized by the production of large amounts of ECM components, such as collagen types I and III, fibronectin, and laminin, leading to the formation of scar tissue within the liver (Mederacke *et al*, 2013; Tsuchida & Friedman, 2017). Normally, the ECM is continuously remodeled by matrix metalloproteinases (MMPs), which degrade the ECM, and their inhibitors, tissue inhibitors of metalloproteinases (TIMPs). In liver fibrosis, however, this balance is disrupted, with increased expression of TIMPs by activated HSCs and decreased expression of MMPs by macrophages, leading to excessive ECM deposition (Baiocchini *et al*, 2016). Myofibroblasts participating in the fibrosis process not only derive from HSCs but also from activation of portal fibroblast, and migration to the liver of precursors from the bone marrow. Portal fibroblasts are mainly activated when the injury is in the portal area (Lei *et al*, 2022). Fibrocytes and mesenchymal stem cells can migrate from the bone marrow and differentiate into hepatic myofibroblasts usually when the disease is in an advanced state (Kisseleva *et al*, 2006; Forbes *et al*, 2004). Multiple factors drive the perpetuation of the fibrotic process. Chronic inflammation and HSC activation create a vicious circle of injury, inflammation, and fibrosis. The inflammatory status is driven not only by KCs but also by other immune cells such as monocytes-derived macrophages and lymphocytes, which are recruited in the damaged liver (Krenkel & Tacke, 2017; Hegde *et al*, 2018). These immune cells contribute to inflammation and HSC stimulation by secreting cytokines, chemokines, and reactive oxygen species (ROS) (Sahin *et al*, 2010). Transforming growth factor-beta (TGF-β) is a key cytokine in the perpetuation of fibrosis, it is produced by various cells, including activated HSCs, Kupffer cells, and hepatocytes (Dewidar *et al*, 2019). TGF-β acts through the SMAD signaling pathway to regulate gene expression (Inagaki & Okazaki, 2007). It promotes the activation of HSCs

and stimulates them to produce ECM components (Deng *et al*, 2024). Another important factor is the platelet-derived growth factor (PDGF) which promotes the activation and proliferation of HSCs. PDGF acts by activating intracellular signaling pathways such as the Ras/MAPK, PI3K/Akt, and JAK/STAT pathways (Ying *et al*, 2017). It is produced by KC, endothelial cells, and even the activated HSCs themselves (Borkham-Kamphorst & Weiskirchen, 2016). ROS are generated by damaged hepatocytes, activated immune cells, and HSCs (Che *et al*, 2023). ROS can directly damage hepatocytes, leading to the release of more DAMPs, which further amplify the inflammatory response. Additionally, oxidative stress can activate HSCs, enhance TGF-β signaling, and promote collagen production (Luedde *et al*, 2014). As liver fibrosis progresses, the normal liver architecture is increasingly disrupted. The loss of hepatocytes and their replacement with fibrotic tissue diminishes the capacity to detoxify the blood and produce proteins like albumin and clotting factors (Berasain *et al*, 2023). Moreover, the excessive deposition of ECM alters the structure of the hepatic sinusoids, leading to increased resistance to blood flow through the liver. In a healthy liver, the sinusoids have a fenestrated endothelium. During fibrosis, these pores are lost in a process known as sinusoidal capillarization, where the endothelium becomes less permeable and more restrictive to the movement of solutes and cells (Baiocchini *et al*, 2019). Moreover, in advanced liver fibrosis, bands of scar tissue are formed, called fibrous septa. These septa can bridge portal tracts and central veins, dividing the liver into isolated nodules (Parola & Pinzani, 2019). This further obstructs blood flow and contributes to increased resistance. In response to these issues, new blood vessels are formed, particularly around fibrotic tissue. The new vessels are an attempt to bypass the fibrotic areas, however, they are often abnormal and contribute to the dysregulated blood flow within the liver (Bocca *et al*, 2015). As a result of the alteration in liver vascularization, the blood pressure in the portal system is increased leading to portal hypertension (Iwakiri & Trebicka, 2021). This causes the redirection of the blood and fluids into other tissues potentially inducing bleeding, commonly in the esophagus and stomach, ascites, exacerbated by the decreased production of albumin, splenomegaly, which can lead to cytopenia, and hepatic encephalopathy, due to the accumulation of toxins (Iwakiri & Trebicka, 2021).

1.8.2 Etiology of liver fibrosis

The etiology of liver fibrosis can be broadly categorized into toxic fibrosis and biliary fibrosis based on the underlying cause. Toxic fibrosis results from direct hepatocyte damage due to viral infections, toxic substances, or metabolic alterations. Toxic fibrosis is characterized by the deposition of ECM more in the pericentral and perisinusoidal regions (Kisseleva & Brenner, 2021). Chronic viral hepatitis, in particular HBV and HCV are the major causes of hepatotoxic fibrosis worldwide (El-Serag, 2012). HBV and HCV directly infect hepatocytes inducing oxidative stress, lipid peroxidation, and mitochondrial dysfunction (Loureiro *et al*, 2023). Moreover, chronic infection causes liver inflammation, activating cytotoxic T cells, which kill infected cells (Zheng *et al*, 2023b). The immune-mediated damage, combined with direct viral effects, leads to chronic inflammation, and fibrosis that can progress to cirrhosis and HCC (Cho & Cheong, 2021). Fibrosis observed with chronic infection creates bridging septa between portal and central veins with marked angiogenesis. Another leading cause of toxic liver fibrosis is excessive alcohol consumption which causes alcoholic liver disease (ALD). The liver metabolizes alcohol, producing toxic metabolites like acetaldehyde, which generate ROS causing oxidative stress, hepatocyte damage, and inflammation (Teschke, 2018). Moreover, alcohol induces the synthesis of fatty acids and cholesterol leading to the formation of steatosis (Gao & Bataller, 2011). Over time, this damage leads to inflammation, activation of HSCs, and fibrosis. Continued alcohol consumption can progress from ALD to alcoholic steatohepatitis with fibrosis, and eventually to cirrhosis and HCC (Gao & Bataller, 2011). Metabolic dysfunction–associated steatotic liver disease (MASLD) is a spectrum of liver conditions associated with metabolic syndrome, obesity, insulin resistance, and type 2 diabetes (Yanai *et al*, 2023). The accumulation of fatty acids, triglycerides, or cholesterol in hepatocytes leads to lipotoxicity, oxidative stress, and the generation of ROS. These ROS cause cellular damage and promote inflammatory responses, which can activate HSCs and cause fibrosis formation (Liu *et al*, 2016). MASLD ranges from simple steatosis to MASH, where inflammation and fibrosis occur. MASH is becoming increasingly prevalent in the population due to rising rates of obesity and metabolic syndrome globally (Yanai *et al*, 2023). In both ALD and MASH, fibrosis deposition occurs mainly around sinusoids and between hepatocytes. Autoimmune hepatitis (AIH) is an autoimmune disease characterized by toxic fibrosis. It

is caused by an autoimmune response against hepatocytes, leading to chronic inflammation and liver damage. If untreated, AIH can progress to cirrhosis and end-stage liver failure (Muratori *et al*, 2023). Finally, different genetic diseases can develop with toxic fibrosis. For example, alpha-1 antitrypsin deficiency is one of the most common genetic disorders, caused by an impairment in protein alpha-1 antitrypsin activity. In healthy conditions, alpha-1 antitrypsin protein is expressed by hepatocytes, and released in the blood to protect lungs from enzyme damage. If mutated, this protein can aggregate inside hepatocytes, leading to damage and fibrosis (Fromme *et al*, 2022). Another example is glycogen storage disease type III (GSD III) that is caused by mutations in the *AGL* gene, encoding for the enzyme amylo-1,6-glucosidase, also called glycogen debranching enzyme. Defects in its activity impair the breakdown of glycogen into glucose. As a result, glycogen accumulates in various tissues, including the liver and muscles (Kishnani *et al*, 2010). This causes skeletal and cardiomyopathy, hepatic dysfunction, and hepatomegaly. Liver damage can progress with fibrosis, cirrhosis, and hepatic failure. Even if the fibrosis induced by GSD III is classified as toxic, due to the direct hepatocyte damage, the fibrosis observed in patients is preferentially periportal with septa bridging between portal areas (Halaby *et al*, 2019). Biliary fibrosis, on the other hand, arises from conditions that cause chronic bile duct injury or obstruction leading to decreased bile flow, called cholestasis. This causes bile accumulation in the liver and in circulation, with liver tissue damage, and inflammation, inducing periportal fibrosis formation (Kisseleva & Brenner, 2021). Biliary fibrosis occurs mostly in autoimmune and genetic diseases. Primary biliary cholangitis (PBC) and primary sclerosing cholangitis (PSC) are two of the most common causes of biliary fibrosis. PBC is an autoimmune disease that targets the small bile ducts within the liver. The destruction of bile ducts leads to cholestasis, chronic inflammation, and fibrosis and can progress to cirrhosis (Gulamhusein & Hirschfield, 2020). PSC is another autoimmune condition, affecting the larger bile ducts both inside and outside the liver. It leads to progressive bile duct strictures and fibrosis, and it is often associated with inflammatory bowel disease (Eaton *et al*, 2013). The main genetic disorders that present biliary fibrosis are cholestatic liver diseases like PFIC2, described above. PFIC2 livers are characterized by inflammation and cholestasis, that progress with ductular proliferation and

sinusoidal/periportal fibrosis. The disease can rapidly progress to cirrhosis and end-stage liver disease (Evason *et al*, 2011).

1.8.3 Liver fibrosis mouse models

Different mouse models have been developed to study the mechanisms and the various types of liver fibrosis (Wu *et al*, 2023), here I will report some representative examples. The most exploited mouse model of toxic liver fibrosis is based on the administration of carbon tetrachloride (CCl_4). CCl_4 is highly hepatotoxic because it is metabolized by the cytochrome P450 2E1 (CYP2E1), generating highly reactive trichloromethyl (CCl_3) radicals. Those radicals cause lipid peroxidation and oxidative stress, leading to hepatocyte damage, inflammation, and fibrosis (Weber *et al*, 2003). The fibrosis obtained with this model is mainly pericentral since CYP2E1 is expressed by hepatocytes in the central zone. Different protocols have been established to generate this mouse model. Usually, CCl_4 is administered with intraperitoneal injections or oral gavage two or three times per week for 6-8 weeks leading to progressive fibrosis (Scholten *et al*, 2015). Another common model of toxic fibrosis is based on thioacetamide (TAA) administration. TAA is a hepatotoxic compound that acts by inducing the formation of reactive metabolites, like sulfur dioxide, leading to hepatocyte necrosis, inflammation, and subsequent fibrosis (Hajovsky *et al*, 2012). TAA is also metabolized by CYP2E1, however, the injury caused is more generalized provoking damage in both zone 1 and zone 3 hepatocytes. This induces the formation of portal-portal and portal-central fibrosis septa, which resembles what is observed in the case of human cirrhosis (Kang *et al*, 2008). TAA is usually administered in drinking water or three times a week by intraperitoneal injection over 8-16 weeks (Wallace *et al*, 2015). To model MASH different diets have been developed. Choline-deficient, L-amino acid-defined (CDAA) diet is a diet without choline that alters lipid metabolism by impairing the production and secretion of very low-density lipoprotein from hepatocytes. After 7-10 weeks of administration, the CDAA diet leads to the accumulation of triglycerides in hepatocytes, steatosis, inflammation, and perisinusoidal fibrosis (Wei *et al*, 2020). Another diet exploited is the high-fat, high-fructose, and high-cholesterol (HFHFC). It induces obesity and insulin resistance leading to steatosis, inflammation, and fibrosis (Kohli *et al*, 2010). However, the development of the disease is slower compared to CDAA since the administration took at least 6 months

to develop fibrosis (Farrell *et al*, 2019). To recapitulate the phenotype of biliary fibrosis the most exploited model is the bile duct ligation (BDL) model. It is based on the surgical ligation of the common extrahepatic bile duct that causes the block of bile flow. This procedure leads to the accumulation of bile in the liver, which triggers inflammation and periportal fibrosis in 21-28 days (Tag *et al*, 2015). Another well-established model of biliary fibrosis is generated with the administration of 3,5-diethoxycarbonyl-1,4-dihydrocollidine (DDC) in the diet for 4-8 weeks (Fickert *et al*, 2007). DDC disrupts the heme metabolism causing the accumulation of porphyrin plugs within the bile duct (Saggi *et al*, 2019). This leads to cholestasis, ductular proliferation, and periportal fibrosis, which resembles human diseases like PSC. Finally, different mouse models of genetic disorders, which recapitulate human conditions with fibrosis involvement, can be exploited. For example, the PFIC2 mouse model recapitulates the human disease described before but with a milder phenotype. *Abcb11* knock-out (*Abcb11*$^{-/-}$) mice accumulate bile acids in hepatocytes and circulation, developing liver injury and cholestatic diseases with ductal proliferation. The disease progressively worsens, with biliary fibrosis starting to develop at 6 months of age (Zhang *et al*, 2012). However, the phenotype remains milder due to alternative bile acid transporters, like *Mdr1a* (Lam *et al*, 2005). Another mouse model of genetic disorder with liver fibrosis is the GSD III one. Like *Abcb11*$^{-/-}$ mice, also this model presents a milder phenotype compared to the human counterpart. Knock-out of *Agl* (*Agl*$^{-/-}$) induced glycogen accumulation in the liver, muscles, and heart. This causes hepatomegaly and periportal fibrosis after 5 months of age (Liu *et al*, 2014).

1.8.4 Liver fibrosis regression and treatments

If the liver damage persists fibrosis can culminate in cirrhosis, with the presence of extensive scars and regenerative nodules that are surrounded by fibrotic septa. Cirrhosis is the latest step of fibrosis and is one of the major risk factors associated with the development of HCC (Parola & Pinzani, 2019). On the contrary, if the underlying causes that induce fibrosis development are eradicated it is possible to obtain fibrosis regression. For example, the antiviral treatment of HBV and HBC, the abstinence from alcohol with ALD, the weight loss and dietary changes with MASH, or the surgical diversion of the bile flow in cholestatic diseases can lead to the activation of anti-fibrogenic mechanisms that can counteract the pro-fibrogenic ones (Marcellin *et al*, 2013; D'Ambrosio *et al*,

2012; Vilar-Gomez *et al*, 2015; Davis *et al*, 2009). However, the time of treatment is crucial since the lower grade of fibrosis can revert more easily compared to the most advanced states (Kisseleva & Brenner, 2021). Fibrosis regression involves different mechanisms starting with the discontinuation of the liver injury, the interruption of HSC activation, and the induction of myofibroblast apoptosis (Kendall *et al*, 2009). Moreover, in fibrosis regression, the balance between MMPs and TIMPs shifts in favor of MMPs, leading to ECM degradation. Macrophages play an important role in this mechanism by switching from a pro-inflammatory to an anti-inflammatory phenotype, secreting MMPs that contribute to the removal of ECM and allow tissue remodeling (Fallowfield *et al*, 2007). They also stop the secretion of pro-inflammatory cytokines, like TNF-α and IL-1, and start the secretion of anti-inflammatory cytokines, like interleukin-10 (IL-10) and interleukin-13 (IL-13) promoting the resolution of inflammation (Ramachandran *et al*, 2012). All these mechanisms contribute to the restoration of normal liver architecture with hepatocyte proliferation, to substitute the scar tissue, and vascular remodeling, with the re-establishment of sinusoidal fenestration. However, the spontaneous regression of fibrosis can be too slow for the prevention of complications in patients. For this reason, over the years, a lot of research has been conducted for anti-fibrotic drugs, targeting metabolic pathways or inflammation involved in fibrosis development, with some candidates in clinical trials. All the drugs tested in clinical and preclinical trials were based on small molecules that can degrade EMC or inhibit key fibrogenic pathways, such as inflammation, TGF-β and PDGF (Shan *et al*, 2022). Nevertheless, all the drugs that reached phase III clinical trials failed to reduce liver fibrosis compared to the placebo groups. Only at the beginning of 2024, positive results of a phase III clinical trial for MASH were announced. Resmetirom, an agonist of the thyroid hormone receptor beta, which is a regulator of cell metabolism, improved fibrosis in a higher percentage of patients compared to the placebo (Harrison *et al*, 2024). Whereas this result is very promising, more effective strategies remain to be developed. Gene therapies have also been tested in preclinical studies. AAV-mediated *in vivo* delivery to the liver was exploited to overexpress or knock down genes or microRNA involved in the fibrotic process. For example, AAVs have been used to overexpress factors to protect hepatocytes from detrimental stimuli, inhibit lipid accumulation in MASH, reduce the inflammatory response, or inhibit the activation of HSCs (Bu *et al*, 2022). However, the abnormal liver

architecture and the alteration of blood flow were demonstrated to be detrimental to hepatocyte transduction mediated by AdV. Fibrosis induced by CCl_4 decreased by half liver transduction while in mice with BDL, the transduction was only 10% of the one obtained in healthy controls. The biodistribution of the vector in other organs was not different comparing mice with or without fibrosis. Anyhow, the transduction was not completely abolished, and by administering AdV encoding for an MMP, the fibrosis was ameliorated (Garcia-Bañuelos *et al*, 2002). On the other hand, in a study exploiting AAV serotype-1, the transduction of hepatocytes was similar in healthy compared to CCl_4- or TAA-treated mice (Sobrevals *et al*, 2012b). The difference in transduction capacity in the presence of liver fibrosis between AdVs and AAVs could be due to the smaller dimension of the latter which could overcome the problems related to ECM deposition and reduction of fenestration. However, also the route of administration was different between the two above-mentioned works since AAVs were administered with injections in the hepatic artery, in the portal vein, or directly into the liver (Sobrevals *et al*, 2012b). In conclusion, a systematic assessment of the *in vivo* gene transfer efficiency to hepatocytes in the presence of different types and stages of liver fibrosis remains to be performed.

2. Aim of the work

The overall goal of this work is to define the optimal strategy for site-specific integration into hepatocytes toward a one-and-done therapy for inherited metabolic diseases in pediatric patients, taking into account the impact of the disease stage. In particular, we aim to:

- Define the best pathway to allow efficient gene editing into the loci involved in two paradigmatic inherited metabolic disorders, namely MSUD and PFIC2, in juvenile mice.
- Determine suitable delivery vehicles and timing of administration for *in vivo* liver-directed gene editing.
- Investigate the impact of liver fibrosis on *in vivo* gene transfer to hepatocytes.

3. Results

3.1 Selection of the best-performing sgRNAs

To set up a CRISPR/Cas9 gene editing strategy for treating PFIC2 and MSUD, we initially performed bioinformatic analysis on the murine and human *DBT* and *ABCB11* genes (Table 1). *DBT* cDNA is 1449 bp in length, while *ABCB11* cDNA is 3966 bp. Since we plan to insert the corrective donor DNA inside the first intron of the two genes, to maintain as much as possible physiological gene regulation, we checked for predicted regulatory regions that were present till around 500bp from the 5' start of the intron. We also confronted the orthologous murine and human introns by BLAST, and they resulted to be very different, indicating the need to design different sgRNA for human and murine cells. There are two described mutations in *DBT* that we would not treat by cDNA insertion in the first intron: a missense mutation in the first exon and a point mutation that alters splicing at the beginning of the first intron (Li *et al*, 2015; Yang *et al*, 2012). No mutations were described for *ABCB11* in the first exon or at the beginning of the first intron.

Table 1. Bioinformatic analysis of human and murine genes

	murine *Dbt*	**human *DBT***	**murine *Abcb11***	**human *ABCB11***
Localization	3G1	1p21	2C2	2q31.1
cDNA length	1449 bp	1449 bp	3966 bp	3966 bp
First intron length	7067 bp	8885 bp	13144 bp	13072 bp
Last predicted regulatory region	550-560 bp	402-418 bp	505-514 bp	400-413 bp

We then exploited Benchling and ChopChop software to design 12 sgRNAs for each murine and human *DBT* and *ABCB11* gene based on predicted efficiency and off-targets. We tested murine sgRNAs exploiting Hepa1.6, a murine hepatoma cell line. We transfected them by nucleofection with a plasmid expressing spCas9 and a plasmid with sgRNAs under the control of the U6 promoter. One week after transfection, we harvested cells and performed T7 and TIDE assays to measure cutting efficiency (Fig. 1A). We detected NHEJ with almost all the sgRNAs selected for *Dbt* and *Abcb11* murine genes,

with some level of discrepancy between the results of the two assays, which was already described in the literature (Sentmanat *et al*, 2018) (Fig. 1B, C). Among the more efficient ones, we chose sgRNA number 11 for *Dbt* and number 9 for *Abcb11,* considering the concordance between T7 and TIDE and the position in the intron. We selected sgRNAs closer to the second exon to maintain the regulatory regions present in the first intron. To test human sgRNAs, we took advantage of Huh7 cells, a hepatocyte-derived carcinoma cell line. Since Huh7 are difficult to transfect, we first transduced them with an LV expressing Cas9 under the control of the PGK promoter (LV.Cas9) (Fig. 1D). In this way, we created a Huh7 cell line with an average of 24.3 vector copies per diploid genome (vector genome copy number, VCN), constitutively expressing Cas9, from now on referred to as Huh7.Cas9. Subsequently, we transfected Huh7.Cas9 using lipofectamine

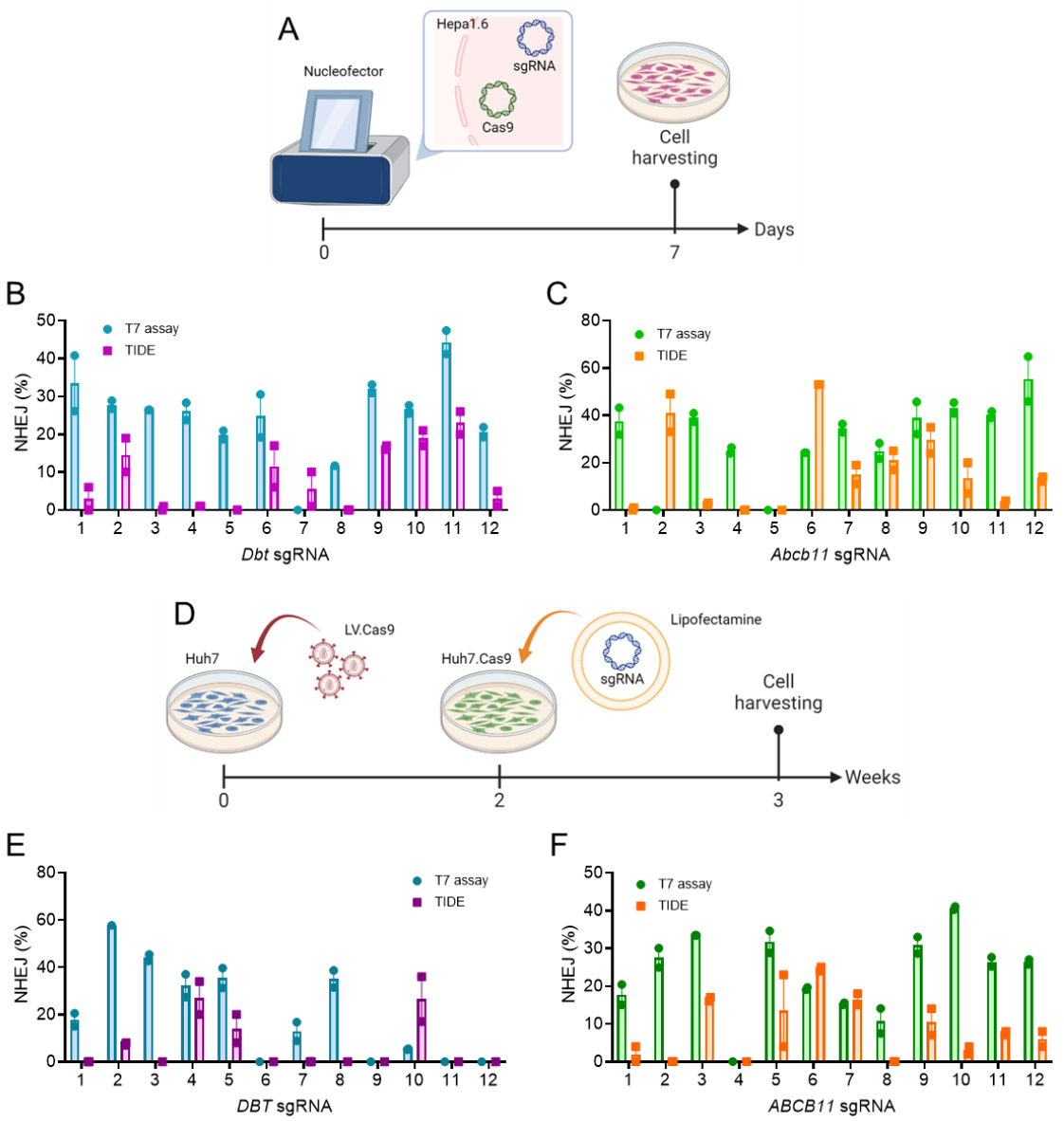


Figure 1. A: Schematics of experimental design with timeline. Cas9 plasmid and sgRNA plasmid 500 ng/each. **B, C**: Individual values and mean ± standard error of the mean (SEM) of percentage (%) of NHEJ of the 12 sgRNA tested for *Dbt* (B) or *Abcb11* (C) gene. **D**: Schematics of experimental design with timeline. LV.Cas9 multiplicity of infection (MOI) 80. sgRNA plasmid 1µg. **E, F**: Individual values and mean ± SEM of percentage (%) of NHEJ of the 12 sgRNA tested for *DBT* (B) or *ABCB11* (C) gene.

with the plasmids expressing sgRNAs (Fig. 1D). One week after transfection, we harvested cells and performed T7 and TIDE assays. Different sgRNAs against *DBT* were poorly efficient, while almost all the ones selected for *ABCB11* were functional (Fig 1E, F). We selected sgRNA number 4 for *DBT* and number 5 for *ABCB11*, considering the concordance between T7 and TIDE and the position in the intron.

3.2 Comparison of HDR- and non-HDR-based donor DNAs in murine and human cell lines

Next, we tested different donor DNAs to understand which pathway allows a higher integration rate in *DBT* and *ABCB11* loci. We compared homology-dependent and independent mechanisms since HDR should allow more precise integration, while MMEJ and HITI have been reported as more efficient in site-specific integrating of exogenous DNA. However, since we aim to treat newborn or juvenile mice where the liver is actively proliferating, we should bypass the main issue of HDR related to its restriction to the S/G2 phase of the cell cycle. We designed four donor DNAs: the first one based on HDR with long homology arms (750 bp, HDR long), the second one also based on HDR but with short homology arms (250 bp, HDR short), the third one based on the PITCh strategy with microhomology arms (20 bp) and sgRNA cut sites (referred as MMEJ), and the last one based on the HITI strategy with only sgRNA cut sites (Fig 2A). We generated donor DNAs by adding a strong splice acceptor sequence to interact with the splice donor of the first exon and a strong poly(A) to end the transcription. To test the different donors, we did not insert the corrective cDNA, but we added the T2A sequence followed by mCherry (Fig. 2A). With these characteristics, we obtained four different constructs for both *Dbt* and *Abcb11* murine gene, cloned them into LV constructs and produced them as IDLVs.

We transduced Hepa1.6 cells with IDLV carrying the described constructs, and 12 hours later, we transfected them by nucleofection with RNP composed of Cas9 and the previously selected sgRNA (Fig. 2B). One-week post-transfection, we harvested cells and performed a digital droplet PCR (ddPCR) to quantify the integration. We designed ddPCR primer and probes on the junctions between the genome and the inserted DNA (Fig. 2C). Due to technical issues, we quantified the product of integration with the 3' junction for the murine *Dbt* gene, while for murine *Abcb11* and the two human genes we measured the 5' junction. The integration was then normalized with the quantification of murine or human genomic DNA by ddPCR on the *Sema3a* or the *TERT* genes, respectively. We then multiplied the results by 2, to quantify the percentage of integrations per diploid genome.

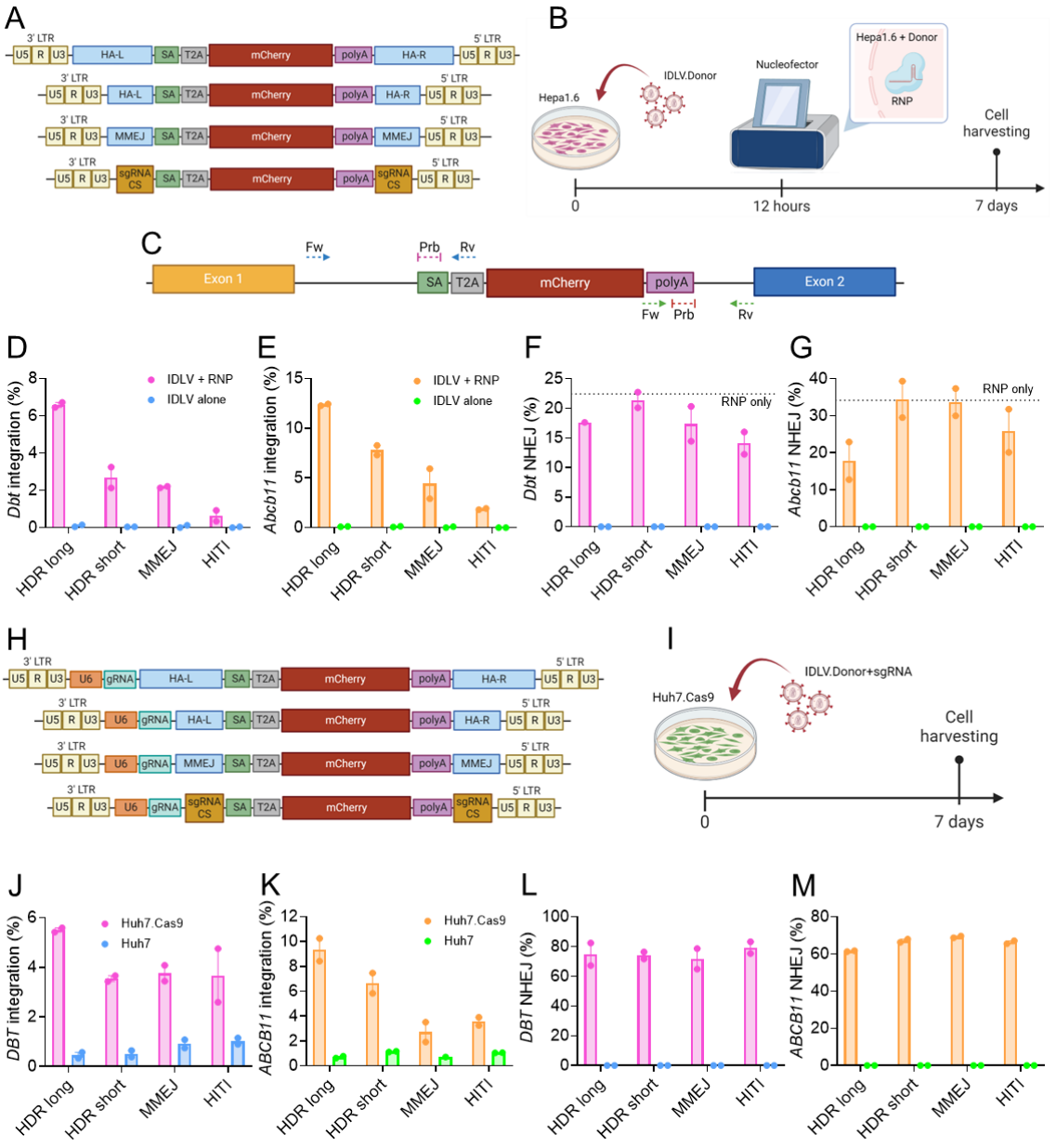


Figure 2. A: Schematic representation of murine donor DNA constructs generated for *in vitro* testing. Homology arm left (HA-L). Splice acceptor (SA). Homology arm right (HA-R). sgRNA cut site (sgRNA CS). **B**: Schematics of experimental design with timeline. IDLV.Donor MOI 150. Cas9 protein 10µg. sgRNA 2.4µg. **C**: Schematic representation of the donor DNA insertion into the first intron, with dotted blue or green arrows indicating a couple of primers (forward, Fw, and reverse, Rv) and a red dotted line indicating probes (Prb). **D, E**: Individual values and mean ± SEM of percentage (%) of integration measured with ddPCR on the junction normalized on the *Sema3a* gene. (D) *Dbt*, (E) *Abcb11*. **F, G**: Individual values and mean ± SEM of percentage (%) of NHEJ of samples treated with the different donor DNAs for *Dbt* (F) or *Abcb11* (G) genes. **H**: Schematic representation of human donor DNA constructs generated for *in vitro* testing. **I**: Schematics of experimental design with timeline. IDLV.Donor MOI 200. **J, K**: Individual values and mean ± SEM of percentage (%) of integration measured with ddPCR on the junction normalized on the *TERT* gene. (J) *DBT*, (K) *ABCB11*. **L, M**: Individual values and mean ± SEM of percentage (%) of NHEJ of samples treated with the different donor DNAs for *DBT* (L) or *ABCB11* (M) genes.

We observed the highest integration rate with HDR long donor DNA (6.6% for *Dbt*, 12.3% for *Abcb11*) and the lowest with the HITI-based ones (0.6% for *Dbt*, 1.9% for *Abcb11*) (Fig 2 D, E). We also measured the cutting efficiency obtained with the RNP. NHEJ was comparable between samples targeted with the same sgRNA (around 20% for *Dbt*, around 30% for *Abcb11*). Only samples treated with HDR long donor and RNP against *Abcb11* showed lower NHEJ (17,8%), probably due to higher integration in that locus (Fig. 2F, G). To test the four donor DNA constructs for the human genes, we added the expression cassettes of the sgRNA in the IDLV transgene together with the donor DNA (Fig. 2H). We transduced Huh7.Cas9 cells with IDLVs carrying the described constructs, and one week later, we harvested the cells (Fig. 2I). We measured the percentage of integration by ddPCR, observing the highest integration rate with HDR long donor DNA in both loci (5.5% for *DBT*, 9.3% for *ABCB11*) (Fig. 2J, K). Moreover, we measured the cutting efficiency, observing similarities between all the samples (around 70% for *DBT*, around 60% for *ABCB11*) (Fig. 2L, M). These data suggest that the HDR pathway allows a higher integration rate in both murine and human hepatoma cell lines.

3.3 Comparison of HDR- and non-HDR-based donor DNAs administration to juvenile Cas9 mice

We then tested the selected sgRNA and all the designed donor DNA configurations *in vivo*. To this end, we exploited Cas9 transgenic mice that express constitutively Cas9 under the control of a CAG promoter (Platt *et al*, 2014). We generated AAVs and IDLVs constructs carrying the murine donor DNAs described above coupled with the expression cassette for sgRNA. We administered 2-week-old Cas9 mice with AAVs carrying the different donor DNAs, or the IDLV carrying HITI-based donor DNA (Fig 3A). We selected a single IDLV to allow comparison with AAV as delivery vehicle for the donor DNA in this setting. In parallel, we treated age-matched wild-type C57BL/6 mice with the same vectors carrying the same donor DNAs as controls for background integration in the absence of Cas9. From now on, all control mice treated with the different donor DNAs will be represented together in the graphs (named C57) since no major differences were detected among donors. Four weeks after AAV or IDLV administration, we harvested the livers and performed molecular analysis (Fig. 3A). Regarding the *Dbt* locus, we detected a high percentage of NHEJ, above 50% with AAV and 42.6% with IDLV (Fig. 3B). We measured integration per diploid genome by ddPCR on the junction normalized with the *Sema3a* gene, as described above. We detected a higher integration rate with non-HDR-based donor DNAs (44% MMEJ, 33.8% HITI) compared to the HDR-based ones (16.3% HDR long, 19.4% HDR short) (Fig. 3C). The comparable integration obtained with long or short homology arms indicates that the presence of longer homology sequence does not confer an advantage to donor DNA. Moreover, we observed integration also by IDLV, but at a lower efficiency compared to AAV (13.6%) (Fig. 3C). We did not detect any integration in control mice administered with any of the donor DNA vectors but without Cas9 expression, suggesting that the presence of Cas9 is crucial to obtain site-specific integrations (Fig. 3C). We measured mCherry expression that followed the same trend of the integration rate for HDR long (0.14-fold on Hprt), HDR short (0.2-fold on Hprt), MMEJ (0.31-fold on Hprt), and HITI carried by IDLV (0.15-fold on Hprt) (Fig. 3D). The exception was the HITI donor carried by AAV, which presented lower mCherry expression compared to the HDR-short (0.17-fold on Hprt). This observation could be caused by the less precise integration that is obtained with the HITI construct. For example, ITRs could be still present when the integration occurs,

resulting in the insertion of the complete AAV that may be less efficient for the expression of the transgene (Fig. 3D). Low level of mCherry expression was detected in control mice treated only with donor DNA vectors, likely due to non-specific integrations into expressed genes. This indicates that the observed mCherry expression in treated mice almost entirely derives from site-specific integrations of the donor DNA in the correct conformation. The donor DNA insertion into the first intron was followed by a 1.5-fold reduction in expression of the endogenous *Dbt* gene (Fig. 3E).

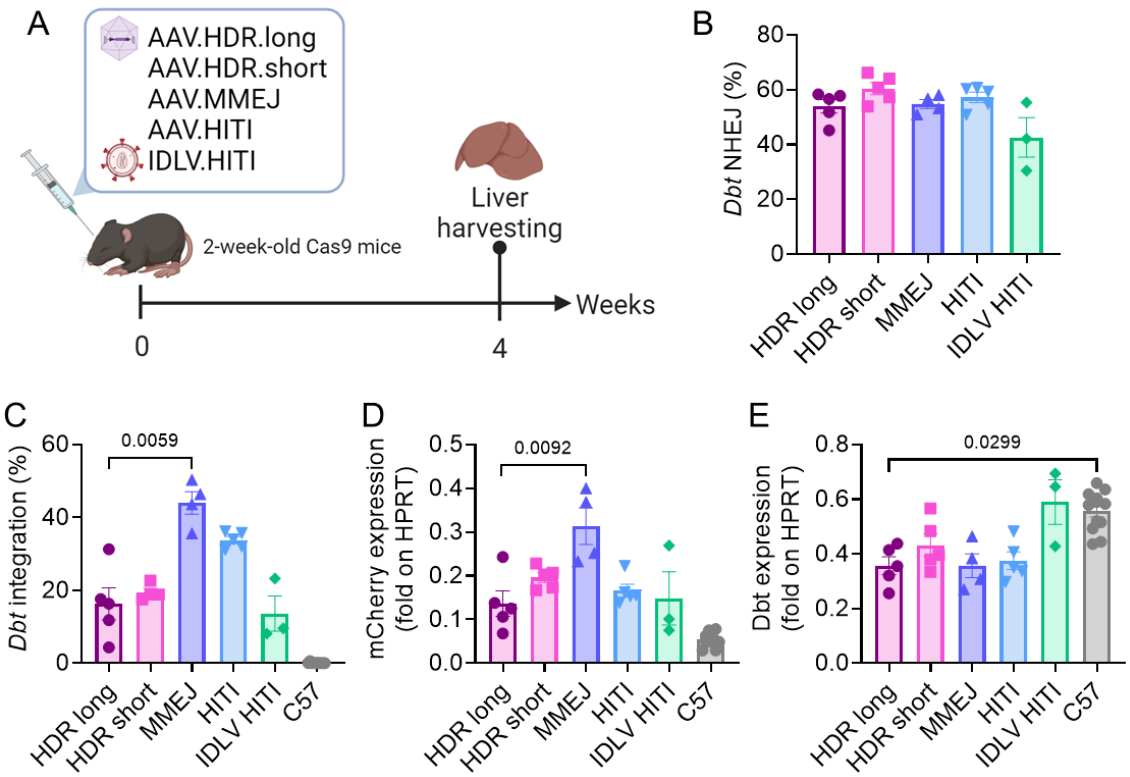


Figure 3. A: Schematics of experimental design with timeline. AAV.donors $3.5x10^{13}$ vg/kg. IDLV.HITI $1x10^{11}$ transducing units (TU)/kg. **B**: Individual values and mean ± SEM of percentage (%) of NHEJ of samples treated with the different donor DNAs. (Kruskal-Wallis test, *p* values not shown are not significant). **C**: Individual values and mean ± SEM of percentage (%) of integration measured with ddPCR on the junction normalized on the *Sema3a* gene. (Kruskal-Wallis test, significant *p* values are shown). **D**: Individual values and mean ± SEM of mCherry expression in the liver normalized on the expression of Hprt. (Kruskal-Wallis test, significant *p* values are shown). **E**: Individual values and mean ± SEM of Dbt expression in the liver normalized on the expression of Hprt. (Kruskal-Wallis test, significant *p* values are shown).

Regarding the *Abcb11* locus we selected two donor DNAs, the HDR short, since *Abcb11* cDNA is long and would not fit inside an AAV if long homology arms are present, and the HITI-based, since we decided to prioritize one representative mechanism of non-

HDR based integration. We administered 2-week-old Cas9 mice with AAV carrying these two donor DNAs, then collected livers 4 weeks after AAV administration (Fig. 4A). As described before, we treated in parallel age-matched wild-type C57BL/6 mice with the same vectors carrying the same donor DNAs as controls for background integration. We detected around 30% of NHEJ with both vectors (Fig. 4B). We observed 5.66% of integration with HDR, 9.15% with HITI, and no site-specific integrations in controls (Fig. 4C). Nevertheless, both the mCherry positive liver area and the mCherry expression were higher when using HDR-based donor DNA compared to HITI (1.3-fold difference) (Fig. 4D, E). Also in this case, we detected very low mCherry expression in control mice, probably due to non-specific integrations. The endogenous *Abcb11* expression was similar to controls, probably due to the low rate of integration and the high level of *Abcb11* expression (more than 3-fold over Hprt) (Fig. 4F). To increase the integration rate, we treated mice doubling the dose of AAV ($7x10^{13}$ vg/kg compared to $3.5x10^{13}$ vector genomes (vg)/kg of the previous experiment). The NHEJ was similar in the two experiments (Fig 4G). However, the integration rate doubled using the HDR-based donor (11.9%) but not with the HITI-based one (6.8%) (Fig. 4H). The significantly higher integration rate obtained with HDR was mirrored by significantly higher mCherry positive liver area (1.4-fold) and mCherry expression (1.9-fold) (Fig. 4I, J). Endogenous Abcb11 expression was not different compared to control mice also in this case (Fig. 4K). These data show that IDLVs can be used as delivery vehicles for donor DNA, however, they result in lower integration compared to AAVs in this setting. Non-HDR-based donor DNA integrates more efficiently at a lower vector dose, however, the higher integration rate does not result in higher transgene expression. On the contrary, increasing the doses of AAVs resulted in more efficient site-specific integration and higher expression of the integrated reporter with HDR-based donors.

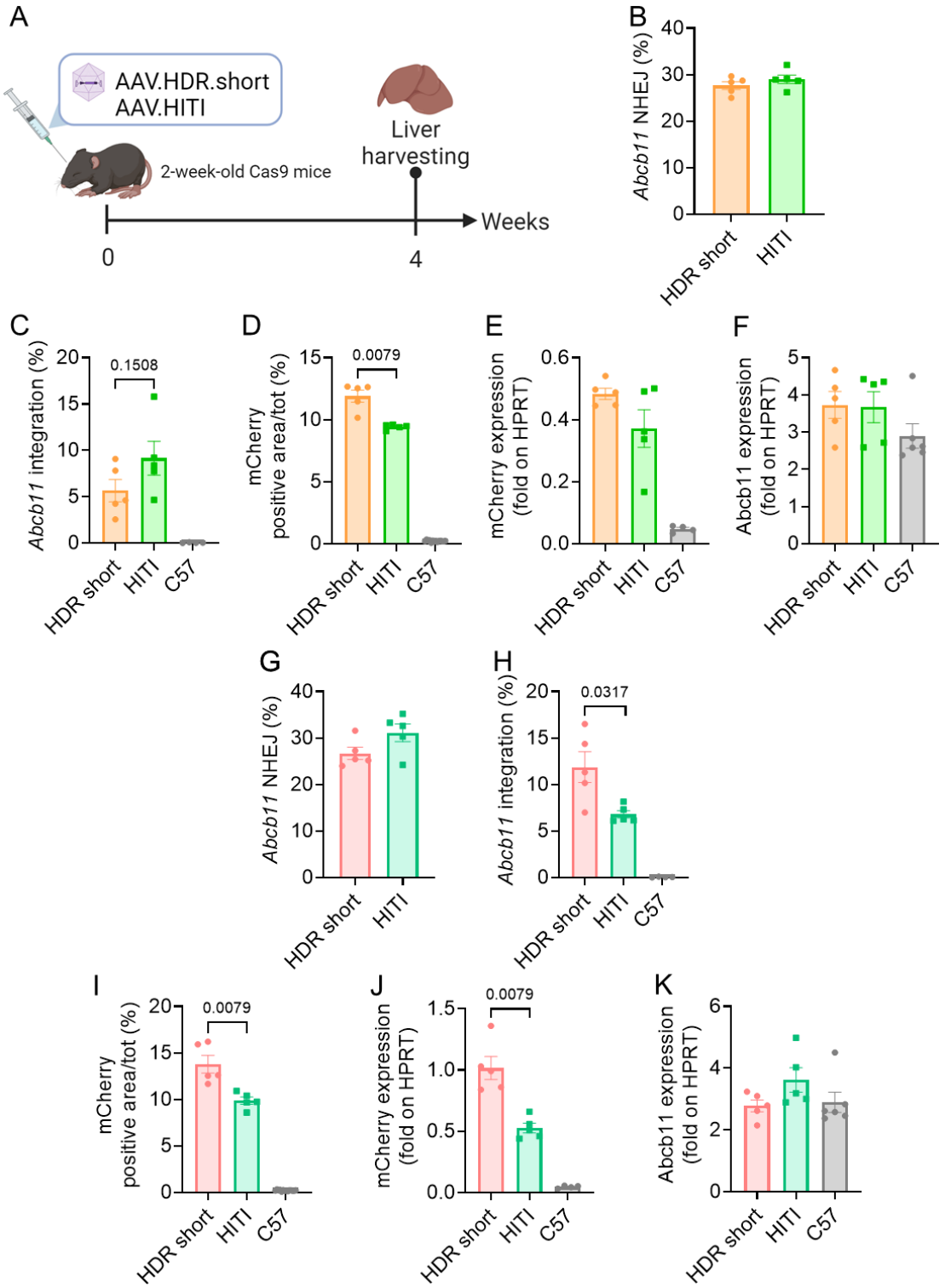


Figure 4. A: Schematics of experimental design with timeline. AAV.donors $3.5x10^{13}$ vg/kg. **B**: Individual values and mean ± SEM of percentage (%) of NHEJ of samples treated with the different donor DNAs. (Mann-Whitney test, *p* values not shown are not significant). **C**: Individual values and mean ± SEM of percentage (%) of integration measured with ddPCR on the junction normalized on the *Sema3a* gene. (p=0.1508, Mann-Whitney test). **D**: Individual values and mean ± SEM of percentage (%) of mCherry-positive liver area expressed over the total area analyzed (p=0.0079, Mann-Whitney test). **E**: Individual values and mean ± SEM of mCherry expression in the liver normalized on the expression of Hprt. (Mann-Whitney test, *p* values not shown are

not significant). **F**: Individual values and mean ± SEM of Abcb11 expression in the liver normalized on the expression of Hprt. (Kruskal-Wallis test, significant *p* values are shown). **G**: Individual values and mean ± SEM of percentage (%) of NHEJ of samples treated with the different donor DNAs. (Mann-Whitney test, *p* values not shown are not significant). **H**: Individual values and mean ± SEM of percentage (%) of integration measured with ddPCR on the junction normalized on the *Sema3a* gene. (p=0.0317, Mann-Whitney test). **I**: Individual values and mean ± SEM of percentage (%) of mCherry-positive liver area expressed over the total area analyzed (p=0.0079, Mann-Whitney test). **J**: Individual values and mean ± SEM of mCherry expression in the liver normalized on the expression of Hprt. (p=0.0079, Mann-Whitney test). **K**: Individual values and mean ± SEM of Abcb11 expression in the liver normalized on the expression of Hprt. (Kruskal-Wallis test, significant *p* values are shown).

3.4 Comparison of HDR- and non-HDR-based donor DNAs administration to newborn Cas9 mice

To test if the different donor DNA configurations resulted in different editing outcomes in newborn compared to juvenile mice, we administered the vectors used in the previous experiments to 2-day-old Cas9 mice and collected livers 6 weeks after vector administration (Fig. 5A). As described in the previous experiment (paragraph 3.3), we treated in parallel age-matched wild-type C57BL/6 mice with the same vectors carrying the same donor DNAs as controls for background integration in the absence of Cas9. Regarding the *Dbt* locus, for technical reasons related to maximum injectable volume, AAV.MMEJ ($2x10^{13}$ vg/kg) and IDLV.HITI ($5x10^{10}$ TU/kg) doses were lower compared to the previous experiment. We observed around 50% of NHEJ with all AAVs and only 20% with IDLV (Fig. 5B). The highest integration rates were observed with HITI (43.3%) and HDR short (36.2%), while HDR long and MMEJ donor DNA configuration showed the lowest (around 21%) (Fig. 5C). Delivery of HITI-based donor DNA by IDLV did not result in detectable integrations (Fig. 5C). Also in this context we did not observe any advantage in using donor DNA with long compared to short homology arms. The mCherry expression levels followed the same trend of the integration, with higher expression obtained by the HDR short and HITI donor DNA design (Fig. 5D). The endogenous Dbt expression was reduced of around 1.4-fold with HDR long, HDR short and MMEJ carried by AAVs, while there were no differences with HITI-based donor (Fig. 5E). Regarding *Abcb11* locus, we obtained around 28% of NHEJ (Fig. 5F), with slightly higher integration exploiting HDR (5.9%) compared to HITI (3.4%) (Fig. 5G). Similarly to previous experiments, the mCherry positive liver area and expression paralleled the integration rates, with a 1.5-fold difference between the two donors (Fig. 5H, I). Abcb11

endogenous expression was not altered by the integrations (Fig. 5J). C57 control mice in both Dbt and Abcb11 contexts did not show any site-specific integration (Fig. 5C, G) and low level of mCherry expression (Fig. 5D, H, I), indicating that the observed transgene expression in experimental mice is prevalently due to correct site-specific integration.

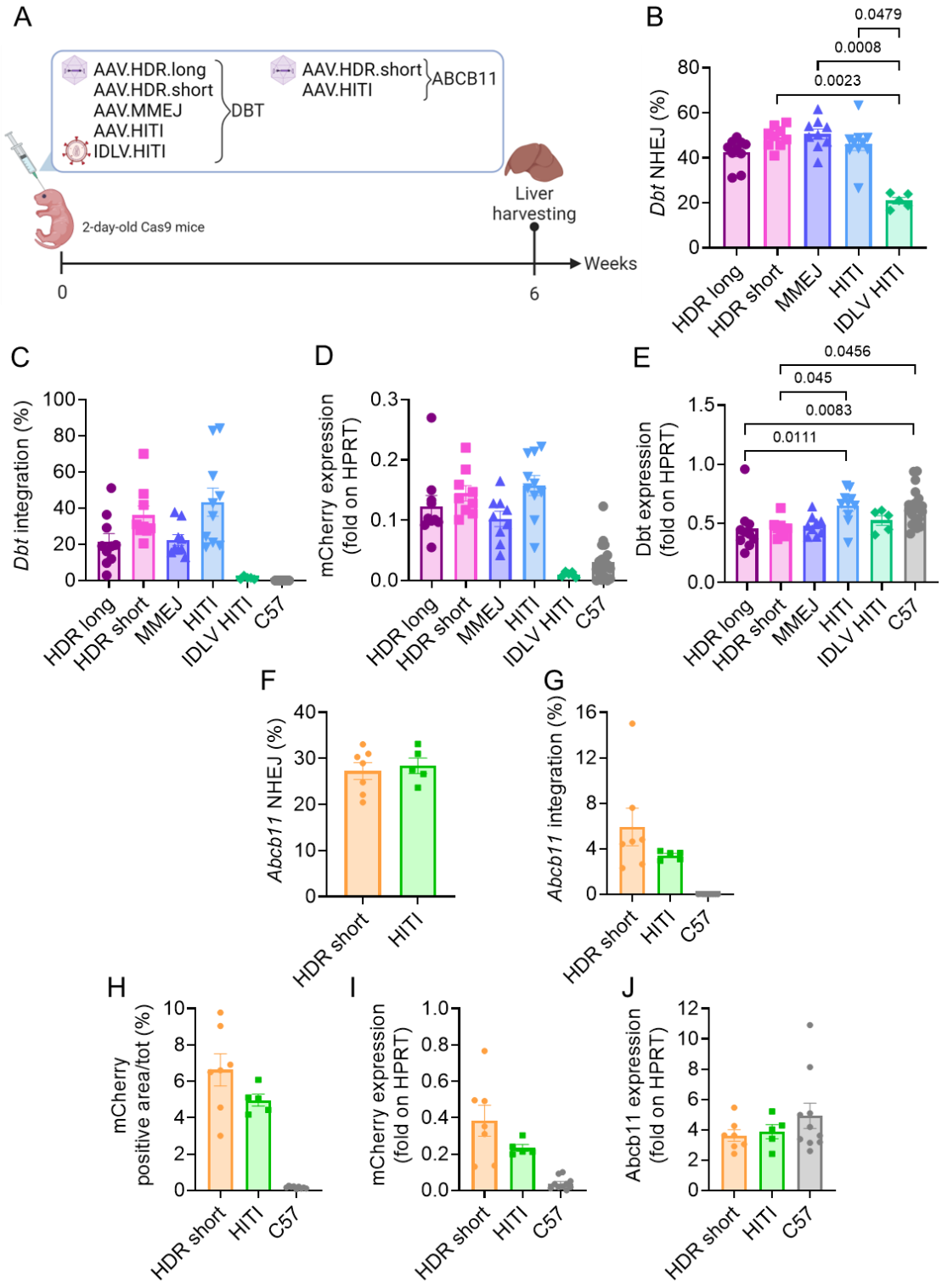


Figure 5. A: Schematics of experimental design with timeline. AAV.HDR.long, AAV.HDR.short, AAV.HITI $3.5x10^{13}$ vg/kg. AAV.MMEJ $2x10^{13}$ vg/kg. IDLV.HITI $5x10^{10}$ TU/kg. **B**: Individual values and mean ± SEM of percentage (%) of NHEJ of samples treated with the different donor DNAs. (Kruskal-Wallis test, significant *p* values are shown) **C**: Individual values and mean ± SEM of percentage (%) of integration measured with ddPCR on the junction normalized on the *Sema3a* gene. (Kruskal-Wallis test, *p* values not shown are not significant). **D**: Individual values and mean ± SEM of mCherry expression in the liver normalized on the expression of Hprt. (Kruskal-Wallis test, *p* values not shown are not significant). **E**: Individual values and mean ± SEM of Dbt expression in the liver normalized on the expression of Hprt. (Kruskal-Wallis test, significant *p* values are shown). **F**: Individual values and mean ± SEM of percentage (%) of NHEJ of samples treated with the different donor DNAs. (Mann-Whitney test, *p* values not shown are not significant). **G**: Individual values and mean ± SEM of percentage (%) of integration measured with ddPCR on the junction normalized on the *Sema3a* gene. (Mann-Whitney test, *p* values not shown are not significant). **H**: Individual values and mean ± SEM of percentage (%) of mCherry-positive liver area expressed over the total area analyzed (Mann-Whitney test, *p* values not shown are not significant). **I**: Individual values and mean ± SEM of mCherry expression in the liver normalized on the expression of Hprt. (Mann-Whitney test, *p* values not shown are not significant). **J**: Individual values and mean ± SEM of Abcb11 expression in the liver normalized on the expression of Hprt. (Kruskal-Wallis test, *p* values not shown are not significant).

These data indicate that different donor DNAs resulted in similar outcomes in newborn and juvenile mice livers, confirming that integrations obtained by the HDR donor DNA configuration resulted in slightly higher reporter gene expression.

3.5 Delivery test of donor DNA with viral vectors in combination with LNP carrying Cas9 and sgRNA

As mentioned above (see paragraph 1.5), the administration of gene editing machinery with viral vectors presents various risks. For this reason, we decided to test LNP for the delivery of Cas9 mRNA and sgRNA, combined with viral vectors to deliver the donor DNA. We administered AAVs or IDLVs carrying HDR short or HITI donor DNAs to 2-week-old C57BL/6 mice. Two days later we injected the same mice with LNPs carrying Cas9 mRNA and sgRNA, and 4 weeks later we collected the livers (Fig. 6A). As controls

for background integration, we treated in parallel age-matched C57BL/6 mice only with vectors carrying the same donor DNAs, without administering LNP (referred as “donor alone”). Regarding the *Dbt* locus, we observed low efficiency of NHEJ when LNPs were administered after AAVs (5.7% HDR short, 7.5% HITI), while NHEJ was undetectable when LNP were administered after IDLVs (Fig. 6A). This was reflected by an absence of integration with IDLVs, while with AAVs we observed low integration rate (less than 4%) that was 1.8-fold lower with HDR-short (Fig. 6C). This difference was not paralleled in mCherry expression where the two donor DNA carried by AAVs showed comparable levels (0.12-fold on Hprt) (Fig. 6D). In the absence of Cas9 no site-specific integrations were detected (Fig. 6C), however, the background mCherry expression was almost half of the mCherry expression detected in experimental mice (Fig. 6D), in line with the low integration observed. Since the integration rate was low, Dbt endogenous expression was not altered (Fig. 6E). Regarding the *Abcb11* locus, the results were similar to what was obtained for *Dbt*. The efficiency of NHEJ when IDVL was administered before the LNP was completely abolished, while we observed around 16% when LNPs were administered after AAV (Fig. 6F). Integrations were absent with IDLV, while with AAV we showed a 2.2-fold higher integration rate with HITI compared to HDR (Fig. 6G). Again, the higher integration was not paralleled by mCherry positive liver area or mCherry expression, where the HDR donor performed better compared to HITI (1.3-fold in mCherry positive area, 1.9-fold in mCherry expression) (Fig. 6H, I). Similarly to what was observed for the *Dbt* locus, in the absence of Cas9 no site-specific integrations were detected (Fig. 7G), however, the background mCherry expression was considerable (Fig. 7H, I), in line with the low integration observed. The low integration rate did not cause perturbation in Abcb11 endogenous expression (Fig. 6J). These results suggest that LNP transfection efficiency is abolished when IDLV is administered 48 hours before. We confirmed that even if more integrations are obtained with HITI donor DNA, the expression of the integrated transgene is higher when exploiting the HDR pathway. However, the efficiency of integration was lower compared to the one observed with Cas9 transgenic mice.

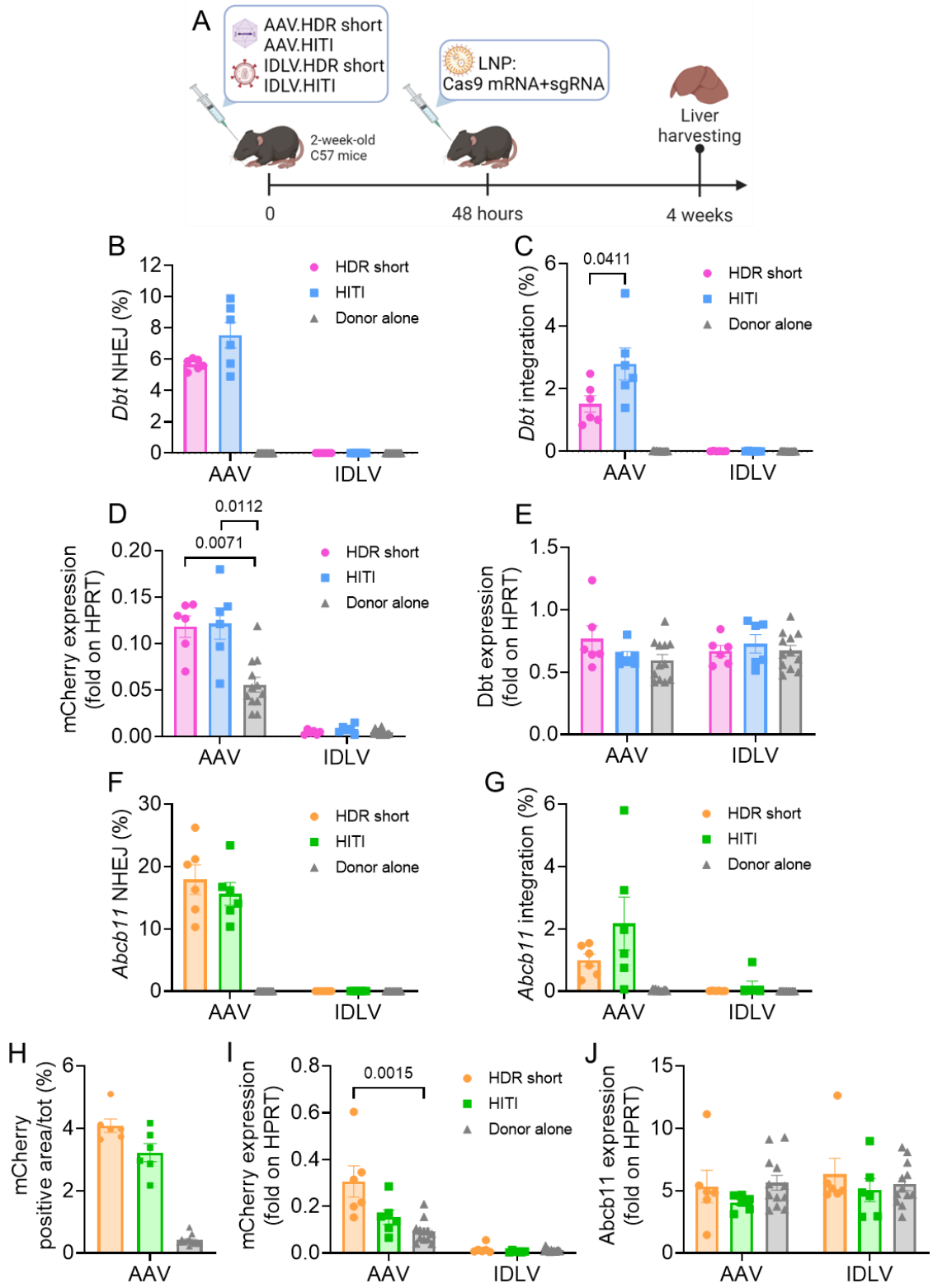


Figure 6. A: Schematics of experimental design with timeline. AAV.donors $5x10^{13}$ vg/kg. IDLV.HDR.short Dbt $4.5x10^{10}$ TU/kg. IDLV.HITI Dbt $2.6x10^{10}$ TU/kg. IDLV.HDR.short Abcb11 $1x10^{11}$ TU/kg. IDLV.HITI Abcb11 $9.4x10^{10}$ TU/kg. LNP Dbt 2.8 mg/kg. LNP Abcb11 3.5 mg/kg. **B**: Individual values and mean ± SEM of percentage (%) of NHEJ of samples treated with the different donor DNAs. (Mann-Whitney test between AAV.HDR.short and AAV.HITI, *p* values not shown are not significant) **C**: Individual values and mean ± SEM of percentage (%) of integration

measured with ddPCR on the junction normalized on the *Sema3a* gene. (Mann-Whitney test between AAV.HDR.short and AAV.HITI, p=0.0411). **D**: Individual values and mean ± SEM of mCherry expression in the liver normalized on the expression of Hprt. (Kruskal-Wallis test between AAV treated mice, p values are shown). **E**: Individual values and mean ± SEM of Dbt expression in the liver normalized on the expression of Hprt. (Kruskal-Wallis test, p values not shown are not significant). **F**: Individual values and mean ± SEM of percentage (%) of NHEJ of samples treated with the different donor DNAs. (Mann-Whitney test between AAV.HDR.short and AAV.HITI, p values not shown are not significant). **G**: Individual values and mean ± SEM of percentage (%) of integration measured with ddPCR on the junction normalized on the *Sema3a* gene. (Mann-Whitney test between AAV.HDR.short and AAV.HITI, p values not shown are not significant). **H**: Individual values and mean ± SEM of percentage (%) of mCherry-positive liver area expressed over the total area analyzed (Mann-Whitney test, p values not shown are not significant). **I**: Individual values and mean ± SEM of mCherry expression in the liver normalized on the expression of Hprt. (Kruskal-Wallis test between AAV treated mice, significant p values are shown). **J**: Individual values and mean ± SEM of Abcb11 expression in the liver normalized on the expression of Hprt. (Kruskal-Wallis test, p values not shown are not significant).

3.6 Assessment of the best time of LNP administration in combination with viral vectors to deliver the gene editing machinery

Since we obtained low to undetectable editing efficiencies with LNP in combination with AAV or with IDLV, respectively, we set up an experiment to investigate different times of administration. We treated 2-week-old C57BL/6 mice with AAV or IDLV carrying HDR short donor for *Abcb11* locus, then we administered LNP with Cas9 mRNA and sgRNA at the same time, 48-hour post or one-week post vector injection (Fig. 7A). We also increased the dose of LNPs to 6 mg/kg. In this experiment, we had three different control groups of age-matched C57BL/6 mice: one treated only with vectors carrying the donor DNAs as control for background integration (referred to as “No LNP”), the second administered only with LNPs carrying Cas9 mRNA and sgRNA as control for the cutting efficiency (referred to as “UT +LNP”), and the third left completely untreated (referred to as “UT No LNP”). We observed a similar NHEJ percentage (around 30%) in all samples including the ones treated with IDLV and the ones administered only with LNP (Fig. 7B). Suggesting that the times of administration tested did not impact LNP transfection capacity. The integration rate was increased compared to the previous experiment. We obtained the highest integration percentage by administering AAV at the same time as LNP (15.1%). The integration rate was reduced when administering LNP 48 hours post AAV (9.1%). The coadministration of IDLV and LNP resulted in low insertion efficiency (1.9%). Administering LNP one week after the viral vector almost completely abolished integration (Fig. 7C). Control mice administered only with vectors

carrying donor DNA did not show site-specific integrations (Fig. 7C). The mCherry positive liver area and mCherry expression confirmed the observation that the concomitant injection is the most effective with 1.7-fold higher positive area and 1.9-fold higher mCherry expression compared to the administration at 48 hours-post viral vectors (Fig. 7D, E).

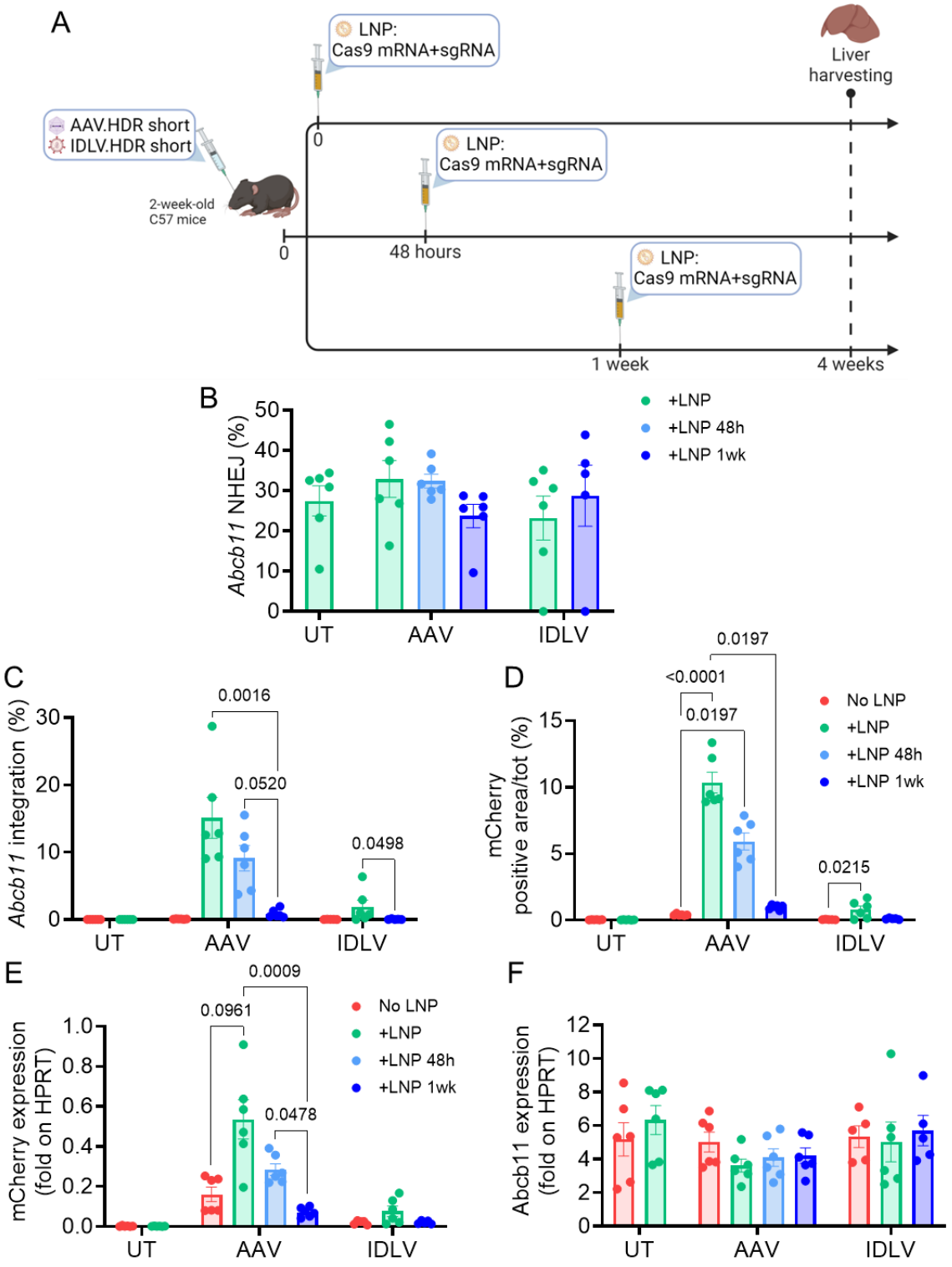


Figure 7. A: Schematics of experimental design with timeline. AAV.HDR short $5x10^{13}$ vg/kg. IDLV.HDR.short Dbt $2.3x10^{10}$ TU/kg. LNP Abcb11 6 mg/kg. **B**: Individual values and mean ± SEM of percentage (%) of NHEJ of samples treated with the different donor DNAs. (Kruskal-Wallis test between AAV treated mice, Mann-Whitney test between IDLV treated mice, *p* values not shown are not significant). **C**: Individual values and mean ± SEM of percentage (%) of integration measured with ddPCR on the junction normalized on the *Sema3a* gene. (Kruskal-Wallis test between AAV treated mice, Mann-Whitney test between IDLV treated mice, significant *p* values are shown). **D**: Individual values and mean ± SEM of percentage (%) of mCherry-positive liver area expressed over the total area analyzed (Kruskal-Wallis test between AAV or IDLV treated mice, significant *p* values are shown). **E**: Individual values and mean ± SEM of mCherry expression in the liver normalized on the expression of Hprt. (Kruskal-Wallis test between AAV or IDLV treated mice, significant *p* values are shown). **F**: Individual values and mean ± SEM of Abcb11 expression in the liver normalized on the expression of Hprt. (Kruskal-Wallis test between AAV or IDLV treated mice, *p* values not shown are not significant).

We obtained 10.4% of mCherry positive area by administering AAV concomitantly to LNP, indicating efficient integration in line with what was observed with Cas9 mice. mCherry-positive liver area and mCherry expression in mice treated only with donor DNAs were not significantly different from the ones obtained in mice treated with LNP 1-week-post vectors (Fig. 7D, E). On the contrary, the coadministration of LNP and viral vectors resulted in significant differences from controls, remarking that it is the most efficient strategy to obtain expression from site-specific correct integration of the transgene. Abcb11 endogenous gene expression was not altered (Fig. 7F). These data indicate that administering LNPs at the same time as viral vectors allows efficient site-specific integration.

3.7 CCl_4-induced liver fibrosis negatively affects LV but not AAV transduction

To study the impact of liver fibrosis on hepatocyte transduction and transfection, we started by setting up a model of toxic liver fibrosis. We administered C57BL/6 (wild-type, WT) mice with CCl_4 for 6 weeks. During CCl_4 treatment, we measured serum levels of alanine transaminase (ALT) and aspartate transaminase (AST) and observed an increase in both liver enzymes over time (ALT >3,000 U/L; AST >2,000 U/L), thus indicating the occurrence of liver damage (Fig. 8A, B). In CCl_4-treated mice, we observed moderate pericentral fibrosis with incomplete and complete fibrous septa, occasionally bridging between central veins, and mild inflammatory cell infiltrate in the liver capsule (Fig. 8C,

Table 2). No major alterations were observed in untreated controls (Table 2). One week after the last CCl_4 injection, we administered LV (VSV.G-pseudotyped) or AAV (serotype 8) to both CCl_4-treated and untreated control mice (Fig. 8D). These vectors express either a secreted reporter transgene (human FIX, hFIX) or a fluorescent reporter transgene

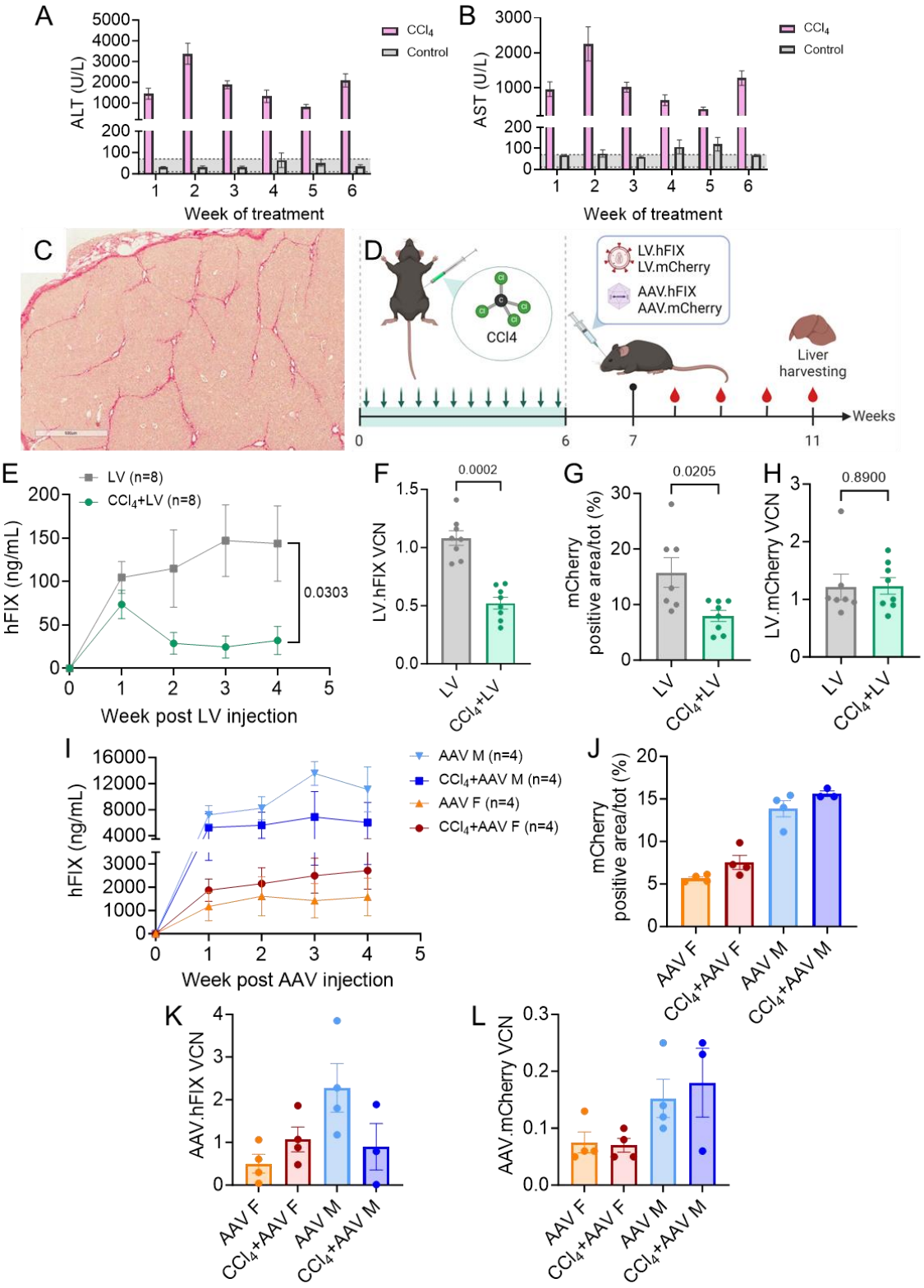


Figure 8. A, B: Mean ± SEM of ALT (A) or AST (B) concentration in the serum of experimental mice. **C**: Representative histological image of a liver section from mice treated with CCl_4 for 6 weeks (bar=600 μm). Picrosirius red staining. **D**: Schematics of experimental design with timeline (green arrows indicate CCl_4 administrations, red drops indicate blood collections). LV.hFIX and LV.mCherry $3.5x10^{10}$ TU/kg. AAV.hFIX $5x10^{11}$ vg/kg. AAV.mCherry $1x10^{11}$ vg/kg. **E**: Mean ± SEM of concentration of hFIX in the plasma of experimental mice at the indicated time after LV.hFIX administration (p=0.0303, Mann-Whitney test at the last time point). **F:** Individual values and mean ± SEM of VCN in the liver of mice administered with LV.hFIX (p=0.0002, Mann-Whitney test). **G**: Individual values and mean ± SEM of percentage (%) of mCherry-positive liver area expressed over the total area analyzed (p=0.0205, Mann-Whitney test). **H**: Individual values and mean ± SEM of VCN in the liver of mice administered with LV.mCherry (p=0.89, Mann-Whitney test). **E**: Mean ± SEM of concentration of hFIX in the plasma of experimental mice at the indicated time after AAV.hFIX administration. **J**: Individual values and mean ± SEM of percentage (%) of mCherry-positive liver area expressed over the total area analyzed. **K, L**: Individual values and mean ± SEM of VCN in the liver of mice administered with (K) AAV.hFIX or (L) AAV.mCherry.

(mCherry) and are referred to hereafter as LV.hFIX, LV.mCherry, AAV.hFIX, and AAV.mCherry (Fig. 8D). The transgenes are expressed under the control of previously described hepatocyte-specific expression cassettes (Milani *et al*, 2019a; Manno *et al*, 2006). We selected LV and AAV doses expected to achieve 5-20% of liver transduction, based on previous experience (Milani *et al*, 2019a; Collaud *et al*, 2019). We longitudinally monitored hFIX amounts in the plasma of treated mice and collected livers at the end of the experiment to determine mCherry expression and VCN 4 weeks after vector administration (Fig. 8D). In LV-treated animals, we observed between 3- and 4-fold lower hFIX output in CCl_4-treated mice compared to controls (Fig. 8E), with a statistically significant difference, paralleled by a reduction of LV VCN in the liver (Fig. 8F). We also observed a significantly 2-fold lower mCherry-positive liver area in CCl_4-treated mice compared to controls (Fig. 8G), without detectable difference in LV VCN in the liver (Fig. 8H). In AAV-treated animals, we analyzed separately males and females since the transduction efficiency is known to be different between the two sexes (Davidoff *et al*, 2003). We did not detect differences in circulating hFIX (Fig. 8I), mCherry-positive liver area (Fig. 8J), or AAV VCN in the liver when comparing mice treated or not with CCl_4 (Fig. 8K, L). These data show that CCl_4-induced pericentral fibrosis caused a reduction in the efficiency of gene transfer into hepatocytes by LV but not AAV.

Table 2. Incidence of microscopic findings in CCl_4-treated mice and controls

	CCl4 3 weeks	Control 3 weeks	CCl4 6 weeks	Control 6 weeks
Total mice analyzed per group	6	5	12	10
Inflammatory mixed cell infiltrate in the capsula				
No abnormality detected	0	5	0	10
Minimal	0	0	2	0
Mild	5	0	10	0
Moderate	1	0	0	0
Inflammatory mixed cell infiltrate in parenchyma				
No abnormality detected	4	2	9	7
Minimal	2	3	2	3
Mild	0	0	1	0
Moderate	0	0	0	0
Perivascular inflammatory lymphohistiocytic cell infiltrate				
No abnormality detected	2	2	2	9
Minimal	1	3	9	1
Mild	3	0	1	0
Moderate	0	0	0	0
Fibrosis in the capsule (Picrosirius red)				
No abnormality detected	0	5	0	10
Minimal	2	0	2	0
Mild	3	0	4	0
Moderate	1	0	6	0
Marked	0	0	0	0
Fibrosis in parenchyme (Picrosirius red)				
Grade 0	0	5	0	10
Grade 1	4	0	1	0
Grade 2	1	0	3	0
Grade 3	1	0	8	0
Grade 4	0	0	0	0

Grade 0: No abnormality detected

Grade 1: minimal pericentral deposition of collagen with or without short septa

Grade 2: mild pericentral deposition of collagen with longer incomplete septa

Grade 3: moderate pericentral deposition of collagen with incomplete and complete bridging septa

Grade 4: marked pericentral deposition of collagen with complete bridging septa and pseudo nodules

3.8 DDC-induced biliary fibrosis negatively affects both LV and AAV transduction

We next fed WT mice with a DDC-supplemented diet for 5 weeks, to induce biliary liver fibrosis. During administration of the DDC diet, we observed the expected elevation of serum ALT and AST (> 1,000 U/L), indicating liver damage (Fig. 9A, B). In DDC-fed mice, we detected cholestasis, marked periportal fibrosis, and complete septa bridging between portal areas, forming pseudo-nodules, sinusoidal lining, and mild to moderate periductular inflammatory cell infiltrate (Fig. 9C, Table 3). We did not detect alterations in untreated control mice (Table 3). One week after the end of DDC treatment, we administered LV.hFIX, LV.mCherry, AAV.hFIX, or AAV.mCherry to DDC-treated and untreated control mice (Fig. 9D). We longitudinally monitored hFIX amounts in the plasma of treated mice and collected livers 4 weeks after vector administration to determine mCherry expression and VCN (Fig. 9D). To reduce the number of experimental animals, we concomitantly delivered AAV.mCherry to CCl_4 or DDC-treated mice, using the same control group for both experiments (as shown in Fig. 8J and Fig. 9J). In LV-treated animals, we observed a remarkable 10-fold reduction in hFIX output at the last time of analysis (Fig. 9E) and a statistically significant 4.5-fold reduction in the mCherry-positive liver area, when comparing DDC-treated mice with controls (Fig. 9F). We detected similar or lower LV VCN in the liver of DDC-fed mice than in controls (Fig. 9G, H). Concerning AAV transduction, we also observed lower circulating hFIX (3.7-fold, Fig. 9I) and mCherry-positive liver area (1.2-fold; Fig.9J) in DDC-pretreated mice compared to controls. To compare fibrotic and non-fibrotic mice, independently of the sex, we normalized each value with the mean of the respective control group (Fig. 9K, L) and showed statistically significant differences. In both AAV.hFIX- and AAV.mCherry-injected mice, we confirmed a reduction of liver transduction, as shown by lower VCN in DDC-fed mice of both sexes (Fig. 9M-P). These data indicate that the presence of DDC-induced periportal fibrosis considerably reduced the efficiency of hepatocyte gene transfer by both LV and AAV.

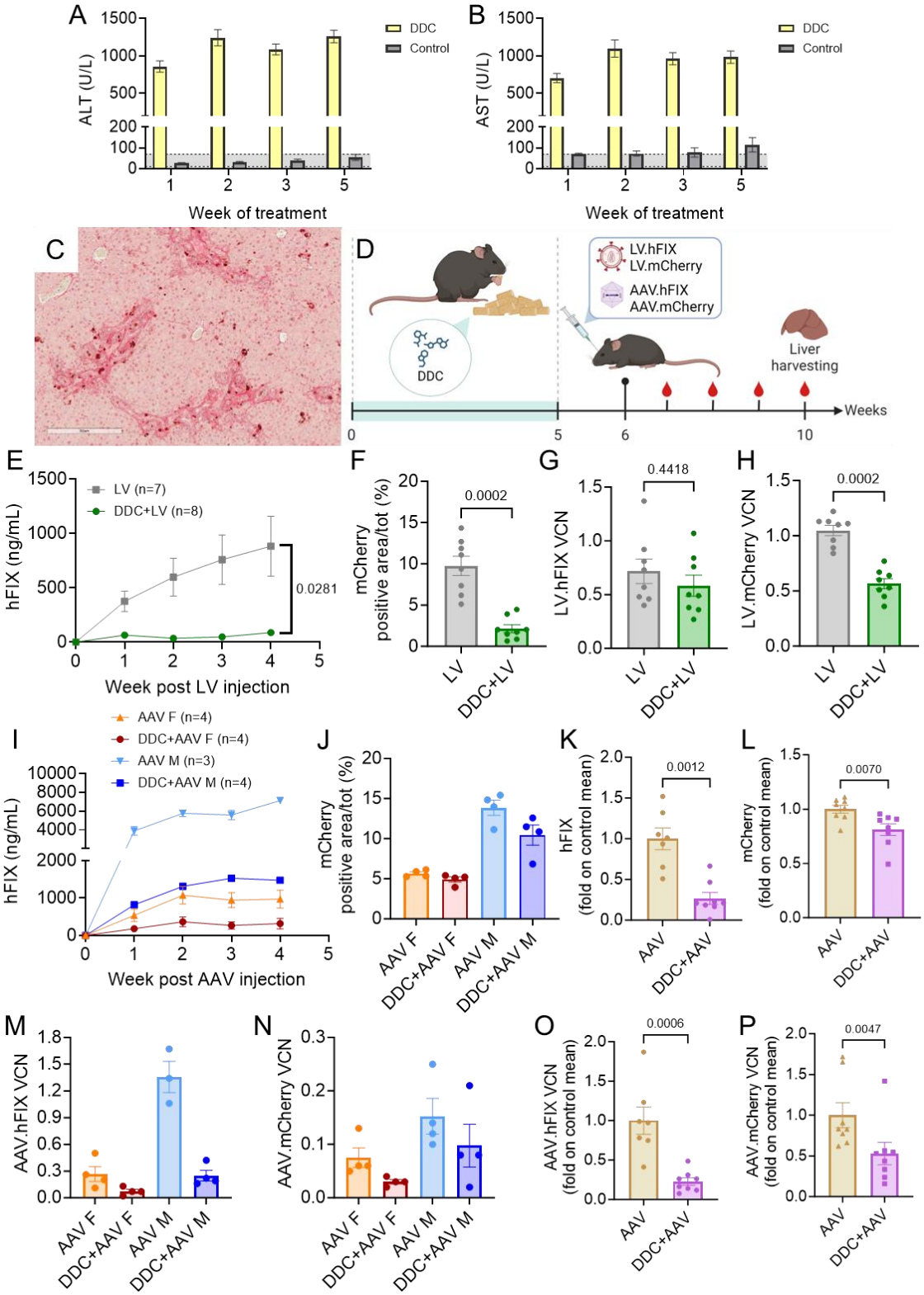


Figure 9. A, B: Mean ± SEM of ALT (A) or AST (B) concentration in the serum of experimental mice. **C**: Representative histological image of a liver section from mice fed with DDC-supplemented diet for 5 weeks (bar=300 µm). Picrosirius red staining. **D**: Schematics of experimental design with timeline (green bar indicates DDC diet, red drops indicate blood collections). LV.hFIX $5x10^{10}$ TU/kg. LV.mCherry $3.5x10^{10}$ TU/kg. AAV.hFIX $2x10^{11}$ vg/kg. AAV.mCherry $1x10^{11}$ vg/kg. **E**: Mean ± SEM of concentration of hFIX in the plasma of

experimental mice at the indicated time after vector administration. (p=0.0281, Mann-Whitney test at the last time point). **F**: Individual values and mean ± SEM of percentage (%) of mCherry-positive liver area expressed over the total area analyzed (p=0.0002, Mann-Whitney test). **G, H**: Individual values and mean ± SEM of VCN in the liver of mice administered with (G) LV.hFIX or (H) LV.mCherry (G, p=0.4418, H, p=0.0002, Mann-Whitney test). **I**: Mean ± SEM of concentration of hFIX in the plasma of experimental mice at the indicated time after vector administration. **J**: Individual values and mean ± SEM of percentage (%) of mCherry-positive liver area expressed over the total area analyzed. AAV F and AAV M, same data as in Fig. 8J, are shown here for comparison. **K, L**: Concentration of hFIX at the last time point analyzed (K) or % of mCherry-positive liver area (L) expressed as fold on the mean of each respective control group (K, p=0.0012, L, p=0.007, Mann-Whitney test). Data are individual values and mean ± SEM. **M, N**: Individual values and mean ± SEM of VCN in the liver of mice administered with (M) AAV.hFIX or (N) AAV.mCherry. **O, P**: AAV VCN expressed as fold on the mean of each respective control group (O, p=0.0006, P, p=0.0047, Mann-Whitney test). Data are individual values and mean ± SEM.

Table 3. Incidence of microscopic findings in DDC-fed mice and controls

	DDC 3 weeks	**Control 3 weeks**	**DDC 5 weeks**	**Control 5 weeks**
Total number analyzed	8	6	10	3
Bile duct hyperplasia				
No abnormality detected	2	6	0	3
Minimal	0	0	0	0
Mild	6	0	4	0
Moderate	0	0	6	0
Cholestasis				
No abnormality detected	0	6	0	3
Minimal	0	0	0	0
Mild	2	0	0	0
Moderate	6	0	4	0
Marked	0	0	6	0
Periductural inflammatory mixed cell infiltrate				
No abnormality detected	0	6	0	3
Minimal	0	0	0	0
Mild	6	0	4	0
Moderate	2	0	6	0
Inflammatory mixed cell infiltrate, in parenchyme				
No abnormality detected	8	6	10	3
Minimal	0	0	0	0
Mild	0	0	0	0
Moderate	0	0	0	0
Fibrosis in parenchyme (Picrosirius red)				
Grade 0	0	6	0	3
Grade 1	0	0	0	0
Grade 2	0	0	0	0
Grade 3	8	0	3	0
Grade 4	0	0	7	0

Grade 0: No abnormality detected

Grade 1: minimal periportal deposition of collagen

Grade 2: mild periportal deposition of collagen

Grade 3: moderate periportal deposition of collagen with incomplete porto-portal bridging septa

Grade 4: marked periportal deposition of collagen with incomplete and complete bridging porto-portal septa, pseudo nodules, sinusoidal lining

3.9 Liver fibrosis reduces LV transduction of hepatocytes and spleen

In the experiments reported above, where LVs were tested in the presence of CCl_4- or DDC-induced fibrosis, VCN measurements were not always concordant with transgene output. This observation is frequent when using LVs to transduce the liver *in vivo*, since they transduce not only hepatocytes but also other liver cell types, while transgene is expressed exclusively by hepatocytes (Milani *et al*, 2019a). We set up an experiment to confirm this observation and to understand the biodistribution of LVs in other organs in the presence of liver fibrosis. We administered CCl_4 for 6 weeks and the DDC diet for 5 weeks to C57 mice as described above. One week after the end of the treatment we injected LV.hFIX or LV.mCherry, and we collected blood 30 minutes, 60 minutes, and 24 hours post-injection to monitor the clearance of LV in circulation (Fig. 10A). Then, we longitudinally measured hFIX amounts in the plasma of treated mice and 5 weeks after LV injection we harvested spleen, kidney, lung, heart, brain and we sorted liver subpopulations, namely hepatocytes, KC, LSEC, HSC, and pDC (Fig. 10A). We determined VCN in all the collected organs and sorted liver cells and we measured the percentage of hepatocytes expressing mCherry with flow cytometry. During CCl_4 and DDC treatment, we monitored the induction of liver damage by elevation of serum ALT, AST (>1,500 U/L for DDC and >3,000 U/L for CCl_4; Fig. 10B, C), and alkaline phosphatase (ALP), elevated just in the presence of biliary damage (>500 U/L for DDC) (Fig. 10D). We confirmed the reduction of hFIX output in CCl_4 and DDC treated mice compared to controls (3- and 65.5-fold respectively) (Fig. 10E). However, by measuring the percentage of mCherry positive hepatocytes, we were able to detect a reduction in transduction just in presence of DDC-induced fibrosis (5.6-fold) and not with CCl_4 treatment (Fig. 10F). Notably, doses of LV were different in this experiment compared to the ones described before (See Fig. 8, 9). By measuring the LV clearance in the blood, we

observed more LV particles 30 minutes and 1 hour after injection in mice treated with CCl_4 compared to the other groups with both LV.hFIX and LV.mCherry, suggesting longer persistence of LV in the blood of mice with pericentral toxic fibrosis (Fig. 10G, H).

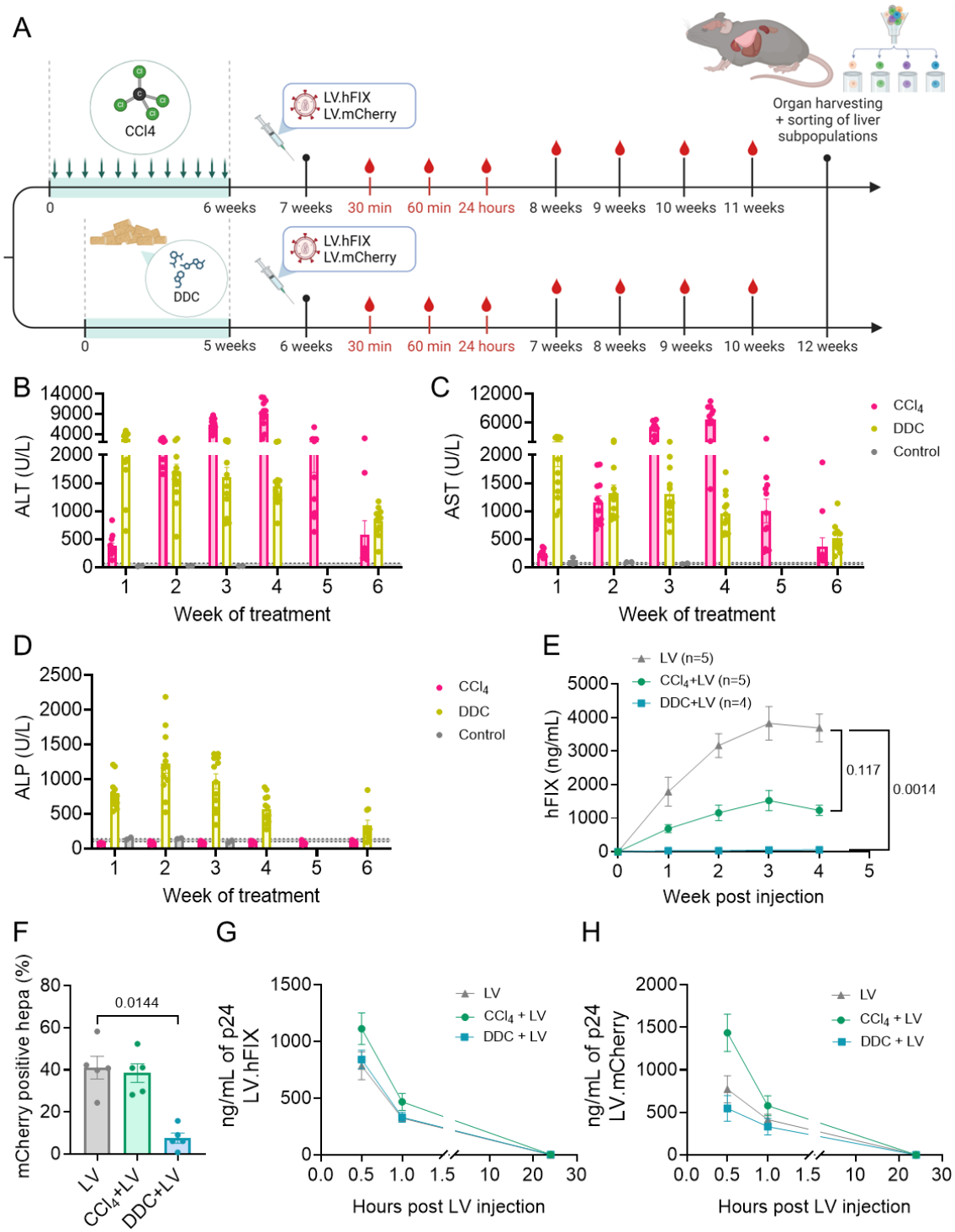


Figure 10. A: Schematics of experimental design with timeline (green arrows indicate CCl_4 administrations, green bar indicates DDC diet, red drops indicate blood collections). LV.hFIX $4.9x10^{10}$ TU/kg and LV.mCherry $4.1x10^{10}$ TU/kg. **B, C, D**: Individual values and mean ± SEM of

ALT (B), AST (C), or ALP (D) concentration in the serum of experimental mice. **E**: Mean ± SEM of concentration of hFIX in the plasma of experimental mice at the indicated time after LV.hFIX administration (Kruskal-Wallis test at the last time point, *p* values are shown). **F**: Individual values and mean ± SEM of percentage (%) of mCherry-positive liver area expressed over the total area analyzed (Kruskal-Wallis test, *p* values are shown). **G, H**: Mean ± SEM of concentration of p24 protein in the serum of experimental mice at the indicated time after LV.hFIX administration.

Then, we assessed VCN in different organs. In the liver, we observed a 1.5-fold VCN reduction with CCl_4 and a 2.3-fold reduction with DDC, for both vectors. Also in the spleen, LV VCN was lower in mice with liver fibrosis compared to controls (LV.hFIX 1.8-fold for both fibrosis, LV.mCherry 1.8-fold with CCl_4, and 1.2-fold with DDC), while kidney, lung, and brain presented very low or no detectable VCN in all mice (Fig. 11A). We then sorted hepatocytes (hepa) by excluding CD45 and CD31 positive cells (Fig. 11B). VCN measured in hepatocytes paralleled as expected the transgene output. For LV.hFIX, we observed a 1.5-fold reduction in hepatocyte VCN with CCl_4 treatment and a 9.6-fold reduction with DDC treatment (Fig. 11C). For LV.mCherry, we observed a 1.2-fold reduction in hepatocyte VCN with CCl_4 treatment and 4.9-fold reduction with DDC treatment (Fig. 11C). We also sorted nPC exploiting surface markers to separate KC, LSEC, pDC, and autofluorescence for HSC (Fig. 11D). We detected VCN in all the subpopulations, without notable differences between the different groups (Fig. 11E). These data suggests that not only liver transduction is reduced in presence of CCl_4- and DDC- induced fibrosis but also spleen transduction. Moreover, we confirmed that hepatocyte VCN reflects the transgene output with both LV.hFIX and LV.mCherry. However, transduction of nPC does not appear to be impacted by liver fibrosis.

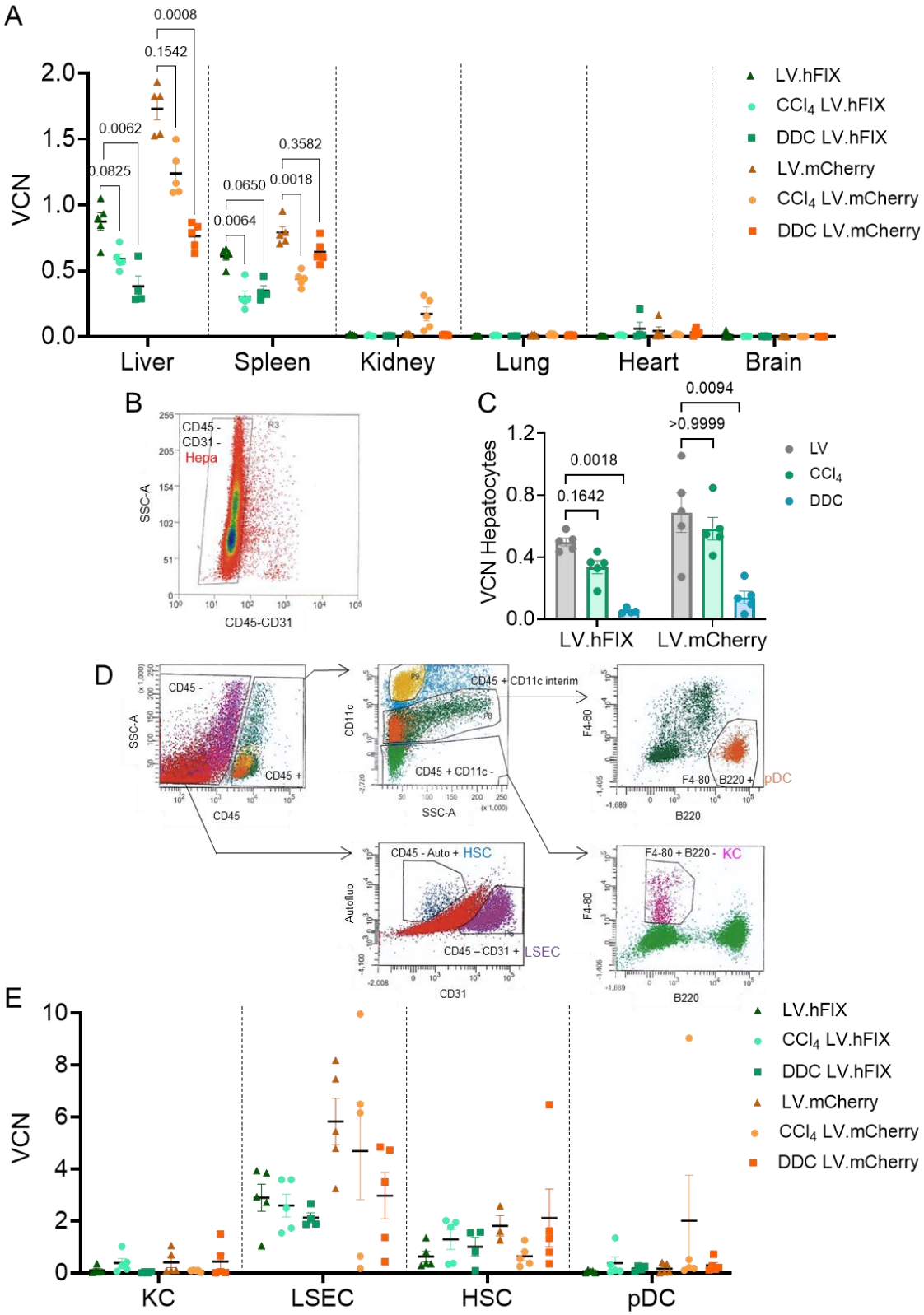


Figure 11. A: Individual values and mean ± SEM of VCN in the liver, spleen, kidney, lung, heart, and brain of mice administered with LV.hFIX (greens) or LV.mCherry (oranges) (Kruskal-Wallis test, *p* values are shown). **B**: Representative dot plot of hepatocyte (hepa) sorting. **C**: Individual values and mean ± SEM of VCN in sorted hepatocytes of mice administered with LV.hFIX or LV.mCherry (Kruskal-Wallis test, *p* values are shown). **D**: Representative scheme of nPC sorting

with dot plots. Sorted populations are indicated in the graphs. **E**: Individual values and mean ± SEM of VCN in KC, LSEC, HSC, and pDC of mice administered with LV.hFIX (greens) or LV.mCherry (oranges).

3.10 Milder fibrosis, induced by CCl_4 or DDC, reduces LV and AAV transduction efficiency

To investigate LV- and AAV-mediated gene transfer in the presence of milder fibrosis, we shortened the time of exposure to CCl_4 or DDC intending to reduce the extent of tissue damage. We administered WT mice with the toxic compounds for 3 weeks. During treatments, we confirmed the induction of liver damage, by showing serum ALT and AST elevation (>1,500 U/L for DDC and >3,000 U/L for CCl_4; Fig. 12A, B). We then analyzed the state of liver fibrosis at the end of the toxic treatments by histopathology. We observed mild pericentral fibrosis in the CCl_4 model and moderate periportal fibrosis induced by the DDC diet (Fig. 12C, D and Tables 2, 3), displaying similar inflammatory cell infiltrate as described above. One week after the last CCl_4 administration or interruption of the DDC diet, we injected LV.mCherry into CCl_4-treated, DDC-treated, or control animals (Fig. 12E). On the other hand, we administered AAV.mCherry only to mice treated with DDC (Fig. 12E), since we did not observe a reduction of AAV transduction in the presence of CCl_4-induced liver fibrosis (see Fig. 8I, J). We observed significant 1.9-fold and 3.2-fold reduction of mCherry-positive liver area in CCl_4+LV and DDC+LV treated mice, respectively (Fig. 12F) paralleled by a reduction of liver VCN (Fig. 12G). Concerning AAV-treated mice, we found a significant 2-fold lower mCherry-positive liver area in DDC-pretreated mice compared to controls of both sexes (Fig. 12H, I). Consistently with the reduced transgene expression, we found a 2-fold reduction in AAV VCN in the liver, as well (Fig. 12J, K). These data show that the milder hepatic damage induced by shorter CCl_4 or DDC treatments negatively influenced both LV and AAV transduction, as the more severe damage induced in the experimental settings mentioned above (see Fig. 8, 9).

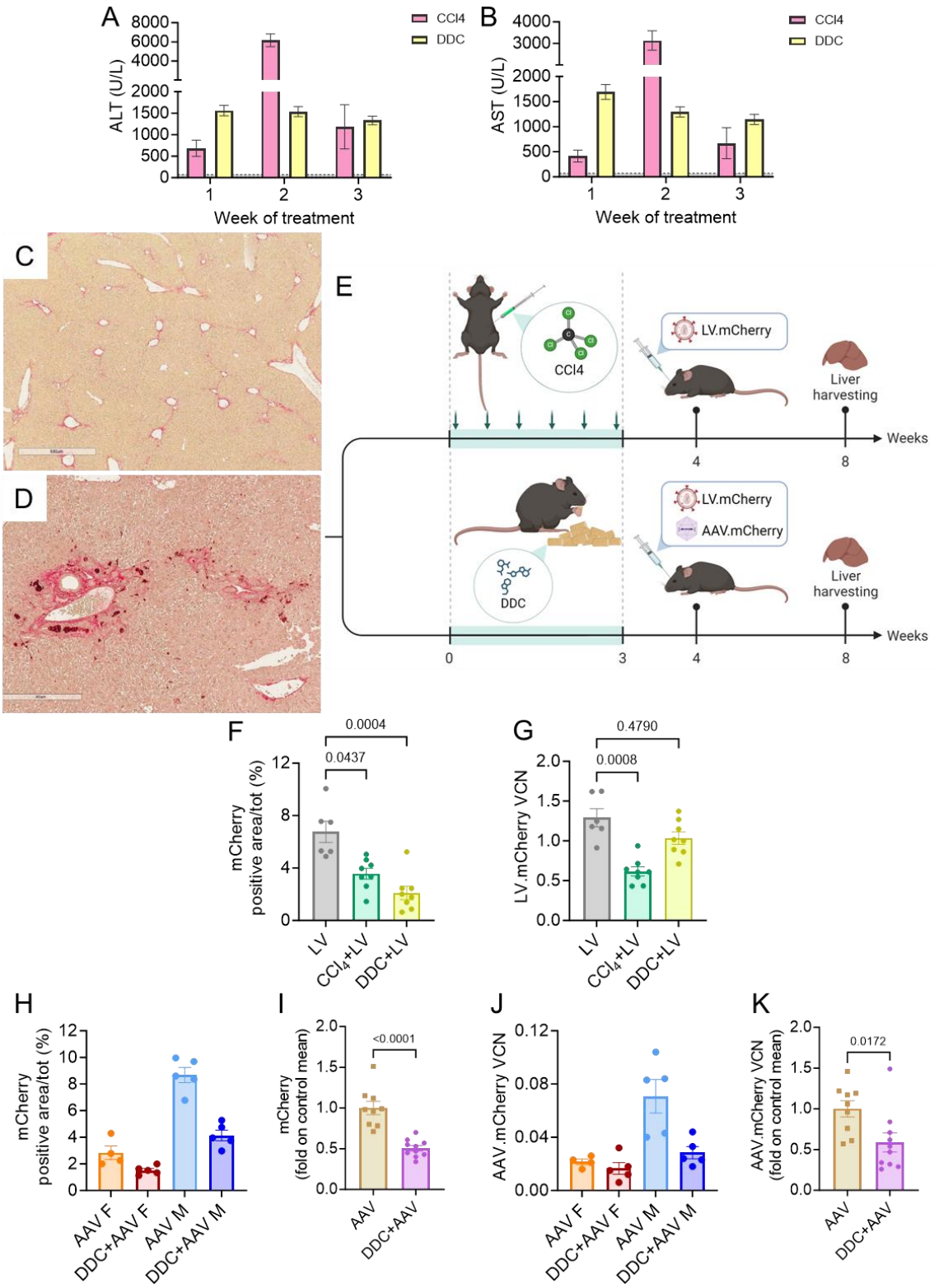


Figure 12. A, B: Mean ± SEM of ALT (A) or AST (B) concentration in the serum of experimental mice. **C, D**: Representative histological images of liver sections from mice treated with CCl_4 or fed with a DDC-supplemented diet for 3 weeks (A, bar=600 µm, B, bar=300 µm). Picrosirius red staining. **E**: Schematics of experimental design with timeline (green arrows indicate CCl_4 administrations, green bar indicates DDC diet). LV.mCherry $1x10^{10}$ TU/kg. AAV.mCherry $1x10^{11}$ vg/kg. **F**: Individual values and mean ± SEM of percentage (%) of mCherry-positive liver area

expressed over the total area analyzed (Kruskal-Wallis test, *p* values are shown). **G**: Individual values and mean ± SEM of VCN in the liver of mice administered with LV.mCherry (Kruskal-Wallis test, *p* values are shown). **H**: Individual values and mean ± SEM of percentage (%) of the mCherry-positive liver area expressed over the total area analyzed **I**: Percentage (%) of the mCherry-positive liver area expressed as fold on the mean of each respective control group ($p<0.0001$, Mann-Whitney test). Data are individual values and mean ± SEM. **J**: Individual values and mean ± SEM of VCN in the liver of mice administered with AAV.mCherry. **K**: AAV VCN expressed as fold on the mean of each respective control group ($p=0.0172$, Mann-Whitney test). Data are individual values and mean ± SEM.

3.11 Hepatocyte transfection mediated by LNP is impaired by CCl_4 and DDC-induced fibrosis

To investigate the impact of fibrosis also on LNP-mediated hepatocyte transfection, we took advantage of a previously described reporter mouse model that expresses TdTomato only after Cre-mediated recombination (Madisen *et al*, 2010). These mice have integrated into the Rosa26 locus a TdTomato constitutive expression cassette with a floxed stop codon that prevents its expression (Fig. 13A). This strain has a C57BL/6 background, thus we exploited the already established protocols to induce liver fibrosis with CCl_4 and DDC administration (See Fig. 8, 9). To monitor the liver damage during treatments, we measured the elevation of serum ALT, AST (>2000 U/L for DDC and >3,000 U/L for CCl_4; Fig. 13B, C), and ALP (>400 U/L with DDC feeding; Fig. 13D). As for previous experiments with vectors, one week after the end of treatments we administered LNP carrying Cre recombinase mRNA (LNP.Cre) and we collected livers 4 weeks after LNP injection to determine TdTomato expression (Fig. 13A). We observed a significant 2-fold reduction in TdTomato positive liver area in mice treated with CCl_4 or DDC when compared to controls (Fig. 13E). These data indicates that both CCl_4-induced toxic pericentral fibrosis and DDC-induced biliary fibrosis negatively affect LNP-mediated gene transfer to the liver.

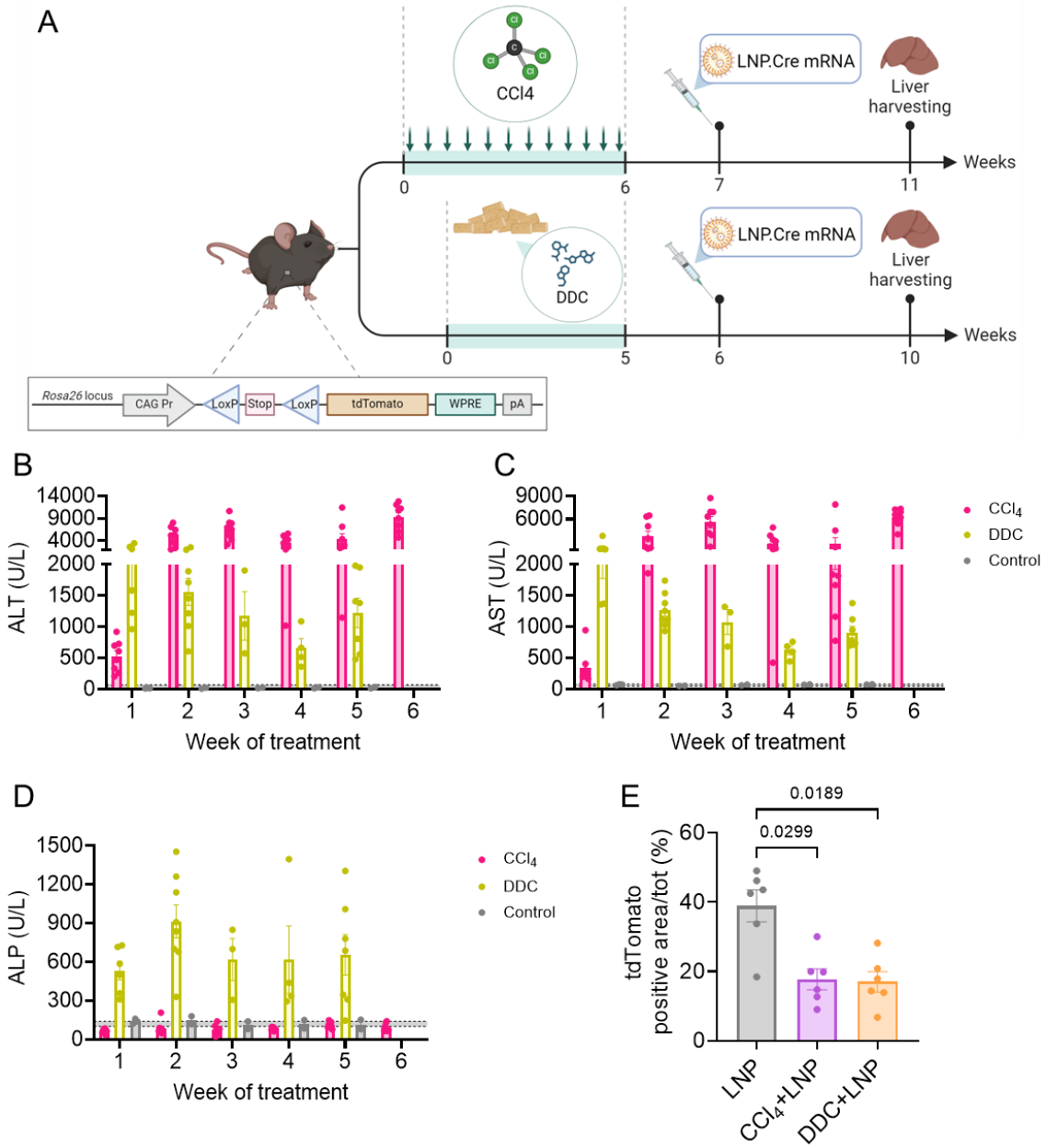


Figure 13. A: Schematics of experimental design with timeline (green arrows indicate CCl_4 administrations, green bar indicates DDC diet). LNP.Cre 0.01 mg/kg. **B, C, D**: Individual values and mean ± SEM of ALT (B), AST (C), or ALP (D) concentration in the serum of experimental mice. **E**: Individual values and mean ± SEM of percentage (%) of TdTomato-positive liver area expressed over the total area analyzed (Kruskal-Wallis test, *p* values are shown).

3.12 Liver fibrosis due to *Abcb11* deficiency slightly reduces LV and AAV transduction

Next, we assessed the impact of liver fibrosis on viral vector transduction in genetic models. We first characterized the state of the liver of 6-month-old *Abcb11*$^{-/-}$ mice or WT age-matched controls by histopathology. In *Abcb11*$^{-/-}$ we observed ductular proliferation,

mild periportal fibrosis with incomplete septa between portal regions, and minimal inflammatory cell infiltrate (Fig. 14A, B, Table 4). None of these alterations were present in control mice (Table 4). We administered *Abcb11*$^{-/-}$ or WT control mice with LV.mCherry or AAV.mCherry and collected livers 2 weeks post vectors injection. In LV-treated mice, we observed a 1.9-fold decrease in the mCherry-positive liver area in *Abcb11*$^{-/-}$ compared to controls (Fig. 14C), paralleled by a similar LV VCN in the liver among the two groups (Fig. 14D). In the livers of mice treated with AAV.mCherry, we detected a 1.3-fold reduction in mCherry-positive tissue area in *Abcb11*$^{-/-}$ compared to WT mice (Fig. 14E), accompanied by a decrease in AAV VCN in the liver (Fig. 14F). These data highlight that the mild periportal fibrosis present in *Abcb11*$^{-/-}$ mice of this age has only a minor negative impact on both LV and AAV mediated gene transfer.

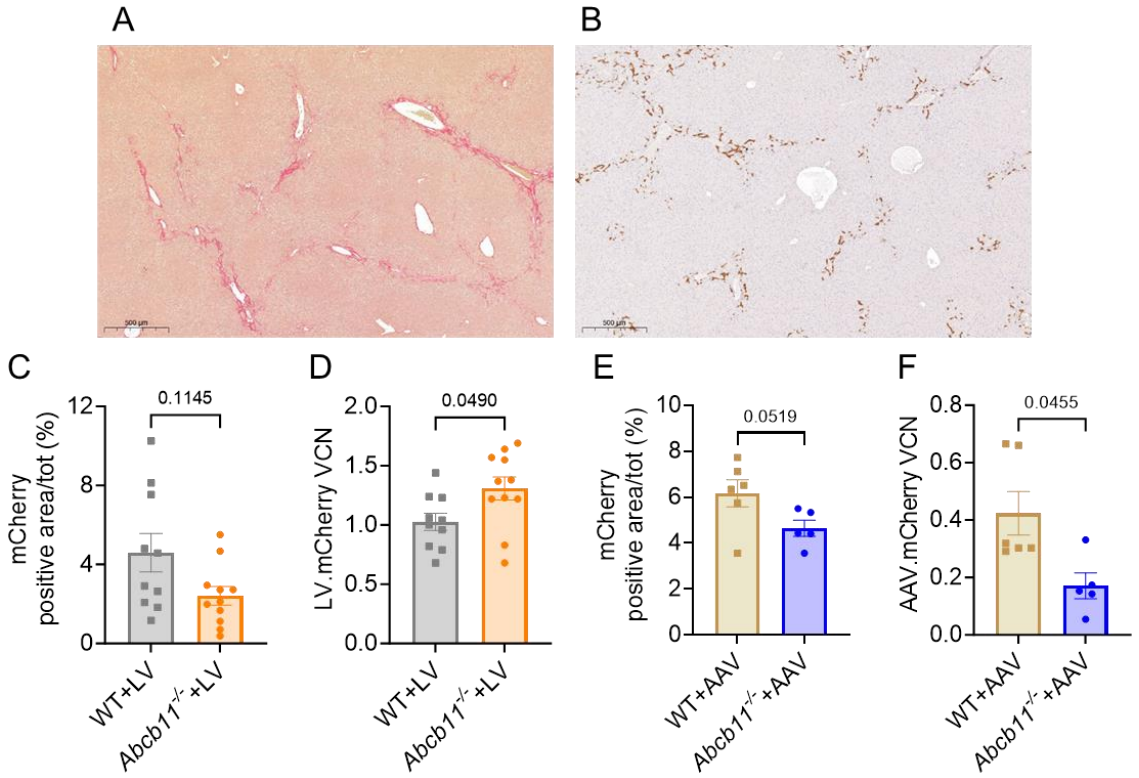


Figure 14. A, B: Representative histological images of liver sections from 6-month-old *Abcb11*$^{-/-}$ mice (bar=500 µm). Picrosirius red staining (A) and IHC CK19 (B). **C**: Individual values and mean ± SEM of percentage (%) of the mCherry-positive liver area expressed over the total area analyzed (p=0.1145, Mann-Whitney test). LV.mCherry 3.5x10^{10} TU/kg. **D**: Individual values and mean ± SEM of VCN in the liver of WT or *Abcb11*$^{-/-}$ mice administered with LV.mCherry (p=0.049, Mann-Whitney test). **E**: Individual values and mean ± SEM of percentage (%) of the mCherry-positive liver area expressed over the total area analyzed (p=0.0519, Mann-Whitney test). AAV.mCherry 1x10^{11} vg/kg. **F**: Individual values and mean ± SEM of VCN in the liver of WT or *Abcb11*$^{-/-}$ mice administered with AAV.mCherry (p=0.0455, Mann-Whitney test).

Table 4. Incidence of microscopic findings in *Abcb11*$^{-/-}$ mice and controls

	***Abcb11* -/-** **6 months**	**WT** **6 months**
Total number analyzed	3	2
Bile ducts proliferation (IHC CK19)		
No abnormality detected	0	2
Minimal	0	0
Mild	1	0
Moderate	2	0
Pigmented macrophages cluster with inflammatory cell infiltrate		
No abnormality detected	0	2
Minimal	1	0
Mild	2	0
Moderate	0	0
Periductural inflammatory mixed cell infiltrate		
No abnormality detected	1	2
Minimal	2	0
Mild	0	0
Moderate	0	0
Fibrosis (Picrosirius red)		
Grade 0	0	2
Grade 1	1	0
Grade 2	2	0
Grade 3	0	0
Grade 4	0	0

Grade 0: No abnormality detected

Grade 1: minimal periportal deposition of collagen with or without short incomplete septa

Grade 2: mild periportal deposition of collagen with short and long incomplete septa

Grade 3: moderate periportal deposition of collagen with long incomplete and complete bridging septa and pseudo nodules

Grade 4: marked periportal deposition of collagen with complete bridging septa and pseudo nodules

3.13 LV and AAV transduction is not significantly impaired in *Agl*$^{-/-}$ mice

We next took advantage of *Agl*$^{-/-}$ mice, a model of GSDIII previously shown to present with a minimal fibrotic state when adults (Gardin *et al*, 2024). We performed histopathology analysis to better characterize the liver fibrosis of 9-month-old *Agl*$^{-/-}$ mice (n=3) or WT age-matched controls (n=2). We detected minimal periportal fibrosis with mostly incomplete bridging septa and pseudo-nodules, while we did not detect alterations in control mice (Fig. 15A). Of note, the fibrosis in this model appears to be less prominent than the one present in *Abcb11*$^{-/-}$ mice or in the chemical models shown above (Fig. 8, 9, 12, 14). We injected 9-month-old *Agl*$^{-/-}$ or age-matched control mice with LV.mCherry or AAV.mCherry and we collected livers 2 weeks post vector administration. In both LV and AAV-treated animals, we did not observe significant differences in mCherry-positive liver area (Fig. 15B, C) or liver VCN (Fig. 15D, E). These data suggest that the minimal periportal liver fibrosis present in *Agl*$^{-/-}$ mice does not substantially impact gene transfer to hepatocytes.

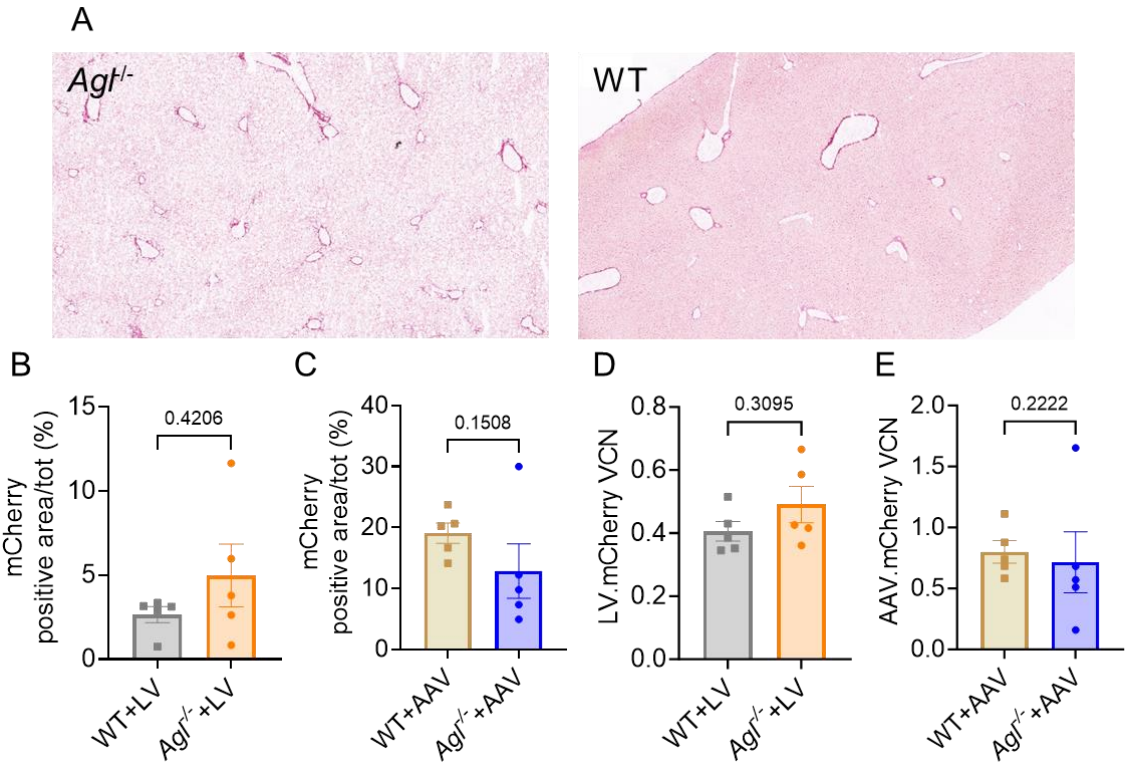


Figure 15. A: Representative histological images of liver sections from 9-month-old *Agl*$^{-/-}$ (left) and age-matched WT male mice (right). Picrosirius red staining. **B, C**: Individual values and mean ± SEM of percentage (%) of the mCherry-positive liver area expressed over the total area analyzed (C, p=0.4206, C, p=0.1508, Mann-Whitney test). LV.mCherry 5x10^{10} TU/kg. AAV.mCherry 1x10^{11} vg/kg. **D**: Individual values and mean ± SEM of VCN in the liver of WT or *Agl*$^{-/-}$ mice administered with LV.mCherry (p=0.3095, Mann-Whitney test). **E**: Individual values and mean ±

SEM of VCN in the liver of WT or *Agl*$^{-/-}$ mice administered with AAV.mCherry (p=0.2222, Mann-Whitney test).

3.14 Liver fibrosis modifies the distribution of gene transfer within the liver lobule

To study the impact of liver fibrosis on gene transfer distribution across different liver lobule zones (zonation), we took advantage of the experiments described above. We exploited the CCl_4 and DDC sever models (Figures 8, 9, 13), the *Abcb11*$^{-/-}$ and the *Agl*$^{-/-}$ mice (Figures 14, 15). We performed immunofluorescence staining to mark the periportal (PP) zone with cytokeratin 7 (CK7), expressed by cholangiocytes, and the pericentral (PC) zone with glutamine synthetase (GS), expressed only by pericentral hepatocytes (Paris & Henderson, 2022). We analyzed the PP and PC mCherry or tdTomato-positive liver area and we performed the fold of the PP over the PC results to understand the gene transfer distribution. LVs in control mice showed a preference for transduction in the PP area, as already demonstrated by our group (Fig 16A) (Starinieri *et al*, 2023). PP transduction bias was significantly reduced in all fibrosis models tested. Transduction bias almost disappeared with DDC-induced fibrosis, while in *Abcb11*$^{-/-}$ and *Agl*$^{-/-}$ mice the transduction became more PC (Fig 16A). By looking at the mCherry positive area in the two zones mouse *per* mouse, we detected a decrease only in the PP and not in the PC transduction with CCl_4-induced fibrosis (Fig. 16B). With DDC-induced fibrosis both PP and PC transduction were reduced, but with a greater extent in the PP zone (Fig. 16B). On the contrary, in *Abcb11*$^{-/-}$ and *Agl*$^{-/-}$ mice PP transduction was reduced but PC transduction was increased (Fig. 16B). AAV serotype 8, showed PC transduction preference in control mice as described in the literature (Fig. 16C) (Bell *et al*, 2011). CCl_4 and DDC-induced liver fibrosis did not impact the transduction bias (Fig. 16C). In *Abcb11*$^{-/-}$ mice, the PC transduction appears prevalent, on the contrary, in *Agl*$^{-/-}$ mice the bias decreased (Fig. 16C). Regarding the mCherry positive liver area, DDC treatment induced an overall decrease in transduction, *Abcb11*$^{-/-}$ mice decrease only PP transduction, and *Agl*$^{-/-}$ mice decreased more the PC transduction (Fig. 16D). LNPs transfection showed a PC bias that became more PP with CCl_4 induced fibrosis, and more PC with DDC treatment (Fig. 16E). Indeed, tdTomato positive liver area showed an overall decrease that was more prominent in the PC area with CCl_4 and the PP area with DDC (Fig. 16F).

These data suggest an overall modification of gene transfer zonation that was dependent by both the delivery method and the liver fibrosis model.

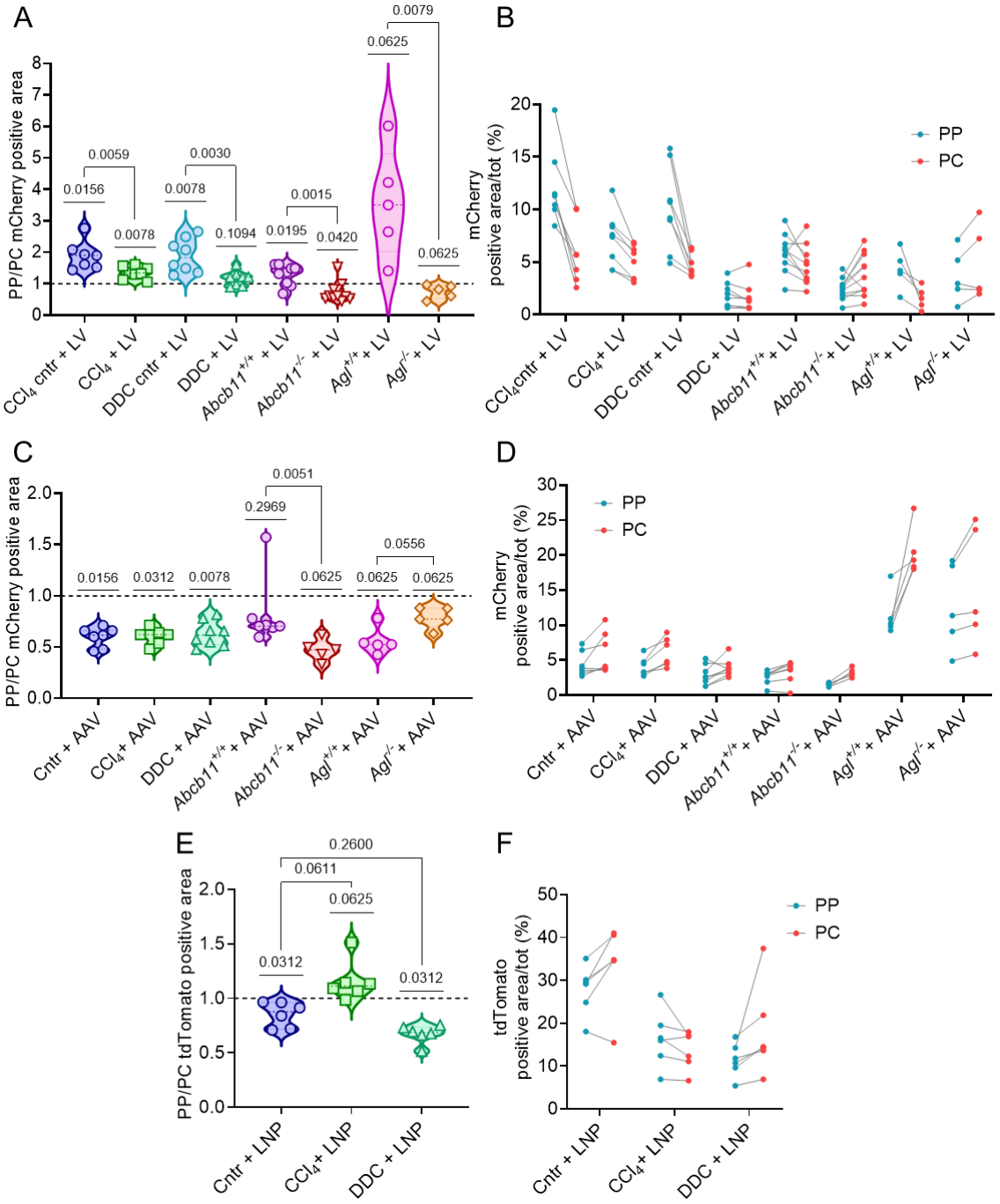


Figure 16. A: Violin plot with individual values median and quartiles of the fold between PP over PC mCherry-positive liver area (Wilcoxon signed-rank test against 1, Mann-Whitney test between test and control groups, *p* values are shown). Dot line represents fold=1. **B**: Individual values of percentage (%) of the mCherry-positive PP (blue) or PC (red) liver area expressed over the total area analyzed. Gray lines connect the two areas of the same mouse. **C**: Violin plot with individual

values median and quartiles of the fold between PP over PC mCherry-positive liver area (Wilcoxon signed-rank test against 1, Kruskal-Wallis test or Mann-Whitney test between test and control groups, significant *p* values are shown). Dot line represents fold=1. **D**: Individual values of percentage (%) of the mCherry-positive PP (blue) or PC (red) liver area expressed over the total area analyzed. Gray lines connect the two areas of the same mouse. **E**: Violin plot with individual values median and quartiles of the fold between PP over PC tdTomato-positive liver area (Wilcoxon signed-rank test against 1, Kruskal-Wallis test between test and control groups, *p* values are shown). Dot line represents fold=1. **F**: Individual values of percentage (%) of the tdTomato-positive PP (blue) or PC (red) liver area expressed over the total area analyzed. Gray lines connect the two areas of the same mouse.

4. Discussion

4.1 Selection of the best-performing sgRNA and donor DNA for *in vivo* liver-directed gene editing

In this work, we have compared the efficiency of different gene-editing strategies for site-specific insertions into the first intron of *ABCB11* and *DBT* genes *in vivo* in hepatocytes of newborn or juvenile mice. Regarding sgRNA selection, notably, sgRNAs with high NHEJ efficiency do not always allow the highest integrations. For this reason, especially regarding the selection of human-specific reagents, it would be important to test additional sgRNA for their ability to mediate integration, to select the best-performing ones for translational purposes. Moreover, by comparing the integration results that we obtained in cell lines and mice with different donor DNAs, we highlight that the formers may not predict the results obtained with *in vivo* studies. Initially, we compared donor DNA based on HDR, MMEJ, or HITI pathway in 2-week- and 2-day-old mice, to understand which mechanism allows more efficient genomic integration in actively proliferating hepatocytes. To test the HDR pathway, we designed donor DNA with long (750bp) or short (250bp) homology arms, to understand if longer regions of homology could increase the rate of integration. However, in the *in vivo* experiments, we did not detect any advantage of long over short homology arms, indicating that 250bp of homology are enough to exploit the HDR pathway, at least in our experimental settings. In all the experiments performed, we exploit mCherry as a reporter gene to more easily detect integrations and expression of the transgene in WT animals. However, mCherry has a shorter cDNA (711 bp) compared to *ABCB11* and *DBT*, which may overestimate the efficiency of site-specific integration compared to longer transgenes. The long *ABCB11* cDNA (3966 bp) may be particularly challenging. Indeed, AAVs have a maximum capacity of ~4.7 kb, meaning that with *ABCB11* cDNA we are at the limit of capacity, with the risk of generating vectors with truncated genomes that may not allow efficient transgene integrations. For these reasons, we tested HDR only with short (250 bp) homology arms in the *Abcb11* locus, since long arms will not fit in an AAV. For the *Abcb11* locus, we tested HITI- but not MMEJ-based donor DNA, since we prioritized one non-HDR-based mechanism to be compared with an HDR-based one. When targeting the *Dbt* locus, we could not measure the mCherry-positive liver area, probably because the

expression of the reporter gene when driven by the DBT promoter is too low to be detected by immunofluorescence. The results obtained in experiments with 2-week-old or 2-day-old Cas9 mice were similar, suggesting that hepatocytes at these two ages have similar responses to genome editing. Our results suggest no major difference in the integration rate of HDR- vs. non-HDR-based methods. Sometimes, the HITI-based donor DNAs seem to allow more efficient integration, however not paralleled by higher mCherry expression in both *loci* tested. Indeed, the use of HDR-based donors usually results in a higher mCherry-positive liver area and mCherry expression. This could derive from how the donor DNA is integrated. If ITRs are not cleaved from the HITI donor DNA, they can integrate with the transgene. This could result in the formation of secondary structures that inhibit the expression of the reporter cDNA. It is important to note that the mCherry expression that we measured likely derived from the site-specific integration since, in all experiments, we have control of background integration and expression in the absence of Cas9. In control mice, we observed low mCherry expression that could derive from non-specific integrations. Indeed, the donor DNAs that we exploited are promoterless, meaning that the mCherry expression observed without Cas9 could derive from insertion into spontaneous breaks inside active genes. Until now, we have measured the integration rate by ddPCR on a single junction. It would be important also to assess the percentage of integration at both junctions to determine the actual ability of the integration strategy tested to allow the complete insertion of the desired construct. Connected to these observations and to better understand which donor DNA is the best for our purposes, it would be interesting to perform long-read sequencing of the target locus. In this way, we could assess the proportion of undesired integration events such as ITRs, concatemer, or truncated constructs.

4.2 Selection of the best delivery vehicles and time of administration for the editing machinery

Other important aspects to be evaluated are the delivery vehicles, the time of administration, and the doses. We decided to rely on LNP to deliver Cas9 and sgRNA, to allow transient expression of the nuclease, and to test both AAV and IDLV for the delivery of donor DNAs. We compared the two vectors since AAVs are the most used vehicles to

reach hepatocytes *in vivo* with an elevated number of copies, while IDLVs have a larger cargo capacity and less detrimental effects in hematopoietic stem cell gene editing (Ferrari *et al*, 2022). Firstly, we set out to administer LNP with Cas9 and sgRNA after donor DNA to allow the completion of vector transduction and the formation of episomes inside the nucleus at the time of nuclease delivery. However, the 48-hour gap between vectors and LNP injection was not the best time point. Indeed, the percentage of integrations with AAV was low, while with IDLV, even the NHEJ was completely abolished in both loci tested. These results indicate that the IDLV administration abrogates LNP transfection in all hepatocytes, not only in the ones transduced by IDLVs. Indeed, at the dose used, we expect to transduce around 20% of hepatocytes by IDLV (Starinieri *et al*, 2023). The injection of enveloped vectors like IDLVs may cause a rearrangement of lipid metabolism in all hepatocytes, which is crucial for LNP transfection. LNP exploits LDLR to enter inside hepatocytes, thus, if LDLR expression is altered, there could be impairments in LNP entry and intracellular trafficking. To understand the changes that occur after IDLV transduction, transcriptomic and metabolomic analyses of the serum and the liver tissue after IDLV administration may be performed. To overcome the limitations encountered, we tested different time points of LNP administration and higher doses of LNP. With 6mg/kg of LNP, we obtained the same NHEJ efficiency observed in Cas9-transgenic mice, where the constitutive expression of Cas9 facilitates the DNA-cutting efficiency with the selected sgRNA. Co-administration of LNP and AAV allows the highest percentage of integration and mCherry expression. These data suggest that it is not necessary to wait for the double-stranded DNA episomes to be completed to serve as substrates for HDR-mediated integration because they may form concatemers (Grimm *et al*, 2006). Actually, the presence of transduction intermediates free single-strand AAV DNA at the time of Cas9 activity may increase the rate of correct integrations (Roth *et al*, 2018). On the contrary, waiting 1 week to administer LNP almost abolished the integration, which might be due to the dilution of AAV episomes caused by the growth of the liver between 2 and 3 weeks of age. With IDLV, we detected integrations and mCherry expression only when administered simultaneously as LNP, but with a lower efficiency than AAV. IDLVs require more time compared to AAVs to enter the nucleus and become substrates for HDR-mediated integration since their RNA genome requires retro-transcription. This may be a problem since the concomitant administration of LNPs

containing short-lived RNAs may not allow Cas9 activity to persist until IDLVs are fully reverse-transcribed. However, it is known that once Cas9 completes the cleavage, it remains attached to the DSB for around 6 hours (Richardson *et al*, 2016). This could give the time for IDLV donor DNA to be retrotranscribed and enter the nucleus. Nevertheless, it could be worth testing higher doses of IDLV and other times of administration of LNP (like 6 or 12 hours after IDLV) to understand when the transfection of LNP starts to be inhibited.

4.3 Future development of a gene-editing strategy for the treatment of MSUD and PFIC2

The most important next step in the project is testing the gene-editing strategy in mouse models of MSUD and PFIC2. We will proceed with the selected sgRNA, the donor DNA based on HDR with short homology arms, and the coadministration of LNP and AAV at the last tested doses. We will exploit *Dbt* and *Abcb11* knock-out mice, models of MSUD and PFIC2, respectively. The first one is a very fragile model that dies in the first days of life, so we will need to treat them as newborns (Skvorak, 2009). The second one has almost the same life expectancy as WT mice, so we will treat them at 2 weeks of age (Zhang *et al*, 2012). The experiments performed suggest that we could obtain around 10-20% of integration. This may be enough for PFIC2 treatment. Indeed, in our laboratory, we treated *Abcb11* knock-out mice with LV carrying a hepatocyte-specific *Abcb11* expression cassette, resulting in therapeutic efficiency. We obtained a similar level of transgene expression by LV transduction, as with our gene editing strategy, suggesting that it can be enough to ameliorate the disease phenotype in mice. In the context of MSUD, we do not have data to support if the transgene expression that we obtained could be enough to revert the phenotype. Looking at a possible clinical translation of the strategy, it would be necessary to screen more human sgRNA to find more efficient guides that could allow higher DNA cleavage efficiency and higher integrations mediated by HDR. Moreover, to select the best sgRNA it would also be important to understand the off-target sites and the potential chromosomal rearrangements that could derive from them. We are planning to investigate those undesired effects only in human settings since the sgRNA designed for the murine genes cannot be translated. While we are prioritizing

AAV at the moment, we will keep investigating the IDLV platform, which is convenient, especially for long transgenes, like *Abcb11*, that hardly fit inside an AAV. Moreover, AAV might induce responses in targeted hepatocytes that may interfere with the proliferation and maturation of the liver during growth, similar to what has been shown in the context of hematopoietic stem and progenitor cells (Schiroli *et al*, 2019; Ferrari *et al*, 2022). Thus, it would be interesting in the future to determine the transcriptional responses to the gene editing procedure *in vivo* with different delivery vehicles and times of administration.

4.4 Impact of liver fibrosis on gene transfer to hepatocytes

As pointed out above, PFIC2 patients develop fibrosis even before one year of age in the most severe cases. For this reason, to set up a gene editing strategy, it is crucial to understand if the delivery of the gene editing components is feasible in the presence of liver fibrosis. In this work, we perform a detailed characterization of the impact of liver fibrosis on *in vivo* gene transfer to hepatocytes in four different mouse models, two chemically induced and two genetic, by LV, AAV, and LNP, widely used viral and non-viral vector platforms. Despite chemical models of fibrosis being relatively artificial, they are extensively adopted to mimic the more common fibrosis types found in human conditions. In particular, the CCl_4 model resembles fibrosis due to toxic damage, similar to what is observed with viral hepatitis, while the DDC model recapitulates biliary fibrosis due to cholestatic diseases like PSC (Parola & Pinzani, 2019). We report that hepatocytes within fibrotic livers are generally transduced with reduced efficiency, although the outcome varied according to the vector used and the state of the tissue at the time of systemic vector administration. Specifically, CCl_4-induced toxic pericentral fibrosis, either scored as moderate or mild, negatively affected LV transduction. On the contrary, this type of fibrosis did not significantly alter AAV transduction. Instead, DDC-induced biliary fibrosis impaired LV- and AAV-mediated gene transfer, both in the presence of moderate and marked periportal damage. Severe CCl_4 and DDC-induced fibrosis also reduce the ability of LNP to transfect hepatocytes *in vivo*. In line with those findings, we observed a slight reduction of LV and AAV transduction in *Abcb11*$^{-/-}$ mice, which display a type of cholestatic fibrosis similar to that induced by the DDC diet. However, the decrease in gene transfer was less pronounced in 6-month-old *Abcb11*$^{-/-}$ mice than in

DDC-fed mice, consistently with the presence of milder biliary fibrosis in the former model. By contrast, the minimal periportal liver fibrosis in 9-month-old Agl-/- mice did not significantly affect LV or AAV transduction. These data suggest that the type and extent of fibrosis determine the impact on gene transfer efficiency. Our results are in line with what was described in the literature for AAV. Indeed, CCl_4-induced fibrosis was shown not to reduce AAV serotype 1 transduction (Sobrevals *et al*, 2012a), while biliary fibrosis present in *Abcb4* knock-out mice, a mouse model of PFIC3, showed to impact AAV8 (Siew *et al*, 2019a). Indications that liver fibrosis could impact the various delivery vehicles differently were suggested by a study with AdV, which showed that both CCl_4 and BDL-induced fibrosis reduced AdV transduction (Garcia-Bañuelos *et al*, 2002). Also, LNPs were tested in the context of CCl_4-induced fibrosis, showing a reduced hepatocyte transfection *in vivo* (Shan *et al*, 2024). However, gene transfer was never completely abolished, meaning that it is possible to work on strategies to reach hepatocytes efficiently, even in a damaged liver. For example, it could be possible to increase the doses to try to reach the same level of transduction or transfection obtained in a healthy liver. This hypothesis could be investigated with a dose-response experiment in the chemical models that we exploited. An indication that this strategy may be efficient is present in the biodistribution experiment shown above (Figure 10), where LV doses administered were higher. In the presence of CCl_4-induced liver fibrosis, the percentage of mCherry-positive hepatocytes was not different from the controls, and the reduction of hFIX output was less pronounced than in previous experiments. It is possible that we could detect differences between controls and LV-treated mice only with hFIX because it is an indirect measurement of transduction since hFIX is secreted from all transduced hepatocytes and remains in circulation, while with mCherry expression, we count transgene-expressing cells without easily distinguishing cells that express at high or low level the transgene. However, this is an indication that by increasing the doses, we may transduce more hepatocytes even in the presence of moderate pericentral fibrosis. On the contrary, DDC-marked periportal fibrosis strongly reduced transduction even at these high doses. Another strategy to overcome the limitation of fibrosis could be the modification of delivery vehicles by changing the AAV serotype, LV pseudotype, or by modifying the LNP formulation. It may be possible that the effect that we observed was linked to the specific composition of the vehicles that we exploited. Indeed, by modifying

the LNP formulation, Shan and colleagues could efficiently transfect the fibrotic liver *in vivo* (Shan *et al*, 2024). Our investigation of the impact of liver fibrosis on gene transfer is missing models that recapitulate the ALD or MASH phenotype, which is characterized by steatosis and perisinusoidal fibrosis. ALD and MASH fibrosis can be defined as toxic since it derives from direct hepatocyte damage. However, the presence of steatosis activates pathways that are not involved in CCl_4-induced fibrosis, so it would be interesting also to assess the impact of ALD or MASH on gene transfer in the future.

4.5 LV biodistribution in liver subpopulation and different organs in the presence of fibrosis

When using AAVs, the reduction of hepatocyte-derived transgene output was always paralleled by a reduction of AAV VCN in the liver since AAV8 has a tropism for hepatocytes. On the other hand, when using LV, the decrease in gene transfer efficiency was not always mirrored by a lower LV VCN in the liver. This finding is expected since VSV.G-pseudotyped LVs also transduce liver nPC (KC and LSEC). Therefore, VCN in the total liver does not directly reflect the transduction of hepatocytes, as previously shown (Milani *et al*, 2019b). However, nothing was known about the biodistribution of LVs in different organs and liver subpopulations in the context of liver fibrosis, so we decided to test two LVs carrying two different transgenes (mCherry and hFIX). As shown in previous reports, we confirmed that hepatocyte VCN reflects the actual transgene output in fibrosis models, being lower compared to healthy controls when the transgene output was lower as well. Not only in the liver but also in the spleen, we observed a decrease in VCN when mice were treated with CCl_4 or DDC. This could be due to an overall alteration of the blood flow caused by portal hypertension in the damaged liver or by alteration of the spleen parenchyma due to chemical treatments. Indeed, it is known that fibrosis alters the blood flow inside the liver, causing portal hypertension that redirects blood into other districts, causing an overall alteration of the blood flow. By altering the blood flow in the spleen, transduction can be altered. However, we have not yet investigated spleen histology after CCl_4 or DDC treatments. In the literature, there are indications that both hypotheses are possible (Das *et al*, 2014; Habashy *et al*, 2021; Kim *et al*, 2020b). VCN in the lung, heart, and brain was very low or undetectable, only mice

with CCl_4-induced fibrosis treated with LV-carrying mCherry showed some detectable VCN. This suggests that the reduction in liver and spleen VCN might be explained by higher transduction of the kidney, probably due to blood flow alteration. However, VCN in the kidney of CCl_4-treated mice injected with LV carrying hFIX was undetectable, not confirming the observation made for LV.mCherry. Nevertheless, an indication of the alteration of blood flow with CCl_4-induced fibrosis also came from the clearance of LV particles from circulation, which was slower than in controls. In the presence of DDC-induced fibrosis, the clearance from the bloodstream was not different compared to controls, even if VCN were reduced in both livers and spleen. A hypothesis to explain this observation is the presence of an important inflammatory infiltrate in the livers of DDC-treated mice that could clear LV particles, abolishing hepatocyte transduction. Moreover, the VCN of different liver resident cells was not different among the groups, indicating that fibrosis reduces only hepatocyte transduction inside the liver.

4.6 Transduction and transfection zonation with liver fibrosis

We analyzed if different types of liver fibrosis could impact the distribution of transduction or transfection across the liver lobule. Regarding LV, our group already reported that by administering LV to adult mice, the transduction is preferentially in the periportal zone (Starinieri *et al*, 2023). We confirmed this observation in all the control groups that we analyzed, but the zonation changed in the presence of fibrosis. With periportal fibrosis (DDC-induced, *Abcb11*$^{-/-}$, *Agl*$^{-/-}$), the transduction in the periportal area was reduced, abolishing the bias or even inducing more pericentral transduction. This is probably due to the collagen deposition that restricts access to periportal hepatocytes. However, also in the context of CCl_4-induced pericentral fibrosis, the periportal transduction was reduced, reducing the bias. This observation could be explained by an overall alteration of the liver metabolism with CCl_4 chronic administration and the formation of fibrosis, which reduces the transduction of periportal hepatocytes even if they are not close to the collagen deposition. AAV8 is known to have a pericentral bias of transduction (17) that is maintained with CCl_4 and DDC-induced fibrosis. CCl_4 treatment does not alter AAV transduction, while DDC treatment seems to impair transduction overall, not in a specific area. *Abcb11*$^{-/-}$ mice seem to increase the pericentral bias, while

Agl$^{-/-}$ mice reduce the bias. All these observations can be better explained by the metabolic state of the liver and not by a physical block of transduction due to ECM deposition. Interestingly, LNP transfection in control mice showed a pericentral bias that became periportal in the presence of peri-central fibrosis and more pericentral in the presence of peri-portal fibrosis. The trend of LNP zonation follows the pattern of fibrosis since the transfection efficiency appears to decrease in the area where there is more deposition of ECM.

4.7 Speculation on the mechanism causing impairment of gene transfer

The different gene transfer outcomes observed in our work are linked to the fibrosis type and the vehicles exploited. Liver fibrosis is generally characterized by an alteration of the tissue architecture with an excessive extracellular matrix deposition. This can lead to the formation of fibrosis septa that can isolate the nodules. Moreover, the fibrogenic process involves an alteration of liver blood flow caused by collagen deposition, sinusoidal capillarization, and angiogenesis. The obstruction of circulation leads to portal hypertension that redirects the blood to other organs. All these changes could hamper the physical accessibility of the viral and non-viral vectors to hepatocytes when administered systemically. Notably, LVs, AAVs, and LNPs have different sizes, approximately 120 nm, 25 nm, and 90 nm, respectively (Li *et al*, 2023). Therefore, a physical barrier may inhibit more strongly LV and LNP rather than AAV delivery to hepatocytes. These observations could explain why pericentral fibrosis induced by CCl_4 administration inhibits gene transfer of LV and LNP but not of AAV. Regarding LNP, the zonation suggests that transfection is reduced more in the lobule zone, where there is a higher presence of fibrosis in both CCl_4 and DDC models, indicating a major contribution of the physical alterations to the transfection impairments. Regarding LVs, we have indications that they remain more in circulation in mice with CCl_4-induced fibrosis, suggesting that access to the liver is impaired, probably due to tissue alteration and blood flow. However, the LV transduction zonation in CCl_4-treated mice is less pericentral, indicating that the less transduced hepatocytes are the ones in the periportal area. These data suggest that the cell-intrinsic metabolic alteration of hepatocytes in a damaged liver plays an important role during gene transfer. Indeed, DDC periportal fibrosis also alters AAV transduction,

even if AAV8 presents a pericentral bias. In DDC-treated mice, the pericentral bias is not altered, while there is an overall decrease in transduction. This can also be explained by the presence of inflammatory infiltrate, which is different between mouse models. The highly present inflammatory infiltrate in the DDC model may cause an increase in phagocytosis and reinforce cellular anti-viral defenses, thus reducing gene transfer. However, the underlying pathogenic mechanisms and the specific cell response play a crucial role in the gene transfer outcomes that we observed. For example, the underlying disease present in *Abcb11*$^{-/-}$ and *Agl*$^{-/-}$ mice could explain the alteration in AAV and LV transduction zonation. When analyzing the total liver transduction, the differences with controls are limited, however, the LV transduction became more pericentral in both models, while the two diseases have opposite effects on AAV. This is probably caused not just by the presence of fibrosis but by other mechanisms. In this regard, an altered metabolic state of hepatocytes and other liver cells could affect the expression of vector receptors and impact other post-entry steps of the vector transduction process, such as capsid trafficking, nuclear import, and nucleic acid synthesis.

4.8 Limitations of the study and its relevance for human pathologies

This study presents some limitations. We selected sgRNA by screening *in vitro* for the one with the highest NHEJ, however this may not be predictive of NHEJ *in vivo*. Using a poorly efficient sgRNA could reduce our capacity to integrate donor DNA. For this reason, it would be crucial to test additional sgRNA for the human genes, ideally by looking at their ability to mediate integration. Moreover, in our experiments, we inserted donor DNA carrying mCherry cDNA, which is shorter than the one of Abcb11 and Dbt. This could have led to an overestimation of the efficiency of integration since longer transgenes may result in a lower integration rate. Our results suggest that the coadministration of LNP and AAV leads to the highest integration percentage. However, we tested just three times of LNP administration, so it would be interesting to perform a more stringent timeframe, for example, by injecting LNP 6 or 12 hours after the vector. To investigate the impact of liver fibrosis on gene transfer, we took advantage of chemically induced models that are artificial, even if extensively exploited, mimicking only some mechanisms found in human conditions. Moreover, among the fibrosis types

that we investigated, we are missing the one characterized by steatosis and perisinusoidal fibrosis, typical of ALD or MASH. Indeed, the presence of steatosis activates different pathways that can not be investigated with the models that we employed. Another important point is the investigation of the gene transfer zonation in the liver lobule. It has been demonstrated that AAV8 has an opposite zonation when transducing murine or NHP livers (Bell *et al*, 2011). For this reason, all the alteration of zonation observed in the presence of liver fibrosis can not be directly translated to an NHP or human context. To address this point, the mechanism underlying the impact of fibrosis on gene transfer and its zonation should be investigated to better predict human outcomes. Nevertheless, this study has potential impacts on human pathologies. The development of a gene-editing strategy for treating PFIC2 and MSUD could allow pediatric patients to receive a one-and-done therapy before the disease worsens, improving patients' quality of life. Moreover, the study's findings may be informative to develop further gene editing strategies for other inherited metabolic diseases that can be treated with liver-directed approaches and in which early intervention is crucial. Investigating the impact of liver fibrosis on gene transfer is relevant when developing liver-directed gene therapy clinical trials for diseases with liver fibrosis. Until now, patients with liver fibrosis have been excluded from clinical trials, but we showed that gene transfer in fibrotic liver can still be achieved. However, it would be important to consider the vector dose, the time of vector administration, and the vector platform based on the target disease and the underlying liver damage.

4.9 Conclusions

Regarding developing a genome editing strategy for treating MSUD and PFIC2, we identify HDR-based donor DNA with short homology arms as the most efficient for integration and transgene expression, at least in our experimental setting. To deliver the editing machinery, we selected the coadministration of LNPs, carrying sgRNA and Cas9 mRNA, with AAVs, carrying the donor DNA. This allows transgene expression similar to what we obtained with LV administration, meaning that we could observe therapeutic efficiency once we move to disease mouse models. The efficacy experiment is the next step in the development of the strategy. Thinking about clinical translation, we consider

the most important next steps would be to investigate deeply the conformation of integrations at the target locus, to find human sgRNAs with the highest DNA cleavage efficiency, and to determine possible off-targets and chromosomal rearrangements. Concerning the analysis of the impact of liver fibrosis, interestingly, we never observed a complete abrogation of transduction and transgene expression in any of the pathological conditions evaluated, suggesting that gene transfer to hepatocytes can still be achieved. However, our findings indicate that the presence of pre-existing liver fibrosis needs to be carefully considered when developing and administering liver-directed gene therapy. Specifically, the vector dose may need to be increased to achieve the same therapeutic efficacy in patients with fibrotic liver compared to those with a non-fibrotic liver. Moreover, the time of vector administration should be anticipated as much as possible to avoid the progression of liver damage, and patient populations should be selected according to the presence and stage of fibrosis. Furthermore, since the presence of hepatic fibrosis may trigger hepatocyte proliferation, AAV-mediated transgene expression may progressively decrease because of the dilution of AAV episomes (Nakai *et al*, 2001). The impact of hepatic fibrosis on gene transfer may also vary according to different vector envelopes/serotypes. Thus, the vector platform and design need to be wisely selected based on the target disease and underlying liver damage. By investigating biodistribution and zonation of gene transfer in the presence of fibrosis, we catch a glimpse of the mechanism that could cause the reduction observed. However, further investigation will be required to understand these mechanisms better and to devise potential strategies to overcome them. Overall, the study reported here represents an important step forward toward the development of gene-editing for the treatment of MSUD and PFIC2, informing about integration pathways and delivery systems suitable for achieving efficiencies associated with an expected therapeutic benefit. Moreover, this study sheds light on the previously unexplored yet critical aspect of the impact of liver fibrosis on liver-directed gene therapy. The work has several implications for future developments and applications of liver-directed gene transfer and editing for inherited metabolic and potentially acquired diseases.

5. Materials and methods

5.1 Bioinformatic analysis

We performed a bioinformatic analysis of the murine and human *DBT* and *ABCB11* genes using NCBI Gene (https://www.ncbi.nlm.nih.gov/gene) and CCDS (https://www.ncbi.nlm.nih.gov/projects/CCDS/CcdsBrowse.cgi) to investigate the position in the genome, the length of the intron, and the cDNA. With Swiss regulon, we investigated the presence of regulatory regions inside the first intron of the four genes (https://swissregulon.unibas.ch/pages/). We compared the first intron of the murine and human orthologous genes to investigate their similarity using BLAST (https://blast.ncbi.nlm.nih.gov/Blast.cgi). Finally, we exploited Benchling (https://benchling.com/editor) and ChopChop (https://chopchop.cbu.uib.no/) software to select 12 sgRNAs for each gene, considering the ones with the highest predicted efficiency and the lower predicted off-targets. We selected the following sgRNAs:

Gene	*sgRNA*	*Sequence (5’- -3)*
Murine *Dbt*	1	AGCTACGAGCACAGGGGAGT
	2	CGGTCCATAAGGAGTTATCT
	3	TTGCTACTAGCTCATAGGAC
	4	ATCTGTAATTAAGAGCAAGG
	5	GCTTCTCTTAGAACACCCCA
	6	CCTGAATGACCAAATCAACA
	7	AGGAATTACTAATAGACTGG
	8	GTTGACAACTTAAAGCTGAG
	9	TGTGTGCACACACACCTGGG
	10	TACCAGTATTCTCAAAACCA
	11	AGCATGTCTACCCACTGATG
	12	CAAAGAACTCAAACTCCTAG
Murine *Abcb11*	1	TTAGTGCCAATCGTTGCCCA
	2	GGAACCAATCTTGATGACCA
	3	GAATACATATCAACCATGAG
	4	ATGCTGATCAACCCTTGGAA
	5	GATGCTGGGAAAGCCCACAA

	6	TTGAGTGCAGGACCTCCACG
	7	TGAGGAGAGAGGGAAATCGA
	8	CTGACATTGAGAATGAAGGG
	9	TTACCTAATTGGGATCACAG
	10	TTTCGTAAGTAGAGCCCCAG
	11	TTGCCTAGCATATGTGACAG
	12	TCCTTAGGGACAAAGTTGGG
Human *DBT*	1	TACTTAGAGATAAGCCGGTA
	2	ACACGTTCAAGATCCCCCGG
	3	ACATAGGCAGTACGTGATAA
	4	ATAGCACGTGTTATAATCAC
	5	TGCAACATACCTCATCCCCG
	6	CTAAAGACACCTAGTTCTAT
	7	ACTGAGGCAGGTGGATCACG
	8	GCTAACGTGTATGTTCCACA
	9	GAGAATCGCATGAACCTGGG
	10	CACTCAATAAATGTTAAGCG
	11	GAGAATCGCTTGAATGCGGG
	12	GCCAAGGTGGGCAGATCACG
Human *ABCB11*	1	ACCGTAATTACTGAACCGTT
	2	TGAATCGAGTGTCTATATCC
	3	ACCATCCATCCAACAACTAG
	4	GTTGCAGGCTATGTTGTGTT
	5	CTGCTTCTGGGATTCCAATT
	6	GTGCCCTTATCTGGAAAACG
	7	ATGAAATGGCATTTAATACG
	8	GAGAATCACATGAACCCAAG
	9	TAAGTGGTTGCCTAATGCTG
	10	GGCTTGCAGAACTTGTGCAT
	11	AAGTGCCCCAAATCAAACAG
	12	CGTCAGCATCCAGACGCTGA

5.2 Generation of plasmids

In this work, we used plasmids already available in the lab or generated by standard cloning techniques. To generate sgRNA expression plasmids, we ordered form Eurofins oligos for sgRNA and we inserted them into a previously described plasmid with U6 promoter by opening it with *BsaI*-HF enzyme (New England Biolabs, NEB, R3733S) (Chen *et al*, 2013). GeneScript synthesized murine donor DNAs combining the following elements:

- 750bp, 250bp, or 20bp homology arms selected by starting from 3bp upstream of the PAM and going towards the 5' end of the gene to generate homology arms left and towards the 3' end of the gene to generate homology arms right. We used gene sequences available online (https://www.ncbi.nlm.nih.gov/gene),
- Splice acceptor sequence, described in the literature (Maddalena *et al*, 2018),
- T2A sequence, described in the literature (Ishibashi *et al*, 2020),
- mCherry sequence, already available in our laboratory (unpublished),
- bovine growth hormone (bGH) polyA, already available in our laboratory (unpublished),
- sgRNA cut site using gene sequences available online (https://www.ncbi.nlm.nih.gov/gene).

GeneScript cloned the donor DNAs into an already available AAV serotype 2 backbone, exploiting *XhoI* and *MluI* restriction enzymes (NEB). Then, we cloned the different murine donor DNAs in antisense by replacing the ET-GFP-polyA sequence into an LV backbone harboring the mutated WPRE sequence outside the LTR (unpublished). Subsequently, we inserted the U6-sgRNA cassettes into AAVs and LVs carrying donor DNAs. We took the U6-sgRNA cassette from expression plasmids previously generated, and we inserted it into the opened backbones. We generated all these plasmids for both murine *Dbt* and *Abcb11* genes. For the human donor DNAs, GeneScript synthesized the 750, 250, and 20bp homology arms and the sgRNA cut site for both *DBT* and *ABCB11* genes. To determine the sequences to be synthesized, we used gene sequences available online as described for the murine donors. Then, we cloned all the different components by replacing the murine sequences with the human ones into IDLVs previously generated. We also substituted the murine sgRNAs with the human counterparts. To produce LV

carrying Cas9, hFIX, or mCherry expression cassette we used already available plasmids in our laboratory (pCCLsin.cPPT.hPGK.Cas9.PuroR.WPRE, pCCLsin.cPPT.ET.co-hFIXR338L.142T.Mwpre.142T, or pCCLsin.cPPT.ET.mCherry.Wpre.4x142-3PT) (unpublished). For AAV production, we used plasmids with hFIX or mCherry expression cassette containing the apolipoprotein E (ApoE) and human alpha1-antitrypsin (hAAT) promoter, the hFIX cDNA, the hFIX intron located just after exon 1 and a bGH poly-A, as previously described (Manno *et al*, 2006).

5.3 LV and IDLV production and titration

We employed human embryonic kidney (HEK) 293T cells for vector production and titration. We maintained HEK293T in Iscove's modified Dulbecco's medium (IMDM, Corning) supplemented with 10% Cytiva HyClone™ FetalClone™ II Serum (U.S.) (Euroclone) and penicillin/streptomycin 100 international units (IU)/ml (Lonza). We detached cells using PBS 0.05% trypsin, 4mM EDTA solution. We maintained cells in a humidified incubator at 37°C 5% CO_2. We produced third-generation self-inactivating (SIN) IDLV or LV by calcium phosphate transfection of HEK 293T cells with a mix of transfer plasmid and the packaging plasmids, as previously described (Milani *et al*, 2022). For IDLV production, we substituted the standard packaging plasmid pMDLg/pRRE with a pMDLg/pRRE carrying the D64V mutation in the integrase encoding gene (Lombardo *et al*, 2007). We filtered IDLV/LV-containing supernatant with a 0.22μm filter (Millipore) and concentrated around 4-fold with Vivaflow 200 Tangential Flow Filtration Cassette 100kDa (Sartorius), according to the manufacturer's instructions. Subsequently, we ultracentrifuged the supernatant in polyallomer tubes (Beckman Optima XL-100K Ultracentrifuge). We concentrated the final IDLV/LV around 500-fold by resuspending the pellet in an appropriate volume of phosphate saline buffer (PBS, Corning). We prepared IDLV/LV aliquots, which were stored at -80°C. We measured the IDLV/LV infectious titer as previously described (Milani *et al*, 2022). For LV production, 10 days after cell transduction, we extracted genomic DNA (gDNA) using Maxwell RSC Cultured Cells DNA Kit (AS1620, Promega) following the manufacturer's instructions. For IDLV production, 3 days after cell transduction, we extracted gDNA using DNeasy Blood and Tissue Kits for DNA Isolation (69504, Qiagen) following the manufacturer's instructions.

We determined VCN and titer by ddPCR, as previously described (Milani *et al*, 2022; Lombardo *et al*, 2007).

5.4 Cell line experiments

For *in vitro* experiments, we employed Hepa1.6 and Huh7 cell lines. We maintained Hepa1.6 and Huh7 in IMDM (Corning) supplemented with 10% Cytiva HyClone™ FetalClone™ II Serum (U.S.) (Euroclone) and penicillin/streptomycin 100 IU/ml (Lonza). We detached cells using PBS 0.05% trypsin, 4mM EDTA solution. We maintained cells in a humidified incubator at 37°C 5% CO_2. In all *in vitro* experiments, we performed technical duplicates. To test murine sgRNAs we transfected 300,000 cells for each condition with 1µg of plasmids in total (Cas9 and sgRNA). We resuspended cells in SF Cell Line solution (Lonza, V4XC-2032) and we used the 4D-Nucleofector X Unit (Lonza) with the CM-137 program. To test human sgRNA, firstly we transduced 500,000 Huh7 cells with LV.Cas9 at MOI 80. 10 days after transduction we collected cells, extracted gDNA using Maxwell RSC Cultured Cells DNA Kit (AS1620, Promega), and determined VCN as described for LV titer. Subsequently, we transfected 200,000 Huh7.Cas9 cells with 0.5µg of sgRNA plasmid using Lipofectamine 3000 Transfection Reagent (Thermo Fisher Scientific, L3000001) following the manufacturer's instructions. To test murine donor DNAs *in vitro*, firstly we transduced 1,500,000 Hepa1.6 cells with IDLVs carrying the different donor DNAs at MOI 150. Then, we mixed Cas9 protein (10µg/condition) with sgRNA (2.4µg/condition) and incubated for 10 minutes at room temperature to form RNP. We bought spCas9 protein (IDT, 1081059), and we synthesized the two selected sgRNA using the GeneArt Precision gRNA Synthesis Kit (Thermo Fisher, A29377) following the manufacturer's instructions. We transfected 300,000 cells for each condition with RNP, by resuspending cells in SF Cell Line solution (Lonza, V4XC-2032) and using the 4D-Nucleofector X Unit (Lonza) with the CM-137 program. In parallel, we mock transfected Hepa1.6 cells to keep controls with only donor DNA transduction. Finally, to test human donor DNAs, we transduced 300,000 Huh7.Cas9 cells for each condition with IDLVs carrying donor DNAs and sgRNA expression cassettes at MOI 200. In parallel, we transduced Huh7 cells with the same IDLVs as controls.

5.5 T7 and TIDE assays

In gene editing experiments, we extracted gDNA from cell lines using Maxwell RSC Cultured Cells DNA Kit (AS1620, Promega) and from 50mg of liver tissue using Maxwell RSC Tissue DNA Kit (AS1610, Promega) following the manufacturer's instructions. Cutting efficiency was measured with T7 or TIDE assay. We used TIDE assay just for *in vitro* experiments. Firstly, we amplified by PCR (GoTaq G2 Hot Start Polymerase, Promega), the region including the sgRNA cut site using the following primers:

Gene	*sgRNA*	*Primer Forward (5'- -3)*	*Primer Reverse (5'- -3)*
Murine *Dbt*	1, 4	GCTGTCCAAGAGATCTCCCG	TCAATCAAGTGGCTTGGGGG
	2, 11, 12	GCATTTTAAAAATAGTTAACAGGGTCA	ACCAGAGAGAAAAGAAAACAAA
	3, 6	GCATGATAGTATGGGGGTGGG	GGAGGCTTAGCTCGACCTTG
	5	CCAGCTCTGAGTGCCCCC	GAGAAGGCATGTCTCCCACC
	7	TGTTTCTCCTAGATTATAGCTTGGA	CCTGGCTCTTGGTCAACAAA
	8	TCTTCAAAAGTTTTAAAGCTGAAA	GTGTCCACCTGGAAACTCAC
	9	TGAGTTTCCAGGTGGACACG	CCCTATTCTAAAAGCAACTAGAATAAA
	10	CTGTCATCAGTCTTTTAATTTTATTC	AGATGACCCTGTTAACTATTTTTAA
Murine *Abcb11*	1, 9, 10	GCATCACTCCTTTGCACAGG	AGTTGGTGAGTAGACAATGATTGTT
	2, 11, 12	TGGTCTTTTATTGAAATATTTCCTCT	TCAAACAAACAAACAAAACCCCC
	4, 8	ACTCCATATTGAGACTTAATGGCCT	TGAGGAAATGATTAGATAGTGAGGA
	5	AGCTTTATCTTTGAGGAGGTTTCA	ACTGCCAGTCACGTCTTCAG
	6	TCTGTTTTATCCTGGTTTTCAAACT	CCATCAATGAAAATGAACGTCAGC
	7	ACATAATTTTACTGAATAGAAATGTGT	AGCCATTGATGAATTGTTCTAGCC
Human *DBT*	1	ACAAGTTTTTCATTGTTTTTAGATGCT	CTTGAGCCCAGGAGTTCAGG
	2	TCTCCCCTTCTTATCTGTGGTCT	CGGCTTGATTTGGCTTGACC
	3, 8	GCACAGTGCAGCTTAAATCT	CCTCCTCAGCTCAGGCAATC
	4, 5	TTTTCTTGTTTAAAACTGCCTTCAG	CACAACAGAAAAATTCCAAATGGCA
	6	ACAAAGTCTCAATGCATTGCCC	TCAAAGACAGGGTTGGCTGG
	7	TGTTCTTCTGTCCTGGTTGTGA	TTCAGCCAGGTGCAGTGA
	9	AAAGATGATGTCTGGGCCGG	CAACATGACGAGACCCCCTC
	10	GCAGTGGTGTGATCTTGGCT	TCCTTCAGCTCCCATAATCCTG
	11, 12	TGCAGAGAAGTAAGCTCAGGG	TCTAGGCTCAAGGGGTCCTC
Human *ABCB11*	1, 9	AAAAAGTGTATGTCTTGACTTTAAAAA	AAACCAAAGGAAATTGCCAAT
	2, 11, 12	TGCTTCTGGGATTCCAATTAGGT	ACTGGTGATATTCTTGAGTCACTGT
	3	AGACTAATCATGACTCTGTCGACA	AGCCACTCACATGATTTATCTGACT
	4	GAAAATCTATCGACATTGTGTTACA	TACGGGTATGAGCCACCATG
	5, 10	AGCCTCTATTGCTGATGAGA	ACCATCTCTTCGCTTGGAGC
	6, 7	CGTTTGTTGAGATTTATCCATGCC	TCCATTCCTGTTTTGAAAACCT
	8	GCATGACGTATCCTTTTCACCC	ACTTTACATAGGTGAACTCTGTGA

To perform the T7 assay, we denatured and reannealed 8uL of the PCR product, then we incubated it at 37° for 1 hour with T7 Endonuclease I enzyme (NEB, M0302L). We ran the digested DNA using the D1000 ScreenTape System (Agilent) and quantified the NHEJ percentage using the formula described in the literature (Sentmanat *et al*, 2018). To perform the TIDE assay, firstly we purified the PCR product using the QIAquick PCR Purification Kit (Qiagen, 28104). Then, Eurofins sequenced by Sanger method 25ng of the PCR products using the forward primers exploited for PCR. We analyzed sequencing results by ICE CRISPR analysis tool (Synthego, https://ice.synthego.com/#/).

5.6 Determination of integrations by ddPCR

In gene editing experiments, we extracted gDNA from cell lines using Maxwell RSC Cultured Cells DNA Kit (AS1620, Promega) and from 50mg of liver tissue using Maxwell RSC Tissue DNA Kit (AS1610, Promega) following the manufacturer's instructions. To determine the percentage of integrations in the murine and human setting we designed the following primer and probes on the junction between the genome and the integrated DNA:

Gene	*Name*	*Sequence*
Murine *Dbt*	bGH Fw	5'-GGAGGATTGGGAAGACAATA-3'
	mDbt int1 Rv	5'-GTCACATCATTCTAGGTGCT-3'
	bGH Probe	5'-(FAM)-CTCTATGGATCGGTACCAAG-(BHQ1)-3'
Murine *Abcb11*	mAbcb11 int1 Fw	5'-TGTCTCATGGCTAACTCTAC-3'
	Splice Acc Rv	5'-TGGAGAGAAAGGCAAAGTGG-3'
	Splice Acc Probe	5'-(FAM)-GGCACCTATTGGTCTTACTG-(BHQ1)-3'
Murine *Sema3a* (normalizer)	Sema Fw long	5'-AGACCTGCCTAAGAGATGCA-3'
	Sema Rv	5'-TCCATATTAATGCAGTGCTTGC-3'
	Sema Probe	5'-(HEX)-AGAGGCCTGTCCTGCAGCTCATGG-(BHQ1)-3'
Human *DBT*	hDBT int1 Fw	5'-CCAAGTAGCTGGCACTACAG-3'
	Splice Acc Rv	5'-TGGAGAGAAAGGCAAAGTGG-3'
	Splice Acc Probe	5'-(FAM)-GGCACCTATTGGTCTTACTG-(BHQ1)-3'
Human *ABCB11*	hABCB11 int1 Fw	5'-TGATTGGCCGTCCTGACATA-3'
	Splice Acc Rv	5'-TGGAGAGAAAGGCAAAGTGG-3'
	Splice Acc Probe	5'-(FAM)-GGCACCTATTGGTCTTACTG-(BHQ1)-3'
	Telo Fw long	5'-GGTGTACGCCGAGACCAAG-3'

Human *TERT* (normalizer)	Telo Rv	5'-GGTGAACCTCGTAAGTTTATGCAA-3'
	Telo Probe	5'-(HEX)-TCAGGACGTCGAGTGGACACGGTG-(BHQ1)-3'

We exploited the ddPCR system by Biorad as described for LV titer. However, we optimized the PCR mix to allow the amplification of long amplicons (>900bp) as follows:

Component	*Producer (Catalog number)*	*Final concentration*
ddPCR Supermix for Probes (No dUTP)	Biorad (1863024)	1X
Primer Fw	Eurofins (custom oligo)	1µM
Primer Rv	Eurofins (custom oligo)	1µM
Probe	Metabion (custom probe)	0.5µM
$MgCl_2$	Promega (A351B)	2mM
dNTPs	Promega (U1330)	0.25mM
GoTaq G2 Hot Start Polymerase	Promega (M740A)	0.625U
gDNA		50ng

We also modified the thermal cycle for PCR amplification as follows:

Temperature	*Time*	*Cycles*	*Ramp rate*
95°C	10 minutes	1x	2°C/second
94°C	30 seconds	40x	
Annealing depending on primers	1 minute		
72°C	2 minutes		
98°C	10 minutes	1x	
4°C	Infinite	1x	

The annealing temperatures were different for the various primer couples: 56°C for murine *Dbt* and *Abcb11*, 60°C for *Sema3a* and *TERT*, and 65°C for human *DBT* and *ABCB11*. We read the results with QX200 or QX600 Droplet Digital PCR System (Biorad), and we calculated the percentage of integration with the formula: $\frac{ng\ gene}{ng\ gDNA} * 2 * 100$.

5.7 AAV production and titration

Innovavector produced and determined the titer of AAV serotype 8 with donor DNA constructs that we cloned. We produced AAV serotype 8 carrying hepatocyte-specific expression cassettes for hFIX or mCherry using an adenovirus-free transient transfection method and performed purification using a chromatographic method as described earlier (Collaud *et al*, 2019). We determined titers of the AAV stocks using a real-time qPCR using primers on the hAAT promoter (Forward: 5' GGC GGG CGA CTC AGA TC 3' and Reverse: 5' GGG AGG CTG CTG GTG AAT ATT 3').

5.8 LNP production and quality assessment

To produce LNP, we exploited the commercially available lipid mix GenVoy-ILM (Cytiva, 1002769). Axolab synthetized sgRNAs, following the previously described nucleotide modification (Finn *et al*, 2018). We purchased Cas9 mRNA (L-7606), and Cre mRNA (L-7211) from Trilink BioTechnologies. We mixed RNA and lipids with NanoAssemblr Ignite nanoparticle formulation systems (Cytiva) using NanoAssemblr Ignite cartridges (Cytiva) following the manufacturer's instructions. We set a total flow rate of 12mL/minute, a flow rate ratio of 3:1 (RNAs:lipids), and a nitrogen-to-phosphate ratio of 4. We diluted the LNP preparation 1:25 with PBS and concentrated again with Amicon Centrifugal Filter (MWCO 100kDa) to remove ethanol. We finally filtered them with a 0.22µm syringe filter. We determined particle size and polydispersity index by analyzing a 1:20 dilution of LNP in PBS with the Zetasizer Ultra instrument (Malvern Panalytical). To determine the RNA concentration and efficiency of encapsulation, we exploited the Quant-it RiboGreen RNA Assay Kit (Thermo Fisher Scientific, R11490) following the protocol developed by Cytiva.

5.9 Mice experiments

We carried out all animal experiments under good animal practices following Italian and European legislation on animal care and experimentation (2010/63/EU) and approved by the local institutional ethical committee. In the experiments, we used C57BL/6, Cas9, TdTomato, *Abcb11*$^{-/-}$, and *Agl*$^{-/-}$ mice. We purchased C57BL/6 mice from Charles River

Laboratories. We purchased Cas9 mice (strain #024858), TdTomato mice (strain #007914), and *Abcb11*$^{-/-}$ mice (strain #004125) from The Jackson Laboratory. The Agl knockout (*Agl*$^{-/-}$) mice were developed in the frame of the International Mouse Phenotyping Consortium (IMPC). Mice were generated in a pure C57BL/6J background by replacing exons 6–10 of the *Agl* gene with a neomycin-expressing cassette. Mice were bred into a mixed BALB/c background. To genotype *Abcb11*$^{-/-}$ mice, we extracted gDNA from tissue biopsies obtained by ear clipping procedure. We resuspended each biopsy in 25µL of QuickExtract DNA extraction solution (Biosearch technologies), incubated at 65°C for 6 minutes, and then at 98°C for 2 minutes. We then performed PCR genotyping, as detailed on The Jackson Laboratory website strain #004125. We genotyped *Agl*$^{-/-}$ mice as previously described (Vidal *et al*, 2018). In experiments with Cas9 mice, we administered IDLV or AAV intravenous (i.v.) retro-orbitally in 2-week-old, and *via* the temporal vein in 2-day-old mice. We treated in parallel with the same vectors aged matched C57BL/6 mice as control. In experiments testing the combination of viral vectors and LNPs for genome editing, we first administered 2-week-old C57BL/6 mice with IDLV or AAV and then right after, 48-hour or 1-week later LNPs both by i.v. retro-orbital injection. In parallel, we treated age-matched mice just with IDLV, AAV, or LNP as controls. In CCl_4 experiments, we intraperitoneally injected 6-week-old C57BL/6 mice with 0.6µL/g of body weight of CCl_4 (289116, Sigma-Aldrich) that was diluted in corn oil to reach a final volume of 50µL. We administered the treatment for a period of 3 or 6 weeks, depending on the experiment. In DDC experiments, we fed 6-week-old C57BL/6 mice with a standard diet supplemented with 0.1% (w/w) of DDC (137030, Sigma-Aldrich), for a period of 3 or 5 weeks, depending on the experiment. In these experiments, we delivered LV or AAV by i.v. retro-orbital administration. We always included age and sex-matched controls injected in parallel with the same doses of LV or AAV. We collected blood samples from the retro-orbital plexus with or without 0.38% sodium citrate anticoagulant buffer pH 7.4 for plasma or serum preparation, respectively. In the experiment with TdTomato mice, we treated 6-week-old mice either with CCl_4 or with DDC for 6 or 5 weeks respectively, as described before. We then administered LNP by i.v. retro-orbital administration, to treated mice as well as age and sex-matched controls. In experiments with *Abcb11*$^{-/-}$ mice, we delivered LV or AAV to 6-month-old male and female mice by i.v. retro-orbital administration including WT (*Abcb11*$^{+/+}$) as controls. In

experiments with *Agl*$^{-/-}$ mice, we administered LV or AAV i.v. *via* the tail vein to 9-month-old male *Agl*$^{-/-}$ mice and WT littermates (*Agl*$^{+/+}$).

5.10 Gene expression assays

We extracted RNA from 50 mg of liver tissue using Maxwell RSC simplyRNA Tissue Kit (AS1340, Promega) and then we retrotranscribed it with SuperScript IV VILO Master Mix with EzDNase Enzyme (Thermo Fisher), following the manufacturer's instructions. We used ddPCR to quantify gene expressions. For mCherry we designed primers (mCherry Fw: 5'-AGAGGCTGAAGCTGAAGGAC-3', mCherry Rv: 5'-GGTGTAGTCCTCGTTGTGGG-3') and probe (mCherry Pr: 5'-(FAM)-GTCAAGACCACCTACAAGGC-(TAMRA)-3'). For *Dbt* and *Abcb11* we used commercially available systems (Thermo Fisher Scientific, respectively Mm00501651_m1 and Mm00445168_m1, FAM). As normalizer, we used a commercial system to detect *Hprt* expression (Biorad, Mus Musculus, dMmuCPE5095493, HEX). We calculated gene expression levels with the formula ng cDNA gene/ng cDNA normalizer.

5.11 Liver immunofluorescence imaging

We fixed mouse livers in PBS 4% paraformaldehyde (PFA) for 4 hours, then moved them to 30% sucrose 0.02% sodium azide for at least 24 hours. We embedded livers in OCT (optimal cutting temperature) compound (Killik, Bio Optica) and prepared 10 µm-thick slices using a cryostat (Histo-line MC5050). We placed slices on Superfrost Plus microscope slides (Epredia) and stored them at -80°C. For the staining, we thawed the slides at room temperature for at least 2 hours, then washed them 3 times in PBS 0.1% X-Triton. We blocked non-specific bindings incubating slides with PBS 0.1% X-Triton 5% FBS 1% BSA for 1 hour at room temperature in a humid chamber. We substituted the blocking solution with a primary antibody mix diluted in blocking solution, which was incubated overnight at 4°C in a humid chamber. After 3 washes with PBS 0.1% X-Triton, we added a secondary antibody mix diluted in blocking solution with Hoechst 33342 (1:2000, H3570, Life technologies), which was incubated for 1 hour at room temperature

in a humid chamber. We washed the slides in PBS and added Fluoromount-G (Invitrogen) to mount the coverslip. We used the following antibodies:

Antigen	*Species*	*Fluorochrome*	*Clone*	*Company (code)*	*Dilution*
mCherry	Chicken	-	Polyclonal	Abcam (ab205402)	1:1000
CK7	Rabbit	-	Polyclonal	Abcam (ab181598)	1:250
GS	Rabbit	-	Polyclonal	Novus Bio (NB110-4104)	1:5000
Chicken IgY	Goat	AF546	Polyclonal	Invitrogen (A11040)	1:1000
Rabbit IgG	Donkey	AF647	Polyclonal	Invitrogen (A31573)	1:1000

We acquired images using the confocal microscope Mavig Rs-G4 (RSG4 software) at 20X magnification and analyzed them with MATLAB software (9.13.0.2126072 (R2022b) Update 3), after manually excluding unwanted areas like fringed borders. We exploited a custom MATLAB script that quantified the mCherry-positive tissue area, automatically calculating the threshold for each image, based on the signal intensity. The script measured the total liver area by saturating the signal from the whole tissue. We identified periportal and pericentral areas by marking tissue areas within a fixed distance from CK7 or GS-positive area using MATLAB.

5.12 Determination of hepatic clinical chemistry

We used commercially available ALT (Instrumentation Laboratory, #0018257440), AST (Instrumentation Laboratory, #0018257540), and ALP (Instrumentation Laboratory, #18259740) controls for the quantitative determination of the serum ALT, AST, and ALP concentration with an International Federation of Clinical Chemistry and Laboratory Medicine–optimized kinetic ultraviolet (UV) method in an ILab650 chemical analyzer (Instrumentation Laboratory). We analyzed SeraChem Control Level 1 and Level 2 (#0018162412 and #0018162512) as quality controls.

5.13 Liver histopathology analysis

We harvested livers from mice and fixed them in buffered 4% buffered formalin by immersion. We embedded livers in paraffin, and then we sectioned and mounted them on

glass slides. We stained 2,5-µm paraffin sections with hematoxylin-eosin and Picrosirius Red for histopathological evaluation and analysis of collagen deposition. We captured images from digitalized slides scanned using Aperio Scanscope (Leica) and Pannoramic Midi (3D Histech). For the cytokeratin 19 immunohistochemistry assay (IHC CK19) we used the rabbit monoclonal antibody anti-CK19 clone EP1580Y (Abcam), diluted 1:1000, and incubated 1 hour at room temperature.

5.14 Enzyme-linked immunosorbent assay (ELISA)

To determine hFIX antigen concentration in mouse plasma, we used a paired antibody set (FIX-EIA, Affinity Biologicals). We coated plates with 100µL of capture antibody (FIX-EIA-C, 1:200 diluted in 50mM carbonate pH 9.6) and incubated them overnight at 4°C. We washed plates 3 times with PBS 0.05% (v/v) Tween-20 and incubated them with 100µL of samples diluted in PBS 0.05%, Tween 1%, bovine serum albumin (BSA) or standard controls for 2 hours at room temperature. We washed plates 3 times, and we added an HRP-conjugated detection antibody (FIX-EIA-D, 1:200 diluted in PBS 0.05% Tween 1% BSA), which was incubated for 1.5 hours at room temperature. After 3 washes, we added 100 µL of 3,3′, 5,5′-Tetrametil-benzidine substrate for 5 minutes and stopped the reaction with 50µL of hydrochloric acid 1 M. We read plates at 450nm using a Multiskan GO microplate reader (Thermo Fisher Scientific).

5.15 VCN determination

In LV experiments, we extracted gDNA from 50 mg of liver, spleen, kidney, lung, and brain tissue using Maxwell RSC Tissue DNA Kit (AS1610, Promega) following the manufacturer's instructions. Moreover, we extracted gDNA from hepatocytes using Maxwell RSC Cultured Cells DNA Kit (AS1620, Promega) and from KC, LSEC, HSC, and pDC using QIAamp DNA Micro Kit (56304, Qiagen) following the manufacturer's instructions. In AAV experiments, we extracted gDNA from 50 mg of liver tissue using DNeasy Blood & Tissue Kit (69504, Qiagen) following the manufacturer's instructions. We determined LV VCN as for LV titration, and AAV VCN by ddPCR using primers (hAAT Fw: 5'- GGCGGGCGACTCAGATC-3', hAAT Rv: 5'-GGGAGGCTGCTGGTGAATATT-3') and a probe (hAAT Pr: 5'-(FAM)-

AGCCCCTGTTTGCTCCTCCGATAACTG-(TAMRA)-3'). For both LV and AAV VCN determination, we quantified mouse gDNA using primers (Sema Fw: 5'-ACCGATTCCAGATGATTGGC-3'; Sema Rv: 5'- TCCATATTAATGCAGTGCTTGC-3') and probe (Sema Pr: 5'-(HEX)-AGAGGCCTGTCCTGCAGCTCATGG-(BHQ1)-3') designed on Sema3a reference gene.

5.16 p24 measurement in serum

We measured LV p24 in the serum of mice using Simple Plex HIV-1 Gag p24 Cartridge (SPCKB-PS-000981, R&D systems) following the manufacturer's instructions. We diluted 1:1000 serum samples collected 30 minutes after injection, 1:100 serum samples collected 60 minutes after, and 1:10 serum samples collected at 24 hours.

5.17 Sorting of liver subpopulations

To sort liver subpopulations, we followed a previously described protocol (Milani *et al*, 2019b). We digested mouse liver exploiting perfusion through the inferior vena cava of collagenase IV (Sigma). We created a cell suspension by passing the liver through a 100μm cell strainer (BD Biosciences). We centrifuged cells at 30, 25, and 20g for 3 minutes sequentially, to separate hepatocytes (pelleted) from nPCs (in the supernatant). We stained hepatocytes by diluting in 200μl of PBS the following antibodies:

Antigen	*Fluorochrome*	*Clone*	*Company (code)*	*Volume*
CD31	APC	MEC 13.3	BD Biosciences (551262)	3μl
CD45	APC	30-F11	BD Biosciences (559864)	3μl
FC Block		2.4G2	BD Biosciences (553142)	5μl

After 20 minutes of incubation at room temperature, we washed them with HBSS (Hank's balanced salt solution, Gibco) 1% HEPES (4-(2-hydroxyethyl)-1-piperazineethanesulfonic acid). We sorted hepatocytes using MoFlo Astrios (Backman Coulter), selecting the APC-negative population and analyzing the percentage of mCherry-positive hepatocytes. We centrifuged nPCs in the supernatant for 10 minutes at 650g. Then, we loaded cells in a Percol gradient of 30%-60% and centrifuged for 15

minutes at 1800g. We collected the nPC interface and washed it twice with HBSS 1% HEPES. Firstly, we incubated nPCs for 15 minutes with 5µL of FC Block, then we stained them with the following antibody mix, diluted in 200µl of PBS:

Antigen	*Fluorochrome*	*Clone*	*Company (code)*	*Volume*
CD31	FITC	MEC 13.3	BD Biosciences (551262)	7µl
CD45	BV786	104	BD Biosciences (563686)	7µl
F4/80	PE	CI:A3-1	BD Biosciences (553142)	7 µl
CD45R/B220	PE-Cy5	RA3-6B2	BD Biosciences (553091)	7 µl
CD11c	PE-Cy7	N418	Invitrogen (25-0114-82)	7 µl

After 20 minutes of incubation at 4°C, we washed them with HBSS 1% HEPES. We sorted KC, LSEC, HSC, and pDC using BD FACSAria Fusion (BD Biosciences).

5.18 Statistical analysis

We presented data as individual values with mean ± standard error of the mean (SEM) or as mean ± SEM. We performed statistical analyses using GraphPad Prism software (10.2.0.392). We applied inferential techniques in the presence of adequate sample sizes ($n \geq 4$), otherwise we reported only descriptive statistics. We performed the two-tailed Mann-Whitney test when comparing two independent groups, or the Kruskal-Wallis test followed by *post hoc* analysis (Dunn's test for multiple comparisons against the reference control group along with Bonferroni's correction) for the comparison of more than two independent groups. For zonation analysis, we presented data as individual values with median and quartiles. To compare the median of our samples with the hypothetical value of 1 we performed the Wilcoxon signed-rank test.

References

A Study of VERVE-101 in Patients With Familial Hypercholesterolemia and Cardiovascular Disease (2024)

A Study of VERVE-102 in Patients With Familial Hypercholesterolemia or Premature Coronary Artery Disease (2024)

A Study to Evaluate the Safety and Efficacy of BEAM-302 in Adult Patients With Alpha-1 Antitrypsin Deficiency (AATD) (2024)

Abudayyeh OO, Gootenberg JS, Essletzbichler P, Han S, Joung J, Belanto JJ, Verdine V, Cox DBT, Kellner MJ, Regev A, *et al* (2017) RNA targeting with CRISPR–Cas13. *Nature* 550: 280–284

Adlat S, Vázquez Salgado AM, Lee M, Yin D & Wangensteen KJ (2023) Emerging and potential use of CRISPR in human liver disease. *Hepatology*

Amabile A, Migliara A, Capasso P, Biffi M, Cittaro D, Naldini L & Lombardo A (2016) Inheritable Silencing of Endogenous Genes by Hit-and-Run Targeted Epigenetic Editing. *Cell* 167: 219-232.e14

An M, Raguram A, Du SW, Banskota S, Davis JR, Newby GA, Chen PZ, Palczewski K & Liu DR (2024) Engineered virus-like particles for transient delivery of prime editor ribonucleoprotein complexes in vivo. *Nat Biotechnol*

Anzalone A V., Gao XD, Podracky CJ, Nelson AT, Koblan LW, Raguram A, Levy JM, Mercer JAM & Liu DR (2022) Programmable deletion, replacement, integration and inversion of large DNA sequences with twin prime editing. *Nat Biotechnol* 40: 731–740

Anzalone A V., Koblan LW & Liu DR (2020) Genome editing with CRISPR–Cas nucleases, base editors, transposases and prime editors. *Nat Biotechnol* 38: 824–844

Anzalone A V, Randolph PB, Davis JR, Sousa AA, Koblan LW, Levy JM, Chen PJ, Wilson C, Newby GA, Raguram A, *et al* (2019) Search-and-replace genome editing without double-strand breaks or donor DNA. *Nature* 576: 149

Aranko AS, Wlodawer A & Iwai H (2014) Nature's recipe for splitting inteins. *Protein Engineering Design and Selection* 27: 263–271

Aronson SJ, Bakker RS, Shi X, Duijst S, ten Bloemendaal L, de Waart DR, Verheij J, Ronzitti G, Oude Elferink RP, Beuers U, *et al* (2019) Liver-directed gene therapy results in long-term correction of progressive familial intrahepatic cholestasis type 3 in mice. *J Hepatol* 71: 153–162

Asrani SK, Devarbhavi H, Eaton J & Kamath PS (2019) Burden of liver diseases in the world. *J Hepatol* 70: 151–171

Bae S, Park J & Kim J-S (2014) Cas-OFFinder: a fast and versatile algorithm that searches for potential off-target sites of Cas9 RNA-guided endonucleases. *Bioinformatics* 30: 1473–1475

Baiocchini A, Montaldo C, Conigliaro A, Grimaldi A, Correani V, Mura F, Ciccosanti F, Rotiroti N, Brenna A, Montalbano M, *et al* (2016) Extracellular Matrix Molecular Remodeling in Human Liver Fibrosis Evolution. *PLoS One* 11: e0151736

Baiocchini A, Del Nonno F, Taibi C, Visco-Comandini U, D'Offizi G, Piacentini M & Falasca L (2019) Liver sinusoidal endothelial cells (LSECs) modifications in patients with chronic hepatitis C. *Sci Rep* 9: 8760

Banskota S, Raguram A, Suh S, Du SW, Davis JR, Choi EH, Wang X, Nielsen SC, Newby GA, Randolph PB, *et al* (2022) Engineered virus-like particles for efficient in vivo delivery of therapeutic proteins. *Cell* 185: 250-265.e16

Barbon E, Kawecki C, Marmier S, Sakkal A, Collaud F, Charles S, Ronzitti G, Casari C, Christophe OD, Denis C V., *et al* (2023) Development of a dual hybrid AAV vector for endothelial-targeted expression of von Willebrand factor. *Gene Ther* 30: 245–254

Baruteau J, Brunetti-Pierri N & Gissen P (2024) Liver-directed gene therapy for inherited metabolic diseases. *J Inherit Metab Dis* 47: 9–21

Barzel A, Paulk NK, Shi Y, Huang Y, Chu K, Zhang F, Valdmanis PN, Spector LP, Porteus MH, Gaensler KM, *et al* (2015) Promoterless gene targeting without nucleases ameliorates haemophilia B in mice. *Nature* 517: 360–364

Beam Therapeutics Announces First Patient Dosed in the Phase 1/2 Study of BEAM-302 in Alpha-1 Antitrypsin Deficiency (AATD) (2024)

Bell P, Wang L, Gao G, Haskins ME, Tarantal AF, McCarter RJ, Zhu Y, Yu H & Wilson JM (2011) Inverse zonation of hepatocyte transduction with AAV vectors between mice and non-human primates. *Mol Genet Metab* 104: 395–403

Bendixen L, Jensen TI & Bak RO (2023) CRISPR-Cas-mediated transcriptional modulation: The therapeutic promises of CRISPRa and CRISPRi. *Molecular Therapy* 31: 1920–1937

Berasain C, Arechederra M, Argemí J, Fernández-Barrena MG & Avila MA (2023) Loss of liver function in chronic liver disease: An identity crisis. *J Hepatol* 78: 401–414

Beyersdorf JP, Bawage S, Iglesias N, Peck HE, Hobbs RA, Wroe JA, Zurla C, Gersbach CA & Santangelo PJ (2022) Robust, Durable Gene Activation In Vivo via mRNA-Encoded Activators. *ACS Nano* 16: 5660–5671

Blackburn P, Gass J, Pinto e Vairo F, Farnham K, Atwal H, Macklin S, Klee E & Atwal P (2017) Maple syrup urine disease: mechanisms and management. *Appl Clin Genet* Volume 10: 57–66

Blair HA (2022) Valoctocogene Roxaparvovec: First Approval. *Drugs* 82: 1505–1510

Bocca C, Novo E, Miglietta A & Parola M (2015) Angiogenesis and Fibrogenesis in Chronic Liver Diseases. *Cell Mol Gastroenterol Hepatol* 1: 477–488

Böck D, Rothgangl T, Villiger L, Schmidheini L, Matsushita M, Mathis N, Ioannidi E, Rimann N, Grisch-Chan HM, Kreutzer S, *et al* (2022) In vivo prime editing of a metabolic liver disease in mice. *Sci Transl Med* 14

Bonam SR, Wang F & Muller S (2019) Lysosomes as a therapeutic target. *Nat Rev Drug Discov* 18: 923–948

Borkham-Kamphorst E & Weiskirchen R (2016) The PDGF system and its antagonists in liver fibrosis. *Cytokine Growth Factor Rev* 28: 53–61

Brooks DL, Carrasco MJ, Qu P, Peranteau WH, Ahrens-Nicklas RC, Musunuru K, Alameh M-G & Wang X (2023) Rapid and definitive treatment of phenylketonuria in variant-humanized mice with corrective editing. *Nat Commun* 14

Brooks DL, Whittaker MN, Said H, Dwivedi G, Qu P, Musunuru K, Ahrens-Nicklas RC, Alameh M-G & Wang X (2024) A base editing strategy using mRNA-LNPs for in vivo correction of the most frequent phenylketonuria variant. *HGG Adv* 5: 100253

Brunetti-Pierri N, Ferla R, Ginocchio VM, Rossi A, Fecarotta S, Romano R, Parenti G, Yildiz Y, Zancan S, Pecorella V, *et al* (2022) Liver-Directed Adeno-Associated Virus–Mediated Gene Therapy for Mucopolysaccharidosis Type VI. *NEJM Evidence* 1

Bu F, Jia P, Zhu Y, Yang Y, Meng H, Bi Y, Huang C & Li J (2022) Emerging therapeutic potential of adeno-associated virus-mediated gene therapy in liver fibrosis. *Mol Ther Methods Clin Dev* 26: 191–206

Burrage LC, Nagamani SCS, Campeau PM & Lee BH (2014) Branched-chain amino acid metabolism: from rare Mendelian diseases to more common disorders. *Hum Mol Genet* 23: R1–R8

Canepari C & Cantore A (2023) Gene transfer and genome editing for familial hypercholesterolemia. *Frontiers in Molecular Medicine* 3

De Caneva A, Porro F, Bortolussi G, Sola R, Lisjak M, Barzel A, Giacca M, Kay MA, Vlahoviček K, Zentilin L, *et al* (2019) Coupling AAV-mediated promoterless gene targeting to SaCas9 nuclease to efficiently correct liver metabolic diseases. *JCI Insight* 4

Cantore A, Ranzani M, Bartholomae CC, Volpin M, Valle P Della, Sanvito F, Sergi LS, Gallina P, Benedicenti F, Bellinger D, *et al* (2015) Liver-directed lentiviral gene therapy in a dog model of hemophilia B. *Sci Transl Med* 7

Cappelluti MA, Mollica Poeta V, Valsoni S, Quarato P, Merlin S, Merelli I & Lombardo A (2024) Durable and efficient gene silencing in vivo by hit-and-run epigenome editing. *Nature* 627: 416–423

Casini A, Olivieri M, Petris G, Montagna C, Reginato G, Maule G, Lorenzin F, Prandi D, Romanel A, Demichelis F, *et al* (2018) A highly specific SpCas9 variant is identified by in vivo screening in yeast. *Nat Biotechnol* 36: 265–271

Cesare Canepari, Michela Milani, Francesco Starinieri, Anna Fabiano, Fabio Russo, Mauro Biffi, Rossana Norata, Martina Rocchi, Francesca Sanvito & Alessio Cantore (2024) Lentiviral Gene Therapy to the Liver for Homozygous Familial Hypercholesterolemia (FH): Assessing the Best Vector Design [abstract n.198]. *27th Annual Meeting ASGCT* [PREPRINT]

Chace DH, Kalas TA & Naylor EW (2003) Use of Tandem Mass Spectrometry for Multianalyte Screening of Dried Blood Specimens from Newborns. *Clin Chem* 49: 1797–1817

Chadwick AC, Wang X & Musunuru K (2017) In Vivo Base Editing of PCSK9 (Proprotein Convertase Subtilisin/Kexin Type 9) as a Therapeutic Alternative to Genome Editing. *Arterioscler Thromb Vasc Biol* 37: 1741–1747

Chandler RJ, Venturoni LE, Liao J, Hubbard BT, Schneller JL, Hoffmann V, Gordo S, Zang S, Ko C-W, Chau N, *et al* (2021) Promoterless, Nuclease-Free Genome Editing Confers a Growth Advantage for Corrected Hepatocytes in Mice With Methylmalonic Acidemia. *Hepatology* 73: 2223–2237

Charlesworth CT, Deshpande PS, Dever DP, Camarena J, Lemgart VT, Cromer MK, Vakulskas CA, Collingwood MA, Zhang L, Bode NM, *et al* (2019) Identification of preexisting adaptive immunity to Cas9 proteins in humans. *Nat Med* 25: 249–254

Che Z, Zhou Z, Li S-Q, Gao L, Xiao J & Wong N-K (2023) ROS/RNS as molecular signatures of chronic liver diseases. *Trends Mol Med* 29: 951–967

Chen B, Gilbert LA, Cimini BA, Schnitzbauer J, Zhang W, Li G-W, Park J, Blackburn EH, Weissman JS, Qi LS, *et al* (2013) Dynamic Imaging of Genomic Loci in Living Human Cells by an Optimized CRISPR/Cas System. *Cell* 155: 1479–1491

Chen H, Shi M, Gilam A, Zheng Q, Zhang Y, Afrikanova I, Li J, Gluzman Z, Jiang R, Kong L-J, *et al* (2019) Hemophilia A ameliorated in mice by CRISPR-based in vivo genome editing of human Factor VIII. *Sci Rep* 9: 16838

Chen X, Du J, Yun S, Xue C, Yao Y & Rao S (2024a) Recent advances in CRISPR-Cas9-based genome insertion technologies. *Mol Ther Nucleic Acids* 35: 102138

Chen Z, Zhang D, Zheng R, Yang L, Huo Y, Zhang D, Fang X, Li Y, Xu G, Li D, *et al* (2024b) In vivo base editing rescues primary hyperoxaluria type 1 in rats. *Kidney Int* 105: 496–507

Cho H-J & Cheong J-Y (2021) Role of Immune Cells in Patients with Hepatitis B Virus-Related Hepatocellular Carcinoma. *Int J Mol Sci* 22: 8011

Christian M, Cermak T, Doyle EL, Schmidt C, Zhang F, Hummel A, Bogdanove AJ & Voytas DF (2010) Targeting DNA Double-Strand Breaks with TAL Effector Nucleases. *Genetics* 186: 757–761

Collaud F, Bortolussi G, Guianvarc'h L, Aronson SJ, Bordet T, Veron P, Charles S, Vidal P, Sola MS, Rundwasser S, *et al* (2019) Preclinical Development of an AAV8-hUGT1A1 Vector for the Treatment of Crigler-Najjar Syndrome. *Mol Ther Methods Clin Dev* 12: 157

CRISPR Therapeutics Provides Business Update and Reports Fourth Quarter and Full Year 2023 Financial Results (2023)

Cunningham SC, Dane AP, Spinoulas A & Alexander IE (2008) Gene Delivery to the Juvenile Mouse Liver Using AAV2/8 Vectors. *Molecular Therapy* 16: 1081–1088

D'Ambrosio R, Aghemo A, Rumi MG, Ronchi G, Donato MF, Paradis V, Colombo M & Bedossa P (2012) A morphometric and immunohistochemical study to assess the benefit of a sustained virological response in hepatitis C virus patients with cirrhosis. *Hepatology* 56: 532–543

D'Amico G, Morabito A, D'Amico M, Pasta L, Malizia G, Rebora P & Valsecchi MG (2018) New concepts on the clinical course and stratification of compensated and decompensated cirrhosis. *Hepatol Int* 12: 34–43

D'Antiga L, Beuers U, Ronzitti G, Brunetti-Pierri N, Baumann U, Di Giorgio A, Aronson S, Hubert A, Romano R, Junge N, *et al* (2023) Gene Therapy in Patients with the Crigler–Najjar Syndrome. *New England Journal of Medicine* 389: 620–631

Das M, Boerma M, Goree JR, Lavoie EG, Fausther M, Gubrij IB, Pangle AK, Johnson LG & Dranoff JA (2014) Pathological Changes in Pulmonary Circulation in Carbon Tetrachloride (ccl4)-Induced Cirrhotic Mice. *PLoS One* 9: e96043

Davidoff AM, Ng CYC, Zhou J, Spence Y & Nathwani AC (2003) Sex significantly influences transduction of murine liver by recombinant adeno-associated viral vectors through an androgen-dependent pathway. *Blood* 102: 480–488

Davis AR, Rosenthal P & Newman TB (2009) Nontransplant surgical interventions in progressive familial intrahepatic cholestasis. *J Pediatr Surg* 44: 821–827

Davis JR, Banskota S, Levy JM, Newby GA, Wang X, Anzalone A V, Nelson AT, Chen PJ, Hennes AD, An M, *et al* (2024) Efficient prime editing in mouse brain, liver and heart with dual AAVs. *Nat Biotechnol* 42: 253–264

Davis JR, Wang X, Witte IP, Huang TP, Levy JM, Raguram A, Banskota S, Seidah NG, Musunuru K & Liu DR (2022) Efficient in vivo base editing via single adeno-associated viruses with size-optimized genomes encoding compact adenine base editors. *Nat Biomed Eng* 6: 1272–1283

Davit-Spraul A, Gonzales E, Baussan C & Jacquemin E (2009) Progressive familial intrahepatic cholestasis. *Orphanet J Rare Dis* 4: 1

Deeks ED (2021) Odevixibat: First Approval. *Drugs* 81: 1781–1786

Deng Z, Fan T, Xiao C, Tian H, Zheng Y, Li C & He J (2024) TGF-β signaling in health, disease, and therapeutics. *Signal Transduct Target Ther* 9: 61

Dewidar B, Meyer C, Dooley S & Meindl-Beinker and N (2019) TGF-β in Hepatic Stellate Cell Activation and Liver Fibrogenesis—Updated 2019. *Cells* 8: 1419

Ding Q, Strong A, Patel KM, Ng S-L, Gosis BS, Regan SN, Cowan CA, Rader DJ & Musunuru K (2014) Permanent Alteration of PCSK9 With In Vivo CRISPR-Cas9 Genome Editing. *Circ Res* 115: 488–492

Doman JL, Raguram A, Newby GA & Liu DR (2020) Evaluation and minimization of Cas9-independent off-target DNA editing by cytosine base editors. *Nat Biotechnol* 38: 620–628

Douglass Wright W, Shital Shah S & Heyer W-D (2018) Homologous recombination and the repair of DNA double-strand breaks. *J Biol Chem* 293: 10524–10535

Dull T, Zufferey R, Kelly M, Mandel RJ, Nguyen M, Trono D & Naldini L (1998) A Third-Generation Lentivirus Vector with a Conditional Packaging System. *J Virol* 72: 8463–8471

Eaton JE, Talwalkar JA, Lazaridis KN, Gores GJ & Lindor KD (2013) Pathogenesis of Primary Sclerosing Cholangitis and Advances in Diagnosis and Management. *Gastroenterology* 145: 521–536

Elena Barbon, Camilla Negri, Andrea Raimondi, Chiara Simoni, Elisabetta Manta, Francesca Sanvito, Giancarlo la Marca, Amy Argabright, Angelo D'Alessandro & Alessio Cantore (2024) Long-Term Efficacy, Safety, and Extrahepatic Benefit of Liver-Directed Lentiviral Gene Therapy in a Methylmalonic Acidemia Mouse Model [abstract n.163]. *27th Annual Meeting ASGCT* [PREPRINT]

Elijah Trefts, Maureen Gannon & David H. Wasserman (2017) The liver. *Current Biology* 27: R1141–R1155

El-Serag HB (2012) Epidemiology of Viral Hepatitis and Hepatocellular Carcinoma. *Gastroenterology* 142: 1264-1273.e1

Esposito F, Dell'Aquila F, Rhiel M, Auricchio S, Chmielewski KO, Andrieux G, Ferla R, Horrach PS, Padmanabhan A, Di Cunto R, *et al* (2024) Safe and effective liver-directed AAV-mediated homology-independent targeted integration in mouse models of inherited diseases. *Cell Rep Med*: 101619

Evason K, Bove KE, Finegold MJ, Knisely AS, Rhee S, Rosenthal P, Miethke AG, Karpen SJ, Ferrell LD & Kim GE (2011) Morphologic Findings in Progressive Familial Intrahepatic Cholestasis 2 (PFIC2). *American Journal of Surgical Pathology* 35: 687–696

Ewing CB, Soltys KA, Strauss KA, Sindhi R, Vockley J, McKiernan P, Squires RH, Bond G, Ganoza A, Khanna A, *et al* (2021) Metabolic Control and "Ideal" Outcomes in Liver Transplantation for Maple Syrup Urine Disease. *J Pediatr* 237: 59-64.e1

Fallowfield JA, Mizuno M, Kendall TJ, Constandinou CM, Benyon RC, Duffield JS & Iredale JP (2007) Scar-Associated Macrophages Are a Major Source of Hepatic Matrix Metalloproteinase-13 and Facilitate the Resolution of Murine Hepatic Fibrosis. *The Journal of Immunology* 178: 5288–5295

Farrell G, Schattenberg JM, Leclercq I, Yeh MM, Goldin R, Teoh N & Schuppan D (2019) Mouse Models of Nonalcoholic Steatohepatitis: Toward Optimization of Their Relevance to Human Nonalcoholic Steatohepatitis. *Hepatology* 69: 2241–2257

FDA NEWS RELEASE FDA Approves First Gene Therapies to Treat Patients with Sickle Cell Disease (2023)

Ferrari S, Jacob A, Cesana D, Laugel M, Beretta S, Varesi A, Unali G, Conti A, Canarutto D, Albano L, *et al* (2022) Choice of template delivery mitigates the genotoxic risk and adverse impact of editing in human hematopoietic stem cells. *Cell Stem Cell* 29: 1428-1444.e9

Fickert P, Stöger U, Fuchsbichler A, Moustafa T, Marschall H-U, Weiglein AH, Tsybrovskyy O, Jaeschke H, Zatloukal K, Denk H, *et al* (2007) A New Xenobiotic-Induced Mouse Model of Sclerosing Cholangitis and Biliary Fibrosis. *Am J Pathol* 171: 525–536

Finn JD, Smith AR, Patel MC, Shaw L, Youniss MR, van Heteren J, Dirstine T, Ciullo C, Lescarbeau R, Seitzer J, *et al* (2018) A Single Administration of CRISPR/Cas9 Lipid Nanoparticles Achieves Robust and Persistent In Vivo Genome Editing. *Cell Rep* 22: 2227–2235

Fiumara M, Ferrari S, Omer-Javed A, Beretta S, Albano L, Canarutto D, Varesi A, Gaddoni C, Brombin C, Cugnata F, *et al* (2024) Genotoxic effects of base and prime editing in human hematopoietic stem cells. *Nat Biotechnol* 42: 877–891

Forbes SJ, Russo FP, Rey V, Burra P, Rugge M, Wright NA & Alison MR (2004) A significant proportion of myofibroblasts are of bone marrow origin in human liver fibrosis☆. *Gastroenterology* 126: 955–963

Frangoul H, Altshuler D, Cappellini MD, Chen Y-S, Domm J, Eustace BK, Foell J, de la Fuente J, Grupp S, Handgretinger R, *et al* (2021) CRISPR-Cas9 Gene Editing for

Sickle Cell Disease and β-Thalassemia. *New England Journal of Medicine* 384: 252–260

Fromme M, Schneider C V., Trautwein C, Brunetti-Pierri N & Strnad P (2022) Alpha-1 antitrypsin deficiency: A re-surfacing adult liver disorder. *J Hepatol* 76: 946–958

Gao B & Bataller R (2011) Alcoholic Liver Disease: Pathogenesis and New Therapeutic Targets. *Gastroenterology* 141: 1572–1585

Gao R, Fu Z-C, Li X, Wang Y, Wei J, Li G, Wang L, Wu J, Huang X, Yang L, *et al* (2022) Genomic and Transcriptomic Analyses of Prime Editing Guide RNA–Independent Off-Target Effects by Prime Editors. *CRISPR J* 5: 276–293

Garcia-Bañuelos J, Siller-Lopez F, Miranda A, Aguilar LK, Aguilar-Cordova E & Armendariz-Borunda J (2002) Cirrhotic rat livers with extensive fibrosis can be safely transduced with clinical-grade adenoviral vectors. Evidence of cirrhosis reversion. *Gene Ther* 9: 127–134

Gardin A, Rouillon J, Montalvo-Romeral V, Rossiaud L, Vidal P, Launay R, Vie M, Krimi Benchekroun Y, Cosette J, Bertin B, *et al* (2024) A functional mini-GDE transgene corrects impairment in models of glycogen storage disease type III. *J Clin Invest* 134

Gaudelli N, Komor A, Rees HA, Packer michael S, badran AH, bryson D & Liu DR (2017) Programmable base editing of A•T to G•C in genomic DNA without DNA cleavage. *Nature* 551

Gemberling MP, Siklenka K, Rodriguez E, Tonn-Eisinger KR, Barrera A, Liu F, Kantor A, Li L, Cigliola V, Hazlett MF, *et al* (2021) Transgenic mice for in vivo epigenome editing with CRISPR-based systems. *Nat Methods* 18: 965–974

Gene Therapy With hLB-001 in Pediatric Patients With Severe Methylmalonic Acidemia (SUNRISE) (2024)

Gillmore JD, Gane E, Taubel J, Kao J, Fontana M, Maitland ML, Seitzer J, O'Connell D, Walsh KR, Wood K, *et al* (2021) CRISPR-Cas9 In Vivo Gene Editing for Transthyretin Amyloidosis. *New England Journal of Medicine* 385: 493–502

Ginn SL, Mandwie M, Alexander IE, Edelstein M & Abedi MR (2024) Gene therapy clinical trials worldwide to 2023—an update. *J Gene Med* 26

Greig JA, Jennis M, Dandekar A, Chorazeczewski JK, Param N, So M, Nayal M, Bell P, Coughlan K, Choi M, *et al* (2024) Lipid nanoparticle mRNA therapy improves survival and reduces serum branched-chain amino acids in mouse models of maple syrup urine disease. *Hum Gene Ther*

Greig JA, Jennis M, Dandekar A, Chorazeczewski JK, Smith MK, Ashley SN, Yan H & Wilson JM (2021) Muscle-directed AAV gene therapy rescues the maple syrup urine disease phenotype in a mouse model. *Mol Genet Metab* 134: 139–146

Grimm D, Pandey K, Nakai H, Storm TA & Kay MA (2006) Liver Transduction with Recombinant Adeno-Associated Virus Is Primarily Restricted by Capsid Serotype Not Vector Genotype. *J Virol* 80: 426–439

Grünewald J, Zhou R, Garcia SP, Iyer S, Lareau CA, Aryee MJ & Joung JK (2019) Transcriptome-wide off-target RNA editing induced by CRISPR-guided DNA base editors. *Nature* 569: 433–437

Gulamhusein AF & Hirschfield GM (2020) Primary biliary cholangitis: pathogenesis and therapeutic opportunities. *Nat Rev Gastroenterol Hepatol* 17: 93–110

Habashy NH, Kodous AS & Abu-Serie MM (2021) Targeting ROS/NF-κB signaling pathway by the seedless black Vitis vinifera polyphenols in CCl4-intoxicated kidney, lung, brain, and spleen in rats. *Sci Rep* 11: 16575

Hajovsky H, Hu G, Koen Y, Sarma D, Cui W, Moore DS, Staudinger JL & Hanzlik RP (2012) Metabolism and Toxicity of Thioacetamide and Thioacetamide S-Oxide in Rat Hepatocytes. *Chem Res Toxicol* 25: 1955–1963

Halaby CA, Young SP, Austin S, Stefanescu E, Bali D, Clinton LK, Smith B, Pendyal S, Upadia J, Schooler GR, *et al* (2019) Liver fibrosis during clinical ascertainment of glycogen storage disease type III: a need for improved and systematic monitoring. *Genetics in Medicine* 21: 2686–2694

Halpern KB, Shenhav R, Matcovitch-Natan O, Tóth B, Lemze D, Golan M, Massasa EE, Baydatch S, Landen S, Moor AE, *et al* (2017) Single-cell spatial reconstruction reveals global division of labour in the mammalian liver. *Nature* 542: 352–356

Han JP, Lee Y, Lee JH, Chung HY, Lee GS, Nam YR, Choi M, Moon K-S, Lee H, Lee H, *et al* (2023) In vivo genome editing using 244-cis LNPs and low-dose AAV achieves therapeutic threshold in hemophilia A mice. *Mol Ther Nucleic Acids* 34: 102050

Harrison SA, Bedossa P, Guy CD, Schattenberg JM, Loomba R, Taub R, Labriola D, Moussa SE, Neff GW, Rinella ME, *et al* (2024) A Phase 3, Randomized, Controlled Trial of Resmetirom in NASH with Liver Fibrosis. *New England Journal of Medicine* 390: 497–509

He L, Pu W, Liu X, Zhang Z, Han M, Li Y, Huang X, Han X, Li Y, Liu K, *et al* (2021) Proliferation tracing reveals regional hepatocyte generation in liver homeostasis and repair. *Science (1979)* 371

He X, Zhang Z, Xue J, Wang Y, Zhang S, Wei J, Zhang C, Wang J, Urip BA, Ngan CC, *et al* (2022) Low-dose AAV-CRISPR-mediated liver-specific knock-in restored hemostasis in neonatal hemophilia B mice with subtle antibody response. *Nat Commun* 13

Hegde P, Weiss E, Paradis V, Wan J, Mabire M, Sukriti S, Rautou P-E, Albuquerque M, Picq O, Gupta AC, *et al* (2018) Mucosal-associated invariant T cells are a profibrogenic immune cell population in the liver. *Nat Commun* 9: 2146

Heo YA (2023) Etranacogene Dezaparvovec: First Approval. *Drugs* 83: 347–352

Inagaki Y & Okazaki I (2007) Emerging insights into Transforming growth factor Smad signal in hepatic fibrogenesis. *Gut* 56: 284–292

Intellia Presents New Interim Data from the Ongoing Phase 1 Study of NTLA-2001 at the 4th International ATTR Amyloidosis Meeting (2023)

Intellia Therapeutics Announces First Quarter 2024 Financial Results and Highlights Recent Company Progress (2024)

Ishibashi R, Abe K, Ido N, Kitano S, Miyachi H & Toyoshima F (2020) Genome editing with the donor plasmid equipped with synthetic crRNA-target sequence. *Sci Rep* 10: 14120

Iwakiri Y & Trebicka J (2021) Portal hypertension in cirrhosis: Pathophysiological mechanisms and therapy. *JHEP Reports* 3: 100316

Jacquemin E (2012) Progressive familial intrahepatic cholestasis. *Clin Res Hepatol Gastroenterol* 36: S26–S35

Jang H, Jo DH, Cho CS, Shin JH, Seo JH, Yu G, Gopalappa R, Kim D, Cho S-R, Kim JH, *et al* (2021) Application of prime editing to the correction of mutations and phenotypes in adult mice with liver and eye diseases. *Nat Biomed Eng* 6: 181–194

Jauze L, Vie M, Miagoux Q, Rossiaud L, Vidal P, Montalvo-Romeral V, Saliba H, Jarrige M, Polveche H, Nozi J, *et al* (2024) Synergism of dual AAV gene therapy and rapamycin rescues GSDIII phenotype in muscle and liver. *JCI Insight* 9

Jiang T, Zhang X-O, Weng Z & Xue W (2022) Deletion and replacement of long genomic sequences using prime editing. *Nat Biotechnol* 40

Jinek M, Chylinski K, Fonfara I, Hauer M, Doudna JA & Charpentier E (2012) A Programmable Dual-RNA–Guided DNA Endonuclease in Adaptive Bacterial Immunity. *Science* 337: 816–821

Kaczmarczyk SJ, Sitaraman K, Young HA, Hughes SH & Chatterjee DK (2011) Protein delivery using engineered virus-like particles. *Proceedings of the National Academy of Sciences* 108: 16998–17003

Kang JS, Wanibuchi H, Morimura K, Wongpoomchai R, Chusiri Y, Gonzalez FJ & Fukushima S (2008) Role of CYP2E1 in thioacetamide-induced mouse hepatotoxicity. *Toxicol Appl Pharmacol* 228: 295–300

Karikó K, Muramatsu H, Welsh FA, Ludwig J, Kato H, Akira S & Weissman D (2008) Incorporation of Pseudouridine Into mRNA Yields Superior Nonimmunogenic Vector With Increased Translational Capacity and Biological Stability. *Molecular Therapy* 16: 1833–1840

Kasianchuk N, Dobrowolska K, Harkava S, Bretcan A, Zarębska-Michaluk D, Jaroszewicz J, Flisiak R & Rzymski P (2023) Gene-Editing and RNA Interference in Treating Hepatitis B: A Review. *Viruses* 15: 2395

Kasiewicz LN, Biswas S, Beach A, Ren H, Dutta C, Mazzola AM, Rohde E, Chadwick A, Cheng C, Garcia SP, *et al* (2023) GalNAc-Lipid nanoparticles enable non-LDLR dependent hepatic delivery of a CRISPR base editing therapy. *Nat Commun* 14: 2776

Katrekar D, Chen G, Meluzzi D, Ganesh A, Worlikar A, Shih Y-R, Varghese S & Mali P (2019) In vivo RNA editing of point mutations via RNA-guided adenosine deaminases. *Nat Methods* 16: 239–242

Katrekar D, Yen J, Xiang Y, Saha A, Meluzzi D, Savva Y & Mali P (2022) Efficient in vitro and in vivo RNA editing via recruitment of endogenous ADARs using circular guide RNAs. *Nat Biotechnol* 40: 938–945

Kazemian P, Yu S-Y, Thomson SB, Birkenshaw A, Leavitt BR & Ross CJD (2022) Lipid-Nanoparticle-Based Delivery of CRISPR/Cas9 Genome-Editing Components. *Mol Pharm* 19: 1669–1686

Kebriaei P, Izsvák Z, Narayanavari SA, Singh H & Ivics Z (2017) Gene Therapy with the Sleeping Beauty Transposon System. *Trends in Genetics* 33: 852–870

Kendall TJ, Hennedige S, Aucott RL, Hartland SN, Vernon MA, Benyon RC & Iredale JP (2009) p75 neurotrophin receptor signaling regulates hepatic myofibroblast proliferation and apoptosis in recovery from rodent liver fibrosis. *Hepatology* 49: 901–910

Khalil A, Quaglia A, Gélat P, Saffari N, Rashidi H & Davidson B (2023) Clinical Medicine New Developments and Challenges in Liver Transplantation. *J Clin Med 2023* 12: 5586

Khirallah J, Eimbinder M, Li Y & Xu Q (2023) Clinical progress in genome-editing technology and in vivo delivery techniques. *Trends in Genetics* 39: 208–216

Kim DY, Moon S Bin, Ko J-H, Kim Y-S & Kim D (2020a) Unbiased investigation of specificities of prime editing systems in human cells. *Nucleic Acids Res* 48: 10576–10589

Kim SY, Kim KH, Schilling JM, Leem J, Dhanani M, Head BP, Roth DM, Zemljic-Harpf AE & Patel HH (2020b) Protective role of cardiac-specific overexpression of caveolin-3 in cirrhotic cardiomyopathy. *American Journal of Physiology-Gastrointestinal and Liver Physiology* 318: G531–G541

Kishnani PS, Austin SL, Arn P, Bali DS, Boney A, Case LE, Chung WK, Desai DM, El-Gharbawy A, Haller R, *et al* (2010) Glycogen Storage Disease Type III diagnosis and management guidelines. *Genetics in Medicine* 12: 446–463

Kisseleva T & Brenner D (2021) Molecular and cellular mechanisms of liver fibrosis and its regression. *Nat Rev Gastroenterol Hepatol* 18: 151–166

Kisseleva T, Uchinami H, Feirt N, Quintana-Bustamante O, Segovia JC, Schwabe RF & Brenner DA (2006) Bone marrow-derived fibrocytes participate in pathogenesis of liver fibrosis. *J Hepatol* 45: 429–438

Klermund J, Rhiel M, Kocher T, Chmielewski KO, Bischof J, Andrieux G, el Gaz M, Hainzl S, Boerries M, Cornu TI, *et al* (2024) On- and off-target effects of paired CRISPR-Cas nickase in primary human cells. *Molecular Therapy* 32: 1298–1310

Klompe SE, Vo PLH, Halpin-Healy TS & Sternberg SH (2019) Transposon-encoded CRISPR–Cas systems direct RNA-guided DNA integration. *Nature* 571: 219–225

Kohli R, Kirby M, Xanthakos SA, Softic S, Feldstein AE, Saxena V, Tang PH, Miles L, Miles M V., Balistreri WF, *et al* (2010) High-fructose, medium chain trans fat diet induces liver fibrosis and elevates plasma coenzyme Q9 in a novel murine model of obesity and nonalcoholic steatohepatitis. *Hepatology* 52: 934–944

Komor AC, Kim B, Packer MS, Zuris JA & Liu DR (2016) Programmable editing of a target base in genomic DNA without double-stranded DNA cleavage. *Nature* 533

Krenkel O & Tacke F (2017) Liver macrophages in tissue homeostasis and disease. *Nat Rev Immunol* 17: 306–321

Kubitz R, Dröge C, Kluge S, Stross C, Walter N, Keitel V, Häussinger D & Stindt J (2015) Autoimmune BSEP Disease: Disease Recurrence After Liver Transplantation for Progressive Familial Intrahepatic Cholestasis. *Clin Rev Allergy Immunol* 48: 273–284

Kubitz R, Dröge C, Stindt J, Weissenberger K & Häussinger D (2012) The bile salt export pump (BSEP) in health and disease. *Clin Res Hepatol Gastroenterol* 36: 536–553

Kullak-ublick GA, Stieger B & Meier PJ (2004) Enterohepatic bile salt transporters in normal physiology and liver disease. *Gastroenterology* 126: 322–342

Labbé RP, Vessillier S & Rafiq QA (2021) Lentiviral Vectors for T Cell Engineering: Clinical Applications, Bioprocessing and Future Perspectives. *Viruses* 13: 1528

Lam P, Wang R & Ling V (2005) Bile Acid Transport in Sister of P-Glycoprotein (ABCB11) Knockout Mice. *Biochemistry* 44: 12598–12605

Lampe GD, King RT, Halpin-Healy TS, Klompe SE, Hogan MI, Vo PLH, Tang S, Chavez A & Sternberg SH (2024) Targeted DNA integration in human cells without double-strand breaks using CRISPR-associated transposases. *Nat Biotechnol* 42: 87–98

Lazaridis KN, Gores GJ & Lindor KD (2001) Ursodeoxycholic acid 'mechanisms of action and clinical use in hepatobiliary disorders'. *J Hepatol* 35: 134–146

Lee CS, Bishop ES, Zhang R, Yu X, Farina EM, Yan S, Zhao C, Zeng Z, Shu Y, Wu X, *et al* (2017) Adenovirus-mediated gene delivery: Potential applications for gene and cell-based therapies in the new era of personalized medicine. *Genes Dis* 4: 43–63

Lee JH, Han JP, Song DW, Lee GS, Choi BS, Kim M, Lee Y, Kim S, Lee H & Yeom SC (2023) In vivo genome editing for hemophilia B therapy by the combination of rebalancing and therapeutic gene knockin using a viral and non-viral vector. *Mol Ther Nucleic Acids* 32: 161–172

Lei L, Bruneau A, El Mourabit H, Guégan J, Folseraas T, Lemoinne S, Karlsen TH, Hoareau B, Morichon R, Gonzalez-Sanchez E, *et al* (2022) Portal fibroblasts with mesenchymal stem cell features form a reservoir of proliferative myofibroblasts in liver fibrosis. *Hepatology* 76: 1360–1375

Leibowitz ML, Papathanasiou S, Doerfler PA, Blaine LJ, Sun L, Yao Y, Zhang C-Z, Weiss MJ & Pellman D (2021) Chromothripsis as an on-target consequence of CRISPR–Cas9 genome editing. *Nat Genet* 53: 895–905

Levy JM, Yeh W-H, Pendse N, Davis JR, Hennessey E, Butcher R, Koblan LW, Comander J, Liu Q & Liu DR (2020) Cytosine and adenine base editing of the brain, liver, retina, heart and skeletal muscle of mice via adeno-associated viruses. *Nat Biomed Eng* 4: 97–110

Li A, Tanner MR, Lee CM, Hurley AE, De Giorgi M, Jarrett KE, Davis TH, Doerfler AM, Bao G, Beeton C, *et al* (2020) AAV-CRISPR Gene Editing Is Negated by Pre-existing Immunity to Cas9. *Molecular Therapy* 28: 1432–1441

Li H, Haurigot V, Doyon Y, Li T, Wong SY, Bhagwat AS, Malani N, Anguela XM, Sharma R, Ivanciu L, *et al* (2011) In vivo genome editing restores haemostasis in a mouse model of haemophilia. *Nature* 475: 217–221

Li X, Ding Y, Liu Y, Ma Y, Song J, Wang Q, Li M, Qin Y & Yang Y (2015) Eleven novel mutations of the BCKDHA, BCKDHB and DBT genes associated with maple syrup urine disease in the Chinese population: Report on eight cases. *Eur J Med Genet* 58: 617–623

Li X, Le Y, Zhang Z, Nian X, Liu B & Yang X (2023) Viral Vector-Based Gene Therapy. *Int J Mol Sci* 24: 7736

Lisjak M, De Caneva A, Marais T, Barbon E, Biferi MG, Porro F, Barzel A, Zentilin L, Kay MA, Mingozzi F, *et al* (2022) Promoterless Gene Targeting Approach Combined to CRISPR/Cas9 Efficiently Corrects Hemophilia B Phenotype in Neonatal Mice. *Front Genome Ed* 4

Lisjak M, Iaconcig A, Guarnaccia C, Vicidomini A, Moretti L, Collaud F, Ronzitti G, Zentilin L & Muro AF (2023) Lethality rescue and long-term amelioration of a citrullinemia type I mouse model by neonatal gene-targeting combined to SaCRISPR-Cas9. *Mol Ther Methods Clin Dev* 31: 101103

Liu K-M, Wu J-Y & Chen Y-T (2014) Mouse model of glycogen storage disease type III. *Mol Genet Metab* 111: 467–476

Liu P, Liang S-Q, Zheng C, Mintzer E, Zhao YG, Ponnienselvan K, Mir A, Sontheimer EJ, Gao G, Flotte TR, *et al* (2021) Improved prime editors enable pathogenic allele correction and cancer modelling in adult mice. *Nat Commun* 12

Liu W, Baker RD, Bhatia T, Zhu L & Baker SS (2016) Pathogenesis of nonalcoholic steatohepatitis. *Cellular and Molecular Life Sciences* 73: 1969–1987

Lombardo A, Genovese P, Beausejour CM, Colleoni S, Lee Y-L, Kim KA, Ando D, Urnov FD, Galli C, Gregory PD, *et al* (2007) Gene editing in human stem cells using zinc finger nucleases and integrase-defective lentiviral vector delivery. *Nat Biotechnol* 25: 1298–1306

Longhurst HJ, Lindsay K, Petersen RS, Fijen LM, Gurugama P, Maag D, Butler JS, Shah MY, Golden A, Xu Y, *et al* (2024) CRISPR-Cas9 In Vivo Gene Editing of KLKB1 for Hereditary Angioedema . *New England Journal of Medicine* 390: 432–441

Loureiro D, Tout I, Narguet S, Bed CM, Roinard M, Sleiman A, Boyer N, Pons-Kerjean N, Castelnau C, Giuly N, *et al* (2023) Mitochondrial stress in advanced fibrosis and cirrhosis associated with chronic hepatitis B, chronic hepatitis C, or nonalcoholic steatohepatitis. *Hepatology* 77: 1348–1365

Luedde T, Kaplowitz N & Schwabe RF (2014) Cell Death and Cell Death Responses in Liver Disease: Mechanisms and Clinical Relevance. *Gastroenterology* 147: 765-783.e4

Lyu P, Wang L & Lu B (2020) Virus-Like Particle Mediated CRISPR/Cas9 Delivery for Efficient and Safe Genome Editing. *Life* 10: 366

Maddalena A, Tornabene P, Tiberi P, Minopoli R, Manfredi A, Mutarelli M, Rossi S, Simonelli F, Naggert JK, Cacchiarelli D, *et al* (2018) Triple Vectors Expand AAV Transfer Capacity in the Retina. *Molecular Therapy* 26: 524–541

Madisen L, Zwingman TA, Sunkin SM, Oh SW, Zariwala HA, Gu H, Ng LL, Palmiter RD, Hawrylycz MJ, Jones AR, *et al* (2010) A robust and high-throughput Cre reporting and characterization system for the whole mouse brain. *Nat Neurosci* 13: 133–140

MAGNITUDE: A Phase 3 Study of NTLA-2001 in Participants With Transthyretin Amyloidosis With Cardiomyopathy (ATTR-CM) (2024)

Makarova KS, Wolf YI, Iranzo J, Shmakov SA, Alkhnbashi OS, J Brouns SJ, Charpentier E, Cheng D, Haft DH, Horvath P, *et al* (2020) Evolutionary classification of

CRISPR–Cas systems: a burst of class 2 and derived variants. *Nat Rev Microbiol* 18: 67–83

Mangeot PE, Risson V, Fusil F, Marnef A, Laurent E, Blin J, Mournetas V, Massouridès E, Sohier TJM, Corbin A, *et al* (2019) Genome editing in primary cells and in vivo using viral-derived Nanoblades loaded with Cas9-sgRNA ribonucleoproteins. *Nat Commun* 10: 45

Manno CS, Arruda VR, Pierce GF, Glader B, Ragni M, Rasko J, Ozelo MC, Hoots K, Blatt P, Konkle B, *et al* (2006) Successful transduction of liver in hemophilia by AAV-Factor IX and limitations imposed by the host immune response. *Nat Med* 12: 342–347

Marcellin P, Gane E, Buti M, Afdhal N, Sievert W, Jacobson IM, Washington MK, Germanidis G, Flaherty JF, Schall RA, *et al* (2013) Regression of cirrhosis during treatment with tenofovir disoproxil fumarate for chronic hepatitis B: a 5-year open-label follow-up study. *The Lancet* 381: 468–475

Marie Payton, Thomas Morgan, Jirair K. Bedoyan, Angela Sun, Hong Li, Daniel Gruskin, Mark A. Kay, Frederic Chereau & Jerry Vockley (2024) Demonstration of Nuclease-Free Genome Editing (GeneRide^{TM}) in Pediatric Patients with Methylmalonic Acidemia [abstract]. *27th Annual Meeting ASGCT* [PREPRINT]

Martínez-García J, Molina A, González-Aseguinolaza G, Weber ND & Smerdou C (2022) Gene Therapy for Acquired and Genetic Cholestasis. *Biomedicines* 10: 1238

Mauer J, Luo X, Blanjoie A, Jiao X, Grozhik A V., Patil DP, Linder B, Pickering BF, Vasseur J-J, Chen Q, *et al* (2017) Reversible methylation of m6Am in the 5′ cap controls mRNA stability. *Nature* 541: 371–375

Mederacke I, Hsu CC, Troeger JS, Huebener P, Mu X, Dapito DH, Pradere J-P & Schwabe RF (2013) Fate tracing reveals hepatic stellate cells as dominant contributors to liver fibrosis independent of its aetiology. *Nat Commun* 4: 2823

Mihm S (2018) Danger-Associated Molecular Patterns (DAMPs): Molecular Triggers for Sterile Inflammation in the Liver. *Int J Mol Sci* 19: 3104

Milani M, Annoni A, Moalli F, Liu T, Cesana D, Calabria A, Bartolaccini S, Biffi M, Russo F, Visigalli I, *et al* (2019a) Phagocytosis-shielded lentiviral vectors improve liver gene therapy in nonhuman primates. *Sci Transl Med*

Milani M, Annoni A, Moalli F, Liu T, Cesana D, Calabria A, Bartolaccini S, Biffi M, Russo F, Visigalli I, *et al* (2019b) Phagocytosis-shielded lentiviral vectors improve liver gene therapy in nonhuman primates. *Sci Transl Med* 11

Milani M, Canepari C, Liu T, Biffi M, Russo F, Plati T, Curto R, Patarroyo-White S, Drager D, Visigalli I, *et al* (2022) Liver-directed lentiviral gene therapy corrects hemophilia A mice and achieves normal-range factor VIII activity in non-human primates. *Nat Commun* 13: 2454

Mirum's LIVMARLI Now Approved for PFIC in Patients 12 Months and Older (2024)

Modica S, Gadaleta RM & Moschetta A (2010) Deciphering the nuclear bile acid receptor FXR paradigm. *Nucl Recept Signal* 8: nrs.08005

Morton DH, Strauss KA, Robinson DL, Puffenberger EG & Kelley RI (2002) Diagnosis and Treatment of Maple Syrup Disease: A Study of 36 Patients. *Pediatrics* 109: 999–1008

Muelly ER, Moore GJ, Bunce SC, Mack J, Bigler DC, Morton DH & Strauss KA (2013) Biochemical correlates of neuropsychiatric illness in maple syrup urine disease. *Journal of Clinical Investigation* 123: 1809–1820

Muratori L, Lohse AW & Lenzi M (2023) Diagnosis and management of autoimmune hepatitis. *BMJ*: e070201

Musunuru K, Chadwick AC, Mizoguchi T, Garcia SP, Denizio JE, Reiss CW, Wang K, Iyer S, Dutta C, Clendaniel V, *et al* (2021) In vivo CRISPR base editing of PCSK9 durably lowers cholesterol in primates. *Nature* 593: 429

Nakade S, Tsubota T, Sakane Y, Kume S, Sakamoto N, Obara M, Daimon T, Sezutsu H, Yamamoto T, Sakuma T, *et al* (2014) Microhomology-mediated end-joining-dependent integration of donor DNA in cells and animals using TALENs and CRISPR/Cas9. *Nat Commun* 5

Nakai H, Yant SR, Storm TA, Fuess S, Meuse L & Kay MA (2001) Extrachromosomal Recombinant Adeno-Associated Virus Vector Genomes Are Primarily Responsible for Stable Liver Transduction In Vivo. *J Virol* 75: 6969–6976

Naldini L, Blömer U, Gallay P, Ory D, Mulligan R, Gage FH, Verma IM & Trono D (1996) In Vivo Gene Delivery and Stable Transduction of Nondividing Cells by a Lentiviral Vector. *Science* 272: 263–267

Neugebauer ME, Hsu A, Arbab M, Krasnow NA, McElroy AN, Pandey S, Doman JL, Huang TP, Raguram A, Banskota S, *et al* (2023) Evolution of an adenine base editor into a small, efficient cytosine base editor with low off-target activity. *Nat Biotechnol* 41: 673–685

NTLA-2002 in Adults With Hereditary Angioedema (HAE) (NTLA-2002) (2024)

Ogier de Baulny H & Saudubray JM (2002) Branched-chain organic acidurias. *Seminars in Neonatology* 7: 65–74

van der Oost J & Patinios C (2023) The genome editing revolution. *Trends Biotechnol* 41: 396–409

Ou L, DeKelver RC, Rohde M, Tom S, Radeke R, St Martin SJ, Santiago Y, Sproul S, Przybilla MJ, Koniar BL, *et al* (2019) ZFN-Mediated In Vivo Genome Editing Corrects Murine Hurler Syndrome. *Molecular Therapy* 27

Ozelo MC, Mahlangu J, Pasi KJ, Giermasz A, Leavitt AD, Laffan M, Symington E, Quon D V., Wang J-D, Peerlinck K, *et al* (2022) Valoctocogene Roxaparvovec Gene Therapy for Hemophilia A. *New England Journal of Medicine* 386: 1013–1025

Packer MS, Chowdhary V, Lung G, Cheng L-I, Aratyn-Schaus Y, Leboeuf D, Smith S, Shah A, Chen D, Zieger M, *et al* (2022) Evaluation of cytosine base editing and adenine base editing as a potential treatment for alpha-1 antitrypsin deficiency. *Molecular Therapy* 30

Padula A, Petruzzelli R, Philbert SA, Church SJ, Esposito F, Campione S, Monti M, Capolongo F, Perna C, Nusco E, *et al* (2022) Full-length ATP7B reconstituted through protein trans-splicing corrects Wilson disease in mice. *Mol Ther Methods Clin Dev* 26: 495–504

Padula A, Spinelli M, Nusco E, Cundin XB, Capolongo F, Campione S, Perna C, Bastille A, Ericson M, Wang C-C, *et al* (2023) Genome editing without nucleases confers proliferative advantage to edited hepatocytes and corrects Wilson disease. *JCI Insight* 8

Pagant S, Huston MW, Moreira L, Gan L, Martin SS, Sproul S, Holmes MC, Meyer K, Wechsler T, Desnick RJ, *et al* (2021) ZFN-mediated in vivo gene editing in hepatocytes leads to supraphysiologic a-Gal A activity and effective substrate reduction in Fabry mice. *Molecular Therapy* 29

Pallarès-Masmitjà M, Ivančić D, Mir-Pedrol J, Jaraba-Wallace J, Tagliani T, Oliva B, Rahmeh A, Sánchez-Mejías A & Güell M (2021) Find and cut-and-transfer (FiCAT) mammalian genome engineering. *Nat Commun* 12: 7071

Pandey S, Gao XD, Krasnow NA, McElroy A, Tao YA, Duby JE, Steinbeck BJ, McCreary J, Pierce SE, Tolar J, *et al* (2024) Efficient site-specific integration of large genes in mammalian cells via continuously evolved recombinases and prime editing. *Nat Biomed Eng*

Pannunzio NR, Watanabe G & Lieber MR (2018) Nonhomologous DNA end-joining for repair of DNA double-strand breaks. *Journal of Biological Chemistry* 293: 10512–10523

Paris J & Henderson NC (2022) Liver zonation, revisited. *Hepatology* 76: 1219–1230

Parola M & Pinzani M (2019) Liver fibrosis: Pathophysiology, pathogenetic targets and clinical issues. *Mol Aspects Med* 65: 37–55

Paunovska K, Loughrey D & Dahlman JE (2022) Drug delivery systems for RNA therapeutics. *Nat Rev Genet* 23: 265–280

Platt RJ, Chen S, Zhou Y, Yim MJ, Swiech L, Kempton HR, Dahlman JE, Parnas O, Eisenhaure TM, Jovanovic M, *et al* (2014) CRISPR-Cas9 Knockin Mice for Genome Editing and Cancer Modeling. *Cell* 159: 440–455

Pontoizeau C, Gaborit C, Tual N, Simon-Sola M, Rotaru I, Benoist M, Colella P, Lamazière A, Brassier A, Arnoux J, *et al* (2024) Successful treatment of severe

MSUD in Bckdhb−/− mice with neonatal AAV gene therapy. *J Inherit Metab Dis* 47: 41–49

Pontoizeau C, Simon-Sola M, Gaborit C, Nguyen V, Rotaru I, Tual N, Colella P, Girard M, Biferi M-G, Arnoux J-B, *et al* (2022) Neonatal gene therapy achieves sustained disease rescue of maple syrup urine disease in mice. *Nat Commun* 13: 3278

Porro F, Bortolussi G, Barzel A, De Caneva A, Iaconcig A, Vodret S, Zentilin L, Kay MA & Muro AF (2017) Promoterless gene targeting without nucleases rescues lethality of a Crigler-Najjar syndrome mouse model. *EMBO Mol Med* 9: 1346–1355

Porto EM & Komor AC (2023) In the business of base editors: Evolution from bench to bedside. *PLoS Biol* 21: e3002071

Porto EM, Komor AC, Slaymaker IM & Yeo GW (2020) Base editing: advances and therapeutic opportunities. *Nat Rev Drug Discov* 19

Prime medicine reports first quarter 2024 financial results and provides business updates (2024)

Pupo A, Fernández A, Low SH, François A, Suárez-Amarán L & Samulski RJ (2022) AAV vectors: The Rubik's cube of human gene therapy. *Molecular Therapy* 30: 3515–3541

Racanelli V & Rehermann B (2006) The Liver as an Immunological Organ. *Hepatology* 43: S54–S62

Raguram A, Banskota S & Liu DR (2022) Therapeutic in vivo delivery of gene editing agents. *Cell* 185: 2806–2827

Ramachandran P, Pellicoro A, Vernon MA, Boulter L, Aucott RL, Ali A, Hartland SN, Snowdon VK, Cappon A, Gordon-Walker TT, *et al* (2012) Differential Ly-6C expression identifies the recruited macrophage phenotype, which orchestrates the regression of murine liver fibrosis. *Proceedings of the National Academy of Sciences* 109

Raper SE, Chirmule N, Lee FS, Wivel NA, Bagg A, Gao G, Wilson JM & Batshaw ML (2003) Fatal systemic inflammatory response syndrome in a ornithine

transcarbamylase deficient patient following adenoviral gene transfer. *Mol Genet Metab* 80: 148–158

Richards DY, Winn SR, Dudley S, Nygaard S, Mighell TL, Grompe M & Harding CO (2020) AAV-Mediated CRISPR/Cas9 Gene Editing in Murine Phenylketonuria. *Mol Ther Methods Clin Dev* 17

Richardson CD, Ray GJ, DeWitt MA, Curie GL & Corn JE (2016) Enhancing homology-directed genome editing by catalytically active and inactive CRISPR-Cas9 using asymmetric donor DNA. *Nat Biotechnol* 34: 339–344

Roehlen N, Crouchet E & Baumert TF (2020) Liver Fibrosis: Mechanistic Concepts and Therapeutic Perspectives. *Cells* 9: 875

Roth TL, Puig-Saus C, Yu R, Shifrut E, Carnevale J, Li PJ, Hiatt J, Saco J, Krystofinski P, Li H, *et al* (2018) Reprogramming human T cell function and specificity with non-viral genome targeting. *Nature* 559: 405–409

Rothgangl T, Dennis MK, C Lin PJ, Oka R, Witzigmann D, Villiger L, Qi W, Hruzova M, Kissling L, Lenggenhager D, *et al* (2021) In vivo adenine base editing of PCSK9 in macaques reduces LDL cholesterol levels. *Nat Biotechnol* 39: 949–957

Rouet P, Smih F & Jasin M (1994) Expression of a site-specific endonuclease stimulates homologous recombination in mammalian cells. *Proceedings of the National Academy of Sciences* 91: 6064–6068

Rovai A, Chung B, Hu Q, Hook S, Yuan Q, Kempf T, Schmidt F, Grimm D, Talbot SR, Steinbrück L, *et al* (2022) In vivo adenine base editing reverts C282Y and improves iron metabolism in hemochromatosis mice. *Nat Commun* 13

Saeed A, Hoekstra M, Hoeke MO, Heegsma J & Faber KN (2017) The interrelationship between bile acid and vitamin A homeostasis. *Biochimica et Biophysica Acta (BBA) - Molecular and Cell Biology of Lipids* 1862: 496–512

Saggi H, Maitra D, Jiang A, Zhang R, Wang P, Cornuet P, Singh S, Locker J, Ma X, Dailey H, *et al* (2019) Loss of hepatocyte β-catenin protects mice from experimental porphyria-associated liver injury. *J Hepatol* 70: 108–117

Sahin H, Trautwein C & Wasmuth HE (2010) Functional role of chemokines in liver disease models. *Nat Rev Gastroenterol Hepatol* 7: 682–690

Sallmyr A & Tomkinson AE (2018) Repair of DNA double-strand breaks by mammalian alternative end-joining pathways. *J Biol Chem*: 10536–10546

Schambach A, Buchholz CJ, Torres-Ruiz R, Cichutek K, Morgan M, Trapani I & Büning H (2024) A new age of precision gene therapy. *The Lancet* 403: 568–582

Schiroli G, Conti A, Ferrari S, della Volpe L, Jacob A, Albano L, Beretta S, Calabria A, Vavassori V, Gasparini P, *et al* (2019) Precise Gene Editing Preserves Hematopoietic Stem Cell Function following Transient p53-Mediated DNA Damage Response. *Cell Stem Cell* 24: 551-565.e8

Scholten D, Trebicka J, Liedtke C & Weiskirchen R (2015) The carbon tetrachloride model in mice. *Lab Anim* 49: 4–11

Schukfeh N, Metzelder ML, Petersen C, Reismann M, Pfister ED, Ure BM & Kuebler JF (2012) Normalization of serum bile acids after partial external biliary diversion indicates an excellent long-term outcome in children with progressive familial intrahepatic cholestasis. *J Pediatr Surg* 47: 501–505

Sentmanat MF, Peters ST, Florian CP, Connelly JP & Pruett-Miller SM (2018) A Survey of Validation Strategies for CRISPR-Cas9 Editing. *Sci Rep* 8: 888

Shan L, Wang F, Zhai D, Meng X, Liu J & Lv X (2022) New Drugs for Hepatic Fibrosis. *Front Pharmacol* 13

Shan X, Zhao Z, Lai P, Liu Y, Li B, Ke Y, Jiang H, Zhou Y, Li W, Wang Q, *et al* (2024) RNA nanotherapeutics with fibrosis overexpression and retention for MASH treatment. *Nat Commun* 15: 7263

Shao Y, Wang L, Guo N, Wang S, Yang L, Li Y, Wang M, Yin S, Han H, Zeng L, *et al* (2018) Cas9-nickase–mediated genome editing corrects hereditary tyrosinemia in rats. *Journal of Biological Chemistry* 293: 6883–6892

Sharma R, Anguela XM, Doyon Y, Wechsler T, DeKelver RC, Sproul S, Paschon DE, Miller JC, Davidson RJ, Shivak D, *et al* (2015) In vivo genome editing of the albumin locus as a platform for protein replacement therapy. *Blood* 126: 1777–1784

Sheridan C (2024) The world's first CRISPR therapy is approved: who will receive it? *Nat Biotechnol* 42: 3–4

Shirley JL, de Jong YP, Terhorst C & Herzog RW (2020) Immune Responses to Viral Gene Therapy Vectors. *Molecular Therapy* 28: 709–722

Siew SM, Cunningham SC, Zhu E, Tay SS, Venuti E, Bolitho C & Alexander IE (2019a) Prevention of Cholestatic Liver Disease and Reduced Tumorigenicity in a Murine Model of PFIC Type 3 Using Hybrid AAV-piggyBac Gene Therapy. *Hepatology* 70: 2047–2061

Siew SM, Cunningham SC, Zhu E, Tay SS, Venuti E, Bolitho C & Alexander IE (2019b) Prevention of Cholestatic Liver Disease and Reduced Tumorigenicity in a Murine Model of PFIC Type 3 Using Hybrid AAV-piggyBac Gene Therapy. *Hepatology* 70: 2047–2061

Simhadri VL, McGill J, McMahon S, Wang J, Jiang H & Sauna ZE (2018) Prevalence of Pre-existing Antibodies to CRISPR-Associated Nuclease Cas9 in the USA Population. *Mol Ther Methods Clin Dev* 10: 105–112

Skvorak KJ (2009) Animal models of maple syrup urine disease. *J Inherit Metab Dis* 32: 229–246

Sobrevals L, Enguita M, Rodriguez C, Gonzalez-Rojas J, Alzaguren P, Razquin N, Prieto J & Fortes P (2012a) AAV vectors transduce hepatocytes in vivo as efficiently in cirrhotic as in healthy rat livers. *Gene Ther* 19: 411–417

Sobrevals L, Enguita M, Rodriguez C, Gonzalez-Rojas J, Alzaguren P, Razquin N, Prieto J & Fortes P (2012b) AAV vectors transduce hepatocytes in vivo as efficiently in cirrhotic as in healthy rat livers. *Gene Ther* 19: 411–417

Srivastava A (2014) Progressive Familial Intrahepatic Cholestasis. *J Clin Exp Hepatol* 4: 25–36

Starinieri F, Milani M, Beretta S, Canepari C, Fabiano A, Simoni C, Cammarota E, Volpin M, Bortolussi G, Russo F, *et al* (2023) Spatio-temporal dynamics of the liver shapes hepatocytes heterogeneity and impacts in vivo gene transfer and editing. *Res Sq*

Stephens CJ, Kashentseva E, Everett W, Kaliberova L & Curiel DT (2018) Targeted in vivo knock-in of human alpha-1-antitrypsin cDNA using adenoviral delivery of CRISPR/Cas9. *Gene Ther* 25: 139–156

Stindt J, Kluge S, Dröge C, Keitel V, Stross C, Baumann U, Brinkert F, Dhawan A, Engelmann G, Ganschow R, *et al* (2016) Bile salt export pump-reactive antibodies form a polyclonal, multi-inhibitory response in antibody-induced bile salt export pump deficiency. *Hepatology* 63: 524–537

Stinson BM & Loparo JJ (2021) Repair of DNA Double-Strand Breaks by the Nonhomologous End Joining Pathway. *Annu Rev Biochem* 90: 137–164

Stoddard BL (2011) Homing Endonucleases: From Microbial Genetic Invaders to Reagents for Targeted DNA Modification. *Structure* 19: 7–15

Stone D, Long KR, Loprieno MA, De Silva Feelixge HS, Kenkel EJ, Liley RM, Rapp S, Roychoudhury P, Nguyen T, Stensland L, *et al* (2021) CRISPR-Cas9 gene editing of hepatitis B virus in chronically infected humanized mice. *Mol Ther Methods Clin Dev* 20: 258–275

Strauss KA, Carson VJ, Soltys K, Young ME, Bowser LE, Puffenberger EG, Brigatti KW, Williams KB, Robinson DL, Hendrickson C, *et al* (2020a) Branched-chain α-ketoacid dehydrogenase deficiency (maple syrup urine disease): Treatment, biomarkers, and outcomes. *Mol Genet Metab* 129: 193–206

Strauss KA, Puffenberger EG & Carson VJ (2020b) Maple Syrup Urine Disease

Strecker J, Ladha A, Gardner Z, Schmid-Burgk JL, Makarova KS, Koonin E V. & Zhang F (2019) RNA-guided DNA insertion with CRISPR-associated transposases. *Science* 365: 48–53

Study to Evaluate Safety, Tolerability, Pharmacokinetics, and Pharmacodynamics of NTLA-2001 in Patients With Hereditary Transthyretin Amyloidosis With

Polyneuropathy (ATTRv-PN) and Patients With Transthyretin Amyloidosis-Related Cardiomyopathy (ATTR-CM) (2023)

Su J, Jin X, She K, Liu Y, Song L, Zhao Q, Xiao J, Li R, Deng H, Lu F, *et al* (2023) In vivo adenine base editing corrects newborn murine model of Hurler syndrome. *Molecular Biomedicine* 4: 6

Suchy FP, Karigane D, Nakauchi Y, Higuchi M, Zhang J, Pekrun K, Hsu I, Fan AC, Nishimura T, Charlesworth CT, *et al* (2024) Genome engineering with Cas9 and AAV repair templates generates frequent concatemeric insertions of viral vectors. *Nat Biotechnol*

Suryawan A, Hawes JW, Harris RA, Shimomura Y, Jenkins AE & Hutson SM (1998) A molecular model of human branched-chain amino acid metabolism. *Am J Clin Nutr* 68: 72–81

Suzuki K, Tsunekawa Y, Hernandez-Benitez R, Wu J, Zhu J, Kim EJ, Hatanaka F, Yamamoto M, Araoka T, Li Z, *et al* (2016) In vivo genome editing via CRISPR/Cas9 mediated homology-independent targeted integration. *Nature* 540: 144–149

Tacke F & Zimmermann HW (2014) Macrophage heterogeneity in liver injury and fibrosis. *J Hepatol* 60: 1090–1096

Tag CG, Sauer-Lehnen S, Weiskirchen S, Borkham-Kamphorst E, Tolba RH, Tacke F & Weiskirchen R (2015) Bile Duct Ligation in Mice: Induction of Inflammatory Liver Injury and Fibrosis by Obstructive Cholestasis. *Journal of Visualized Experiments*

Tao J, Bauer DE & Chiarle R (2023) Assessing and advancing the safety of CRISPR-Cas tools: from DNA to RNA editing. *Nat Commun* 14: 212

Tao J, Wang Q, Mendez-Dorantes C, Burns KH & Chiarle R (2022) Frequency and mechanisms of LINE-1 retrotransposon insertions at CRISPR/Cas9 sites. *Nat Commun* 13: 3685

Teschke R (2018) Alcoholic Liver Disease: Alcohol Metabolism, Cascade of Molecular Mechanisms, Cellular Targets, and Clinical Aspects. *Biomedicines* 6: 106

Thakore PI, Kwon JB, Nelson CE, Rouse DC, Gemberling MP, Oliver ML & Gersbach CA (2018) RNA-guided transcriptional silencing in vivo with S. aureus CRISPR-Cas9 repressors. *Nat Commun* 9: 1674

The Human Gene Mutation Database

Torella L, Klermund J, Bilbao-Arribas M, Tamayo I, Andrieux G, Chmielewski KO, Vales A, Olagüe C, Moreno-Luqui D, Raimondi I, *et al* (2024) Efficient and safe therapeutic use of paired Cas9-nickases for primary hyperoxaluria type 1. *EMBO Mol Med* 16: 112–131

Tornabene P, Ferla R, Llado-Santaeularia M, Centrulo M, Dell'Anno M, Esposito F, Marrocco E, Pone E, Minopoli R, Iodice C, *et al* (2022) Therapeutic homology-independent targeted integration in retina and liver. *Nat Commun* 13

Tou CJ, Orr B & Kleinstiver BP (2023) Precise cut-and-paste DNA insertion using engineered type V-K CRISPR-associated transposases. *Nat Biotechnol* 41: 968–979

Trapani I, Colella P, Sommella A, Iodice C, Cesi G, de Simone S, Marrocco E, Rossi S, Giunti M, Palfi A, *et al* (2014) Effective delivery of large genes to the retina by dual AAV vectors. *EMBO Mol Med* 6: 194–211

Treacy E, Clow CL, Reade TR, Chitayat D, Mamer OA & Scriver CR (1992) Maple syrup urine disease: Interrelations between branched-chain amino-, oxo- and hydroxyacids; implications for treatment; associations with CNS dysmyelination. *J Inherit Metab Dis* 15: 121–135

Tsai SQ, Nguyen NT, Malagon-Lopez J, Topkar V V, Aryee MJ & Joung JK (2017) CIRCLE-seq: a highly sensitive in vitro screen for genome-wide CRISPR–Cas9 nuclease off-targets. *Nat Methods* 14: 607–614

Tsai SQ, Zheng Z, Nguyen NT, Liebers M, Topkar V V, Thapar V, Wyvekens N, Khayter C, Iafrate AJ, Le LP, *et al* (2015) GUIDE-seq enables genome-wide profiling of off-target cleavage by CRISPR-Cas nucleases. *Nat Biotechnol* 33: 187–197

Tsuchida T & Friedman SL (2017) Mechanisms of hepatic stellate cell activation. *Nat Rev Gastroenterol Hepatol* 14: 397–411

Tsuji S, Stephens CJ, Bortolussi G, Zhang F, Baj G, Jang H, de Alencastro G, Muro AF, Pekrun K & Kay MA (2022) Fludarabine increases nuclease-free AAV- and CRISPR/Cas9-mediated homologous recombination in mice. *Nat Biotechnol* 40: 1285–1294

Tucci F, Galimberti S, Naldini L, Valsecchi MG & Aiuti A (2022) A systematic review and meta-analysis of gene therapy with hematopoietic stem and progenitor cells for monogenic disorders. *Nat Commun* 13: 1315

Turchiano G, Andrieux G, Klermund J, Blattner G, Pennucci V, el Gaz M, Monaco G, Poddar S, Mussolino C, Cornu TI, *et al* (2021) Quantitative evaluation of chromosomal rearrangements in gene-edited human stem cells by CAST-Seq. *Cell Stem Cell* 28: 1136-1147.e5

Ueda J, Yamazaki T & Funakoshi H (2023) Toward the Development of Epigenome Editing-Based Therapeutics: Potentials and Challenges. *Int J Mol Sci* 24: 4778

Urnov FD, Rebar EJ, Holmes MC, Steve Zhang H & Gregory PD (2010) Genome editing with engineered zinc finger nucleases. *Nat Rev Genet* 11: 636–646

U.S. FDA Approves Pfizer's BEQVEZ^{TM} (fidanacogene elaparvovec-dzkt), a One-Time Gene Therapy for Adults with Hemophilia B (2024)

Vakulskas CA, Dever DP, Rettig GR, Turk R, Jacobi AM, Collingwood MA, Bode NM, McNeill MS, Yan S, Camarena J, *et al* (2018) A high-fidelity Cas9 mutant delivered as a ribonucleoprotein complex enables efficient gene editing in human hematopoietic stem and progenitor cells. *Nat Med* 24: 1216–1224

Venturoni LE, Chandler RJ, Liao J, Hoffmann V, Ramesh N, Gordo S, Chau N & Venditti CP (2022) Growth advantage of corrected hepatocytes in a juvenile model of methylmalonic acidemia following liver directed adeno-associated viral mediated nuclease-free genome editing. *Mol Genet Metab* 137: 1–8

Verve Therapeutics Announces Pipeline Progress and Reports First Quarter 2024 Financial Results (2024)

Verve Therapeutics Announces Updates on its PCSK9 Program (2024)

Vidal P, Pagliarani S, Colella P, Costa Verdera H, Jauze L, Gjorgjieva M, Puzzo F, Marmier S, Collaud F, Simon Sola M, *et al* (2018) Rescue of GSDIII Phenotype with Gene Transfer Requires Liver- and Muscle-Targeted GDE Expression. *Molecular Therapy* 26: 890–901

Vilar-Gomez E, Martinez-Perez Y, Calzadilla-Bertot L, Torres-Gonzalez A, Gra-Oramas B, Gonzalez-Fabian L, Friedman SL, Diago M & Romero-Gomez M (2015) Weight Loss Through Lifestyle Modification Significantly Reduces Features of Nonalcoholic Steatohepatitis. *Gastroenterology* 149: 367-378.e5

Villiger L, Joung J, Koblan L, Weissman J, Abudayyeh OO & Gootenberg JS (2024) CRISPR technologies for genome, epigenome and transcriptome editing. *Nat Rev Mol Cell Biol* 25: 464–487

Villiger L, Man Grisch-Chan H, Lindsay H, Ringnalda F, Pogliano CB, Allegri G, Fingerhut R, Häberle J, Matos J, Robinson MD, *et al* (2018) Treatment of a metabolic liver disease by in vivo genome base editing in adult mice. *Nat Med* 24

Wagner DL, Peter L & Schmueck-Henneresse M (2021) Cas9-directed immune tolerance in humans—a model to evaluate regulatory T cells in gene therapy? *Gene Ther* 28: 549–559

Wallace M, Hamesch K, Lunova M, Kim Y, Weiskirchen R, Strnad P & Friedman S (2015) Standard Operating Procedures in Experimental Liver Research: Thioacetamide model in mice and rats. *Lab Anim* 49: 21–29

Wang D, Mou H, Li S, Li Y, Hough S, Tran K, Li J, Yin H, Anderson DG, Sontheimer EJ, *et al* (2015) Adenovirus-Mediated Somatic Genome Editing of *Pten* by CRISPR/Cas9 in Mouse Liver in Spite of Cas9-Specific Immune Responses. *Hum Gene Ther* 26: 432–442

Wang D, Tai PWL & Gao G (2019a) Adeno-associated virus vector as a platform for gene therapy delivery. *Nat Rev Drug Discov* 18: 358–378

Wang JY & Doudna JA (2023) CRISPR technology: A decade of genome editing is only the beginning. *Science* 379

Wang L, Wang H, Bell P, McMenamin D & Wilson JM (2012) Hepatic Gene Transfer in Neonatal Mice by Adeno-Associated Virus Serotype 8 Vector. *Hum Gene Ther* 23: 533–539

Wang L, Yang Y, Breton C, Bell P, Li M, Zhang J, Che Y, Saveliev A, He Z, White J, *et al* (2020) A mutation-independent CRISPR-Cas9-mediated gene targeting approach to treat a murine model of ornithine transcarbamylase deficiency. *Sci Adv* 6: 5701–5713

Wang L, Yang Y, Breton CA, White J, Zhang J, Che Y, Saveliev A, Mcmenamin D, He Z, Latshaw C, *et al* (2019b) CRISPR/Cas9-mediated in vivo gene targeting corrects hemostasis in newborn and adult factor IX-knockout mice. *Blood* 133

Wanisch K & Yáñez-Muñoz RJ (2009) Integration-deficient Lentiviral Vectors: A Slow Coming of Age. *Molecular Therapy* 17: 1316–1332

Weber LWD, Boll M & Stampfl A (2003) Hepatotoxicity and Mechanism of Action of Haloalkanes: Carbon Tetrachloride as a Toxicological Model. *Crit Rev Toxicol* 33: 105–136

Weber ND, Odriozola L, Martínez-García J, Ferrer V, Douar A, Bénichou B, González-Aseguinolaza G & Smerdou C (2019) Gene therapy for progressive familial intrahepatic cholestasis type 3 in a clinically relevant mouse model. *Nat Commun* 10: 5694

Weber T (2021) Anti-AAV Antibodies in AAV Gene Therapy: Current Challenges and Possible Solutions. *Front Immunol* 12

Wei G, An P, Vaid KA, Nasser I, Huang P, Tan L, Zhao S, Schuppan D & Popov Y V. (2020) Comparison of murine steatohepatitis models identifies a dietary intervention with robust fibrosis, ductular reaction, and rapid progression to cirrhosis and cancer. *American Journal of Physiology-Gastrointestinal and Liver Physiology* 318: G174–G188

Wei G, Cao J, Huang P, An P, Badlani D, Vaid KA, Zhao S, Wang DQ-H, Zhuo J, Yin L, *et al* (2021) Synthetic human ABCB4 mRNA therapy rescues severe liver disease phenotype in a BALB/c.Abcb4 mouse model of PFIC3. *J Hepatol* 74: 1416–1428

Wu S, Wang X, Xing W, Li F, Liang M, Li K, He Y & Wang J (2023) An update on animal models of liver fibrosis. *Front Med (Lausanne)* 10

Yan K, Feng J, Liu X, Wang H, Li Q, Li J, Xu T, Sajid M, Ullah H, Zhou L, *et al* (2021) Inhibition of Hepatitis B Virus by AAV8-Derived CRISPR/SaCas9 Expressed From Liver-Specific Promoters. *Front Microbiol* 12

Yanai H, Adachi H, Hakoshima M, Iida S & Katsuyama H (2023) Metabolic-Dysfunction-Associated Steatotic Liver Disease—Its Pathophysiology, Association with Atherosclerosis and Cardiovascular Disease, and Treatments. *Int J Mol Sci* 24: 15473

Yang N, Han L, Gu X, Ye J, Qiu W, Zhang H, Gong Z & Zhang Y (2012) Analysis of gene mutations in Chinese patients with maple syrup urine disease. *Mol Genet Metab* 106: 412–418

Yao X, Wang X, Liu J, Hu X, Shi L, Shen X, Ying W, Sun X, Wang X, Huang P, *et al* (2017) CRISPR/Cas9 – Mediated Precise Targeted Integration In Vivo Using a Double Cut Donor with Short Homology Arms. *EBioMedicine* 20: 19–26

Yarnall MTN, Ioannidi EI, Schmitt-Ulms C, Krajeski RN, Lim J, Villiger L, Zhou W, Jiang K, Garushyants SK, Roberts N, *et al* (2023) Drag-and-drop genome insertion of large sequences without double-strand DNA cleavage using CRISPR-directed integrases. *Nat Biotechnol* 41: 500–512

Yi Z, Qu L, Tang H, Liu Z, Liu Y, Tian F, Wang C, Zhang X, Feng Z, Yu Y, *et al* (2022) Engineered circular ADAR-recruiting RNAs increase the efficiency and fidelity of RNA editing in vitro and in vivo. *Nat Biotechnol* 40: 946–955

Yilmaz BS, Gurung S, Perocheau D, Counsell J & Baruteau J (2020) Gene therapy for inherited metabolic diseases. *J Mother Child* 24: 53–64

Yin H, Song C-Q, Suresh S, Wu Q, Walsh S, Rhym LH, Mintzer E, Bolukbasi MF, Zhu LJ, Kauffman K, *et al* (2017) Structure-guided chemical modification of guide RNA enables potent non-viral in vivo genome editing. *Nat Biotechnol* 35: 1179–1187

Ying H-Z, Chen Q, Zhang W-Y, Zhang H-H, Ma Y, Zhang S-Z, Fang J & Yu C-H (2017) PDGF signaling pathway in hepatic fibrosis pathogenesis and therapeutics. *Mol Med Rep* 16: 7879–7889

Yuen MF, Chen DS, Dusheiko GM, Janssen HLA, Lau DTY, Locarnini SA, Peters MG & Lai CL (2018) Hepatitis B virus infection. *Nat Rev Dis Primers* 4

Zabaleta N, Unzu C, Weber ND & Gonzalez-Aseguinolaza G (2023) Gene therapy for liver diseases — progress and challenges. *Nat Rev Gastroenterol Hepatol* 20: 288–305

Zhang Y, Li F, Patterson AD, Wang Y, Krausz KW, Neale G, Thomas S, Nachagari D, Vogel P, Vore M, *et al* (2012) Abcb11 Deficiency Induces Cholestasis Coupled to Impaired β-Fatty Acid Oxidation in Mice. *Journal of Biological Chemistry* 287: 24784–24794

Zhao G, Ma Q, Yang H, Jiang H, Xu Q, Luo S, Meng Z, Liu J, Zhu L, Lin Q, *et al* (2024) Base editing of the mutated TERT promoter inhibits liver tumor growth. *Hepatology* 79: 1310–1323

Zheng C, Liang S-Q, Liu B, Liu P, Kwan S-Y, Wolfe SA & Xue W (2022) A flexible split prime editor using truncated reverse transcriptase improves dual-AAV delivery in mouse liver. *Molecular Therapy* 30

Zheng C, Liu B, Dong X, Gaston N, Sontheimer EJ & Xue W (2023a) Template-jumping prime editing enables large insertion and exon rewriting in vivo. *Nat Commun* 14

Zheng P, Dou Y & Wang Q (2023b) Immune response and treatment targets of chronic hepatitis B virus infection: innate and adaptive immunity. *Front Cell Infect Microbiol* 13

Zufferey R, Nagy D, Mandel RJ, Naldini L & Trono D (1997) Multiply attenuated lentiviral vector achieves efficient gene delivery in vivo. *Nat Biotechnol* 15: 871–875

Zuo E, Sun Y, Wei W, Yuan T, Ying W, Sun H, Yuan L, Steinmetz LM, Li Y & Yang H (2019) Cytosine base editor generates substantial off-target single-nucleotide variants in mouse embryos. *Science* 364: 289–292

